Hans Tausen Iskappe North Greenland

Studies Using an Ice Flow Model

Master Thesis

by

Anne Munck Solgaard

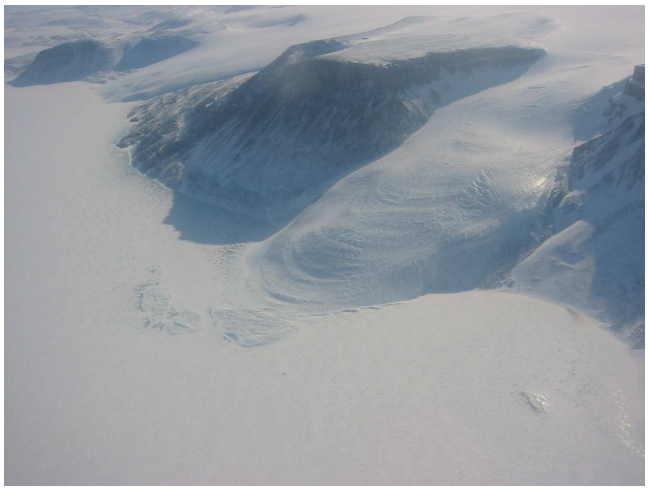

SUPERVISOR: Christine Schøtt Hvidberg

February 2008

CENTRE FOR ICE AND CLIMATE

Niels Bohr Institute, University of Copenhagen

Abstract

Hans Tausen Iskappe is a local ice cap located in Peary Land, North Greenland. The ice cap is approximately 75 km from north to south and 50 km from east to west and rests on a $\sim$ 1000 m high plateau. Different studies of an ice core drilled to bedrock at the Central Dome indicates an age of the ice cap of 3500-4000 years meaning that it did not survive the warmer climate of the Climatic Optimum 6000-8000 BP. The re-building together with the present and future state of the ice cap are studied using a 2D vertically integrated ice flow model based on the shallow ice approximation.

Investigations of the build-up using simple parameterizations of accumulation show that a change in accumulation pattern has occurred over the life time of the ice cap. The surface height of the Central Dome has been measured in 1994 and 2004 and a decrease of $1 - 1.5$ m $\pm$ 0.5m is reported ascribed to local effects. The most likely mechanisms are believed to be increased melting during the period in the dome area and ice flow transporting ice away from the dome combined with low accumulation. These mechanisms are able to explain a decrease within the lower bound of the observations but are not sufficient to account for decreases in the upper bound.

The future state of Hans Tausen Iskappe is investigated by forcing the ice flow model using future predictions of temperature and precipitation by *Stendel et al.* [2007]. All applied scenarios show thinning and retreat of the ice margin leading to a steeper ice cap over the next century.

Resumé

Hans Tausen Iskappe er en selvstændig iskappe beliggende i Peary Land i Nordgrønland. Iskappen er ca. 75 km fra nord til syd og ca. 50 km fra øst til vest, og den hviler på et $\sim$ 1000 m højt plateau. Studier af en iskerne boret på den Centrale Dome viser, at Hans Tausen Iskappe ikke er ældre end 3500-4000 år, og at den dermed ikke overlevede de varmere temperaturer under det klimatiske optimum 6000-8000 år BP. En 2D vertikalt integreret isflydningsmodel baseret på shallow ice approximationen er anvendt til at undersøge iskappens nuværende og fremtidige tilstand samt opbygningsfasen.

Undersøgelser af opbygningsfasen ved brug af simple parametriseringer af akkumulationsraten viser, at der sket ændringer i nedbørsmønsteret i løbet af iskappens levetid. Højden af den Central Dome blev målt i både 1994 og 2004. Der er sket et fald i højden på $1 - 1.5$ m $\pm$ 0.5m, som tilskrives lokale processer. De to mest sandsynlige mekanismer anses for at være øget smeltning samt flydning, der transporterer is væk fra området kombineret med lav akkumulation. Disse mekanismer er i stand til at forklare et fald i højden i den lave grænse, men kan ikke redegøre for et fald i den høje ende af $1 - 1.5$ m $\pm$ 0.5m.

Hans Tausen Iskappes fremtidige tilstand er undersøgt ved at forcere isflydemodellen ved brug af model forudsigelser udført af [*Stendel et al.*, 2007] af temperatur og nedbør i området. Alle anvendte scenarier viser udtynding og tilbagetrækning af isranden. Dette vil i løbet af det næste århundrede føre til en stejlere iskappe.

Preface

The work for this thesis has been carried out in the period from February 2007 to February 2008 under the supervision of Christine Schøtt Hvidberg at the Centre for Ice and Climate at the Niels Bohr Institute, University of Copenhagen.
Many people have been very helpful along the way and I owe you many thanks for ideas and discussions. First, I would like to thank my supervisor Christine Schøtt Hvidberg for helpful and inspiring supervision. I am also grateful for the ideas and assistance provided by Guðfinna Aðalgeirsdóttir for the last part of this thesis.
Several people have kindly provided data sets for this study: I would like to thank Niels Reeh for providing the data of the digital elevation models, Martin Stendel for sharing the results of his model simulation of the Greenland region and the Danish National Space Center for the data of the measurements of Hans Tausen Iskappe in 1994 and 2004. Furthermore, I would like to thank Kristian Keller, Lars Stenseng and Finn Bo Madsen for assistance with the geodetic data.
For help in the last hectic phase I would like to thank Susanne Lilja Buchardt and Hans Christian Steen-Larsen for useful suggestions and corrections. Last but not least, I thank Kasper Jørgensen for unlimited help and understanding.

Anne Munck Solgaard
University of Copenhagen, 21st February 2008

Contents

Chapter 1

Introduction

The Hans Tausen Iskappe (ice cap) studied in this thesis is a local ice cap in Peary Land, Northern Greenland just 20 km north of the Greenland Ice Sheet. The location of the ice cap is shown in Fig. 1.3. A map showing the vicinity of the ice cap is displayed in Fig. 1.4 and a map of Peary Land can be seen in Fig. A.3 in the Appendix. Peary Land is named after the American

Figure 1.1: *Hans Tausen Iskappe is located on an approximately* 1000 m *high plateau and has several outlet glaciers. Photo: Danmarks Rumcenter 2004*

polar explorer Robert Edwin Peary who made several dog sledge expeditions to North Greenland. The conditions during these expeditions were tough and often food supplies were limited. For this reason the Inuits who assisted these

expeditions called Peary Land: 'Kingmersoriartorfigssuak', -the place where you eat dogs. The sledgedogs were often a part of food supply [*Dawes*, 2003].

Hans Tausen Iskappe is approximately 75 km from north to south and 50 km from east to west and rests on a ca. 1000 m high plateau as seen in Fig. 1.1 [*Reeh et al.*, 2001]. The fjords surrounding the ice cap are covered by semi-permanent sea ice [*Landvik et al.*, 2001]. In the central parts the surface elevation can reach 1200-1300 m as seen in Fig. 1.2. The ice thickness varies over the area: In the southern part it is $\sim$ 300 m except in a north-south trending valley where it reaches up to 600 m. In the northern part the bedrock topography is very mountainous and the ice thickness varies between 100-400 m. Hans Tausen Iskappe has several local domes as seen in Fig. 1.2 and

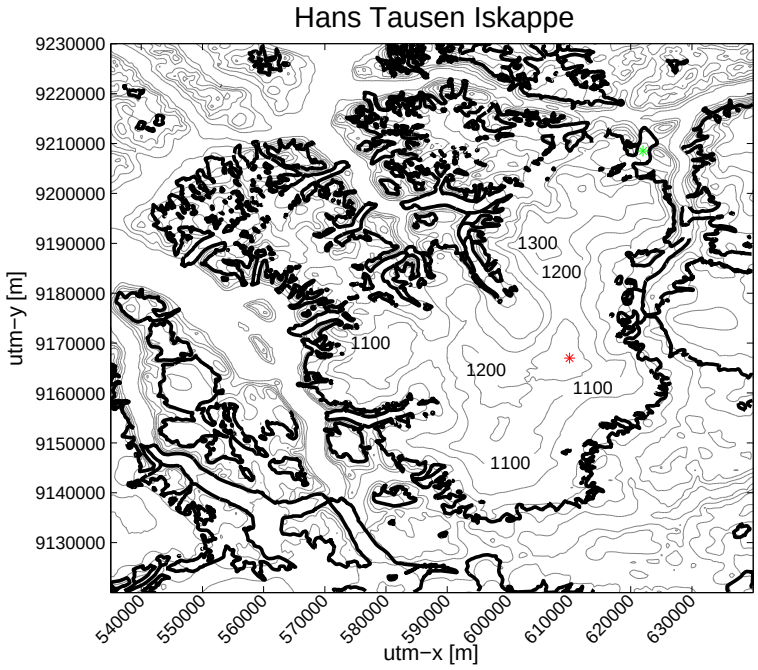

Figure 1.2: *Map of Hans Tausen Iskappe, North Greenland. The* ***red*** *star indicates the Central Dome where the ice core was drilled. The* ***green*** *star shows the location of the small outlet glacier, Hare Glacier, where mass balance studies were carried out during the field work. The contour lines indicate surface elevation in* [m.a.s.l.] *with an equidistance of* 100 m. *The thick black line indicates the ice margin.*

several outlet glaciers drain the northern, western and eastern part of the ice cap. Some of these are calving glaciers terminating at sea level while others terminate up to some few hundred meters above sea level. This is in contrast

to the southern part which is more 'quiet' and covered by snow drifts that survive summer melt. Summer melting occurs even at high elevations [*Reeh et al.*, 2001]. The accumulation at the Central Dome is 0.1 $^{m_{ice}}/_{yr}$ and a little higher on the northern part of the ice cap. In general precipitation in the North Greenland area is very modest [*Cappelen et al.*, 2001].

North Greenland is an area where climatological data are very sparse and this makes studies of the ice cap especially exciting and important. A larger field work was carried out on this basis in the period from 1993-1995 including a wide range of different studies:

- An ice core 345 m long was drilled to bedrock at the Central Dome along with several firn cores
- Elevation and ice thickness were measured both as part of an airborne survey in 1993 and a ground survey in 1994-1995 from snow scooter
- Strain net observations were carried at the Central Dome
- Mass balance studies were performed along a flow line starting at the North Dome and extending to a small outlet glacier, Hare Glacier
- Glacio-geological investigations were carried out north of the ice cap.

In the seventies further two firn cores were drilled a bit south of the Central Dome. The location of the drill-site and Hare Glacier are marked in Fig. 1.2. The results of the field work will be discussed and described in the later chapters. One of the main discoveries was that the ice cap did not survive the higher temperatures of the Climatic Optimum 6000-8000 years ago. Different studies of the ice core show that the age estimate of the ice cap lies in the range 3500-4000 years *Madsen and Thorsteinsson* [2001]; *Clausen et al.* [2001]; *Hammer et al.* [2001].

The aim of this thesis is to investigate the build-up following the Climatic Optimum along with the present and the future state of Hans Tausen Iskappe. This is done using a 2D vertically integrated ice flow model developed for this purpose together with the results of the above mentioned field work. Also newly obtained information from a remeasurement of the Central Dome [*Dalå et al.*, 2005] and model predictions of future values of temperature and precipitation are used. An earlier modelling study of Hans Tausen Iskappe using a 1D ice flow model concentrated on fixing bounds on the age of the ice cap *Madsen* [1997]. This is not attempted in this study, rather the age estimate is taken as starting point to investigate the accumulation pattern

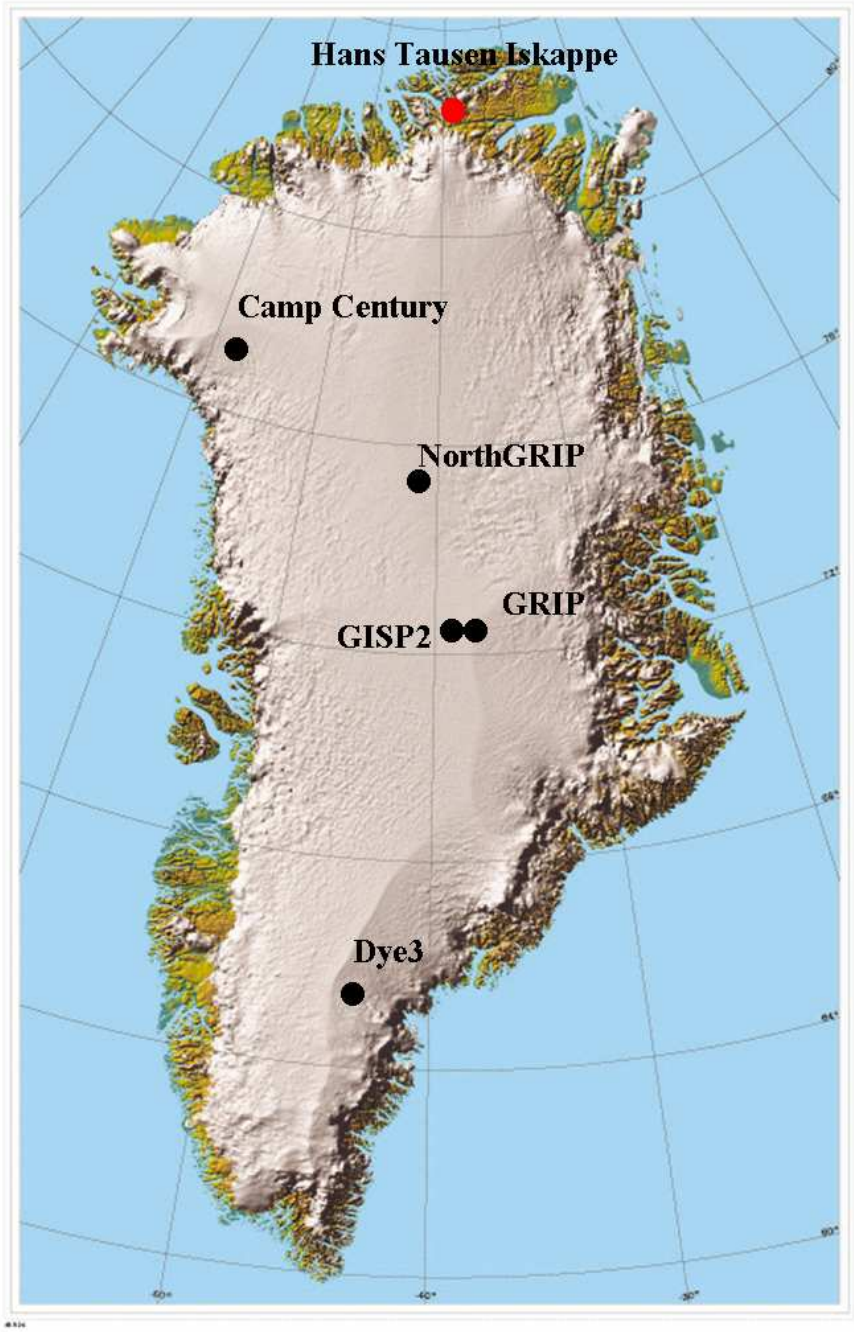

Figure 1.3: *Figure showing the location of the Hans Tausen Iskappe along with the drillings on the Greenland Ice Sheet. Map: S. Ekholm, Danish National Survey and Cadastre.*

during the rebuilding of the ice cap.

Understanding the response of ice masses to changes in climate is essential, especially in the view of the projected preferential warming of the Arctic regions [*Anisimov et al.*, 2007]. Glaciers and ice caps outside the two major ice sheets of Greenland and Antarctica are believed to very important contributors to the rise in global sea level not attributable to thermal expansion in this century *Meier et al.* [2007].

The structure of the thesis is outlined below:

Chapter 2: In this chapter the development of the 2D vertically integrated ice flow model based on the shallow ice approximation is described.

Chapter 3: The model is validated using the EISMINT benchmarks and tested for conservation of mass.

Chapter 4: The input data sets of ice thickness and bedrock topography are described together with parameterizations of temperature and accumulation. Different special circumstances related to Hans Tausen Iskappe are accounted for.

Chapter 5: Hans Tausen Iskappe did not survive the warmer climate of the Climatic Optimum. In this chapter the build-up of the ice cap is studied using different simple parameterizations of the accumulation.

Chapter 6: The present state of the Hans Tausen Iskappe is investigated. The Central Dome area was remeasured in 2004 ten years after the field work and a decrease in elevation is reported. The state of the ice cap is also investigated by comparing the 1994 mass balance with the one representing a steady state.

Chapter 7: The future state of Hans Tausen Iskappe is investigated. The ice flow model is forced by future predictions of temperature and precipitation from a transient run using a RCM by *Stendel et al.* [2007].

Chapter 8: This chapter presents the main conclusions of the thesis.

Figure 1.4: *Figure showing the vicinity of Hans Tausen Iskappe in Peary Land, North Greenland. Map: GEUS 2003 from the anthology: Peary Land At tænke sig til Peary Land - Og kommer der. Redaktion: Gunnar Martens, Jens Fog Jensen, Morten Meldgaard og Hans Meltofte.*

Chapter 2

The Ice Flow Model

Ice flow models have a wide range of applications ranging from investigation of the past and future climate to dating of deep ice cores. The complexity of the numerical ice flow models has evolved following the increase in computer power, and now the variety of models ranges from flow line models and 2D map plane models to complex higher order models. For each model type the complexity can vary depending e.g. on the choice of flow model, whether temperature calculations are performed or whether basal sliding is included. It is still, however, very time consuming to solve the full system of equations governing the flow of ice and therefore most models still make use of the shallow ice approximation (SIA)(to be described in Section 2.2) to simplify the equations. The SIA has its limitations but it is currently the best choice for simulating time dependent changes in geometry over long periods of time while the more complex models give a much better understanding of the dynamics on smaller spatial scales. For an overview of the present achievements in ice dynamics see *Marshall* [2005].

This chapter will focus on the development of the 2D map plane model used in this study of Hans Tausen Iskappe. In Sections 2.1 - 2.3 the basic concepts and equations used to develop the model are described. Sections 2.4 and 2.5 will focus on the discretization of the problem in space and time and how the equations are solved. The applied mass balance model is described in Section 2.6 and in the last Section 2.7 an overview of the model is given.

2.1 The Basic Equations and Definitions

A cross section of the model to be developed in this section is shown in Fig. 2.1. x and y are the horizontal coordinates and z is the vertical co-

ordinate which is positive above sealevel. $S(x, y)$ is the height of the ice surface at a given point (x, y), $B(x, y)$ denotes the bedrock topography and $H(x, y) = S(x, y) - B(x, y)$ is the ice thickness.

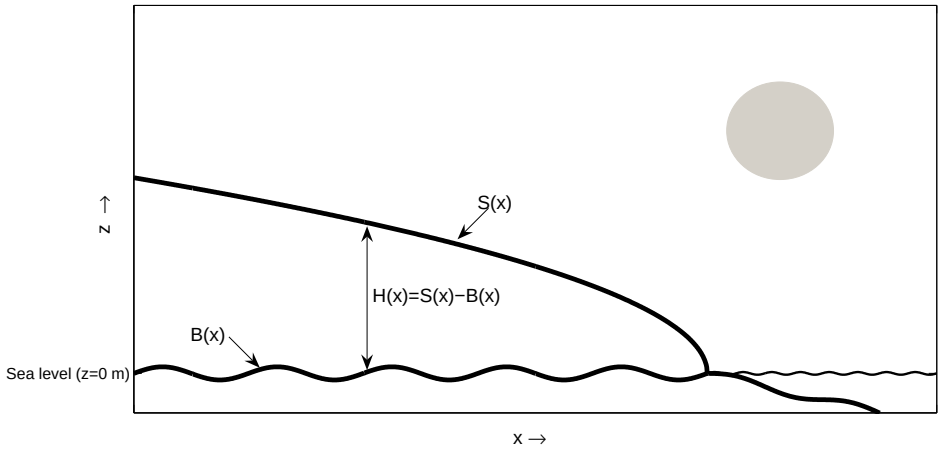

Figure 2.1: *Defining the coordinate system. The z coordinate is pointing upwards opposite the gravitational force and is positive above sealevel. The y axis points into the paper.* $S(x, y)$ *is the height of the surface above sealevel,* $B(x, y)$ *the bedrock topography and* $H(x, y)$ *is the ice thickness.*

2.1.1 The Continuity Equation

Ice sheet models are based on the principles of conservation of momentum, mass and heat. In this model the ice is assumed to be isothermal and therefore no temperature calculations are performed. It is also assumed that the ice is incompressible reducing the equation of continuity which expresses conservation of mass to:

$$\nabla \cdot \mathbf{U} = \frac{\partial u}{\partial x} + \frac{\partial v}{\partial y} + \frac{\partial w}{\partial z} = 0 \tag{2.1}$$

$\mathbf{U}$ is the velocity vector and u, v and w denote the velocity in the x, y and z-direction respectively. Vertical integration of Eq. (2.1) leads to the prognostic equation describing the evolution of the local ice thickness expressing conservation of mass in a vertical column in the ice (see e.g. p. 256 in *Paterson* [1994] for a derivation). The equation is also illustrated in Figure 2.2:

$$\frac{\partial H}{\partial t} = -\nabla \cdot \mathbf{q} + b_s + b_b = \nabla \cdot (H\bar{\mathbf{U}}) + b_s + b_b \tag{2.2}$$

Here $\mathbf{q}$ is the local horizontal mass flux vector, b_s and b_b are the mass balances at the surface and bottom respectively and $\bar{\mathbf{U}}$ is the vertically mean velocity vector. The ice cap is assumed to be frozen to bedrock and therefore only internal deformation contributes to the velocity. It is also assumed that no ice loss/gain occurs at the bottom and therefore $b_b = 0$.

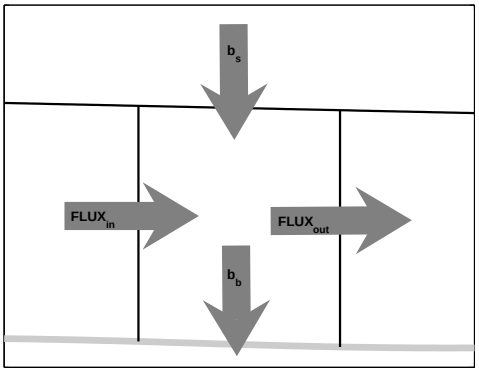

Figure 2.2: *The local change in ice thickness of an element is controlled by the fluxes in and out of the element. In this model it is assumed that there is no bottom melting ($b_b = 0$).*

2.1.2 The Stress Equilibrium Equations

The flow of a glacier or an ice cap is sufficiently slow to neglect acceleration. This reduces the equations of motion to equations of static equilibrium. They express a balance between the forces acting on the surfaces of an element and the forces acting on the entire element (See Fig. 2.3):

$$\begin{aligned} \frac{\partial \sigma_x}{\partial x} + \frac{\partial \tau_{xy}}{\partial y} + \frac{\partial \tau_{xz}}{\partial z} &= 0 \\ \frac{\partial \tau_{xy}}{\partial x} + \frac{\partial \sigma_y}{\partial y} + \frac{\partial \tau_{yz}}{\partial z} &= 0 \\ \frac{\partial \tau_{xz}}{\partial x} + \frac{\partial \tau_{yz}}{\partial y} + \frac{\partial \sigma_z}{\partial z} &= \rho g \end{aligned} \tag{2.3}$$

σ_x, σ_y and σ_z denote the normal stresses and τ_{xz}, τ_{yz} and τ_{xy} denote the shear stresses. ρ and g denote the density of ice and the acceleration of gravity respectively both assumed to be constants. For a derivation see eg. *Hooke* [2005] p. 261. The stress tensor is symmetric meaning that (using tensor notation) $\tau_{ij} = \tau_{ji}$.

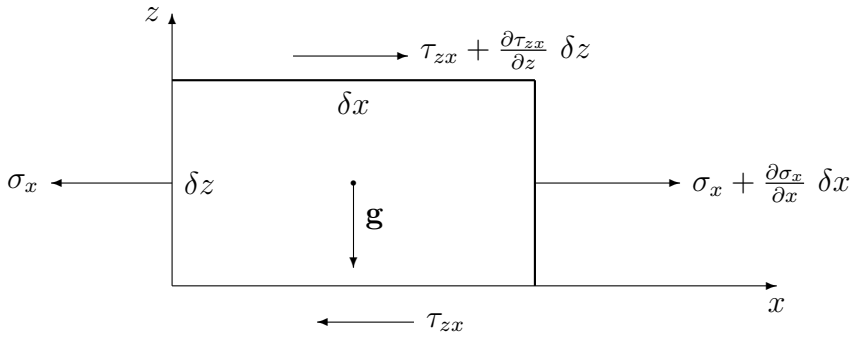

Figure 2.3: *Stresses acting on a small element in the x-direction. Illustration in 2D.*

2.1.3 The Flow Law

The constitutive relation used in this model is Glen's law (Eq. (2.6)) [*Glen*, 1955]. It is an empirical relation describing the flow of isotropic polycrystalline ice and it is the most widely used flow law for ice. It relates the deviatoric stresses, σ'_{ij}, to the strain rates defined as:

$$\dot{\epsilon}_{ij} = \frac{1}{2}\left(\frac{u_{\partial i}}{\partial x_j} + \frac{\partial u_j}{\partial u_i}\right) \tag{2.4}$$

It is convenient to work with stress deviators since experiments show that the flow relation is almost unaffected by hydrostatic pressure [see eg. *Paterson*, 1994, p. 89]. The deviatoric stress is defined as:

$$\sigma'_{ij} = \sigma_{ij} - P \tag{2.5}$$

Where P is the hydrostatic pressure (the mean normal stress) given by: $P = \frac{1}{3}\sigma_{kk}$ meaning that the shear stress components are unchanged. Glen's flow law takes the generalized form:

$$\dot{\epsilon}_{ij} = A\tau^{n-1}\tau'_{ij} \tag{2.6}$$

Here $\dot{\epsilon}_{ij}$ is the strain rate, τ is the second invariant of the stress tensor also called the effective shear stress and is defined as $\tau = \sqrt{\frac{1}{2}\sigma'_{ij}\sigma'_{ij}}$ and σ'_{ij} is the deviatoric stresses defined above. The exponent n is a constant but it is not well determined. For the present study the recommended value of 3 by *Paterson* [1994] is used. The value of A is dependent on the temperature of the ice, impurity content, crystal orientation and water content, but other things may influence the value as well. A depends on temperature according to the Arrhenius relation:

$$A = A_0 \exp(-Q/RT) \tag{2.7}$$

where A_0 is independent of temperature, R is the universal gas constant and Q is the activation energy for creep [*Paterson*, 1994]. Ice with a lower temperature is generally stiffer than ice with a higher temperature. This is reflected in A meaning that low/high temperatures give smaller/larger values for the parameter. Eq.(2.6) is a flow law for isotropic ice but the right hand side is sometimes multiplied by an enhancement factor E trying to account for the effect of crystal orientation on the strain rate [*Marshall*, 2005]. This does not account, though, for crystal orientation favoring flow in a certain direction.

2.2 The Shallow Ice Approximation

As mentioned in the introduction to this chapter the shallow ice approximation (SIA) is widely used in ice flow modelling (eg. Ralf Greve's model SICOPOLIS which is used to model the ice sheets of Greenland and Antartica). It was introduced in glaciology by *Fowler and Larson* [1978] and is also briefly described in e.g. *Hooke* [2005].

In the shallow ice approximation the equations are scaled making use of the fact that for ice sheets the horizontal extent ($\mathbb{L}$) is much greater than the vertical extent ($\mathbb{H}$). This is also the case for the horizontal ($\mathbb{V}_\mathbb{L}$) and vertical ($\mathbb{V}_\mathbb{H}$) velocity and therefore the horizontal derivatives are much smaller than the vertical ones in both cases.

The typical velocities are chosen so that

$$\frac{\mathbb{H}}{\mathbb{L}} = \frac{\mathbb{V}_\mathbb{H}}{\mathbb{V}_\mathbb{L}} = \gamma \tag{2.8}$$

For the great ice sheets γ is typically of the order of 10^{-3}. By introducing this ratio into Eq. (2.1, 2.3 and 2.6) it is possible to identify the relative importance of the different terms. By removing all terms including γ to a power ≥ 1 the zeroth-order shallow ice approximation is obtained which is the basis for this model.

When applying the SIA to the stress equilibrium equations Eq. (2.3) only the vertical shear stresses are left:

$$\frac{\partial P}{\partial x} + \frac{\partial \tau_{xz}}{\partial z} = 0 \tag{2.9}$$

$$\frac{\partial P}{\partial y} + \frac{\partial \tau_{yz}}{\partial z} = 0 \tag{2.10}$$

$$\frac{\partial P}{\partial z} = \rho g \tag{2.11}$$

P comes from the substitution of the deviatoric stress, Eq. (2.5), into the stress equilibrium equations (Eq. (2.3)). The effective stress reduces to:

$$\tau^2 = \tau_{xz}^2 + \tau_{yz}^2 \tag{2.12}$$

while the equation of continuity remains unchanged.

The SIA has its limitations because the longitudinal stresses and the horizontal shear stresses are neglected. This means that the gravitational driving stress is balanced only by vertical shearing i.e. for an ice column the gravitational driving stress is balanced locally by basal shear alone with no direct influence of up- or downstream effects. The scaling breaks down in the margin area where the surface gradient is large and near the ice divide. Here the proportionality between coordinates and velocity, Eq. (2.8), breaks down and the vertical shear is no longer dominant. Variations in bedrock topography also affect the validity of the SIA since it can change the local flow pattern [*Le Meur et al.*, 2004].

Despite the limitations models based on the SIA reproduce the large scale dynamics of ice sheets and glaciers correctly when compared to full-stokes models as studied by *Le Meur et al.* [2004] and *Leysinger Vieli and Gudmundson* [2004].

In this thesis the time dependent large scale dynamics of a small ice cap assumed to be frozen to bedrock is studied and therefore the zeroth-order SIA seems to be an appropriate scaling of the equations.

2.3 Deriving the Model Equations

To obtain an expression for the mean vertical velocity in Eq. (2.2) the reduced equations in Section 2.2 are solved for the two shear stresses. The shear stress expressions are then inserted into the flow law, Eq. (2.6), and it is then possible to integrate for the velocity. First, the mean pressure, P, is calculated by integrating equation 2.11 from a height z in the ice to the surface:

$$P = -\rho g(S - z) \tag{2.13}$$

The vertical shear stresses can now be calculated by inserting Eq. (2.13) in Eqs. (2.9) and (2.10) and integrating as before:

$$\tau_{xz} = -\rho g \frac{\partial S}{\partial x}(S - z) \tag{2.14}$$

$$\tau_{yz} = -\rho g \frac{\partial S}{\partial y}(S - z) \tag{2.15}$$

By using Eqs. (2.14) and (2.15) the horizontal velocities $u(z)$ and $v(z)$ can be derived using Glen's flow law (Eq. (2.6)). In the following an expression for $u(z)$ is derived. The calculation for the velocity in the y-direction is obtained similarly. From Glen's flow law, Eq. (2.6), and Eq. (2.4) we have:

$$A\tau^{n-1}\tau_{xz} = \frac{1}{2}(\frac{du}{dz} + \frac{dw}{dx}) \tag{2.16}$$

By using Eq. (2.8) it can be shown that $\frac{\partial w}{\partial x} << \frac{\partial u}{\partial z}$ which simplifies Eq. (2.16) to:

$$\frac{1}{2}\frac{du}{dz} = A\tau^{n-1}\tau_{xz} \tag{2.17}$$

The vertical shear stresses are the only non-zero stresses and inserting them in the scaled expression for the effective shear stress (Eq. (2.12)) yields:

$$\begin{aligned} \tau^2 &= (-\rho g \frac{\partial S}{\partial x}[S - z])^2 + (-\rho g \frac{\partial S}{\partial y}[S - z])^2 \\ \tau^2 &= (\rho g[S - z])^2\Big((\frac{\partial S}{\partial x})^2 + (\frac{\partial S}{\partial y})^2\Big) \\ \tau &= \rho g[S - z]|\nabla S| \end{aligned} \tag{2.18}$$

Inserting Eq. (2.18) into Eq. (2.17) and integrating from a height z above bedrock to the ice surface S gives the following expression for $u(z)$:

$$\int_{u(z)}^{u_s} du = \int_z^S -2A[\rho g(S-z)]^n |\nabla S|^{n-1} \frac{\partial S}{\partial x} dz \tag{2.19}$$

$$u(z) = u_s - \frac{2A}{n+1}(\rho g)^n |\nabla S|^{n-1} \frac{\partial S}{\partial x}(S-z)^{n+1} \tag{2.20}$$

To find an expression for the mean **u**-velocity, $\bar{u}$, of the ice column the expression for the flux is integrated over the ice thickness. The flux through a vertical section can be written as:

$$\bar{u}H = \int_B^S u(z) dz \tag{2.21}$$

Remembering that $S(x,y) - B(x,y) = H(x,y)$ and integrating Eq. (2.21) over the ice thickness yields an expression for the vertical mean velocity in the x-direction:

$$\bar{u} - u_b = \frac{2A}{n+2}(\rho g)^n |\nabla S|^{n-1} \frac{\partial S}{\partial x} H^{n+1} \tag{2.22}$$

By performing similar calculations for the vertical mean velocity in the y-direction, $\bar{v}(z)$, the vertical mean velocity vector becomes:

$$\bar{\mathbf{U}} = \frac{2A}{n+2}(\rho g)^n |\nabla S|^{n-1} H^{n+1} \nabla S \tag{2.23}$$

This can be inserted in the vertically integrated continuity equation (Eq. (2.2)) to find an expression for the time derivative of the local ice thickness:

$$\begin{aligned}
\frac{\partial H}{\partial t} &= -\nabla \cdot (H\bar{\mathbf{U}}) + b_s \\
&= \nabla \cdot (H \frac{2A}{n+2} (\rho g)^n |\nabla S|^{n-1} \nabla S \; H^{n+1}) + b_s \\
&= \nabla \cdot \Big(\frac{2A}{n+2} (\rho g)^n \, |\nabla S|^{n-1} \, \nabla S \, H^{n+2} \Big) + b_s \\
&= \nabla \cdot \Big(\frac{2A}{n+2} (\rho g)^n \Big[\Big(\frac{\partial S}{\partial x} \Big)^2 + \Big(\frac{\partial S}{\partial y} \Big)^2 \Big]^{\frac{n-1}{2}} \nabla S \, H^{n+2} \Big) + b_s
\end{aligned} \tag{2.24}$$

b_s denotes the surface mass balance. The equation can be written in the form of a non-linear diffusion equation:

$$\frac{\partial H}{\partial t} = \nabla \cdot (D \nabla S) + b = -\nabla \cdot \mathbf{q} + b \tag{2.25}$$

where:

$$D = \frac{2A}{n+2} (\rho g)^n H^{n+2} \Big[\Big(\frac{\partial S}{\partial x} \Big)^2 + \Big(\frac{\partial S}{\partial y} \Big)^2 \Big]^{\frac{n-1}{2}} \tag{2.26}$$

The model resulting from these equations is called a 2D map-plane or vertically integrated model. It is not a 3D model because the basic elements are columns of ice and parameters like velocity are averaged over a column.

2.4 Discretizising the Problem

The equation describing the evolution of the ice cap, (Eq. (2.2)), is a non-linear equation and cannot be solved analytically. Instead, it is solved numerically using finite differences and adopting a staggered grid. The independent variables are discretized as:

$$x = i\Delta_x; \quad y = j\Delta_y, \quad i \in (0, N_x) \;\; j \in (0, N_y) \tag{2.27}$$

where x and y are the horizontal dimensions over the domain:

$$0 \leq x \leq L_x \quad \text{and} \quad 0 \leq y \leq L_y \tag{2.28}$$

N_x and N_y are the number of grid points and L_x and L_y are the length of the domain in the x- and y-direction respectively. In *Hindmarsh and Payne* [1996] different ways to make the spatial descretization are presented and for this model method 3 from that paper is used. It uses a 13 point computational molecule as seen in Fig. 2.4.

D is calculated at the gridpoints:

$$D_{i,j} = \frac{2A}{n+2} (\rho g)^n H_{i,j}^{n+2} |\nabla(S)_{i,j}|^{n-1} \tag{2.29}$$

where

$$|\nabla S_{i,j}| = \sqrt{\Big(\frac{S_{i+1,j} - S_{i-1,j}}{2\Delta_x} \Big)^2 + \Big(\frac{S_{i,j+1} - S_{i,j-1}}{2\Delta_y} \Big)^2} \tag{2.30}$$

The flux in the x-direction, q^x, is evaluated at the staggered points in the x-direction:

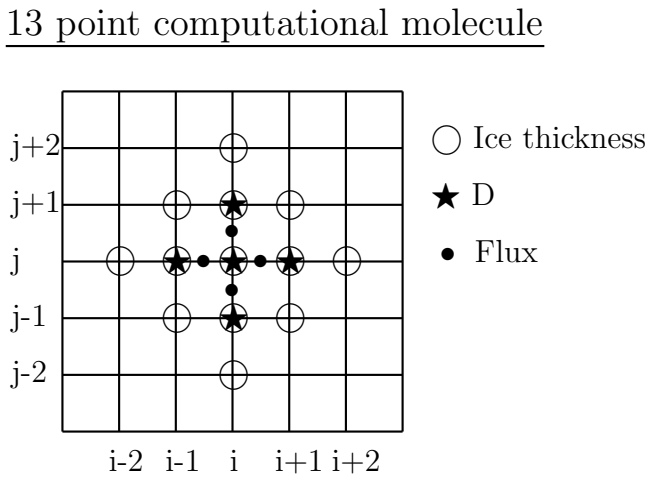

Figure 2.4: *The 13 point computational molecule for calculating* $(\nabla \cdot \mathbf{q})_{i,j}$. *The height of the bedrock,* B, *is used at all grid points to calculate the height of the surface:* $S = H + B$ *used to calculate both the diffusion,* D *and the flux,* q.

$$q^x_{i+\frac{1}{2},j} = -(\frac{D_{i+1,j} + D_{i,j}}{2})(\frac{S_{i+1,j} - S_{i,j}}{\Delta_x}) \tag{2.31}$$

And likewise for the flux in the y-direction, q^y. Calculating the flux at the staggered grid points enables the margin to advance and retreat. $D = 0$ if calculated at the grid points at the glacier front because the ice thickness is zero. As a result the flux calculated at the same (not staggered) point would also equal zero meaning that snout would be stagnant as described in *Oerlemans* [2001]. The divergence of the flux is then calculated as:

$$(\nabla \cdot \mathbf{q})_{i,j} = \frac{q^x_{i+\frac{1}{2},j} - q^x_{i-\frac{1}{2},j}}{\Delta_x} + \frac{q^y_{i,j+\frac{1}{2}} - q^y_{i,j-\frac{1}{2}}}{\Delta_y} \tag{2.32}$$

In the EISMINT benchmarks (European Ice Sheet Modelling INiTiative) [*Huybrechts and Payne*, 1996] (see also section 3.1), which provide a tool for validating ice flow models, the participating ice flow models were divided into two types according to the way D is constructed at the staggered grid points. Type I models construct the diffusion directly at the staggered points while type II models calculate it as the mean of two diffusivities evaluated at the neighboring points i and $i + 1$:

$$\begin{aligned} \text{Type I: } D_{i+\frac{1}{2}} &= f\Big(\frac{H_{i+1}+H_i}{2}, \frac{H_{i+1}+H_i}{\Delta_x}\Big) \\ \text{Type II: } D_{i+\frac{1}{2}} &= \frac{D_{i+1}+D_i}{2} \end{aligned}$$

Type I models are numerically more precise than type II models, but type II models have the great advantage of being stable for much larger time steps [*Huybrechts and Payne*, 1996]. The spatial discretization used for this model means that it is a type II model. It uses a 13 point computational molecule (Fig. 2.4) for calculating $(\nabla \cdot \mathbf{q})_{i,j}$ contrary to the two other methods discussed in *Hindmarsh and Payne* [1996] which use a 9 point molecule. This can be understood as method 3 includes additional artificial diffusion. *Hindmarsh and Payne* [1996] tested the accuracy of different spatial descretizations and found that the model using the 13 point molecule consistently underpredicts the ice thickness and they ascribe this to the extra artificial diffusion. Both model types have difficulties capturing the slope of the ice sheet near the margin because of the discontinuity of the surface and the central differences method used for calculating the slope. Different methods have been suggested to improve this (See e.g. *Van den Berg et al.* [2006] and *Saito et al.* [2007]) but is not applied in this study.

In order to discretize in time a Crank-Nicolson method is used:

$$\frac{\partial H}{\partial t} = \frac{H_{i,j}^{k+1} + H_{i,j}^{k}}{\Delta_t} = \frac{\Theta_{i,j}^{k+1} + \Theta_{i,j}^{k}}{2} \tag{2.33}$$

Here the superscript k denotes the time step, Δ_t the time step size and Θ the right hand side of the Eq. (2.25) describing the evolution of H. This is an implicit method in time meaning that to calculate the state of the system at a later time it uses both the current and the later state of the system. The Crank-Nicolson method uses the average of the two states and is second order in time [see e.g. *Press et al.*, 2003, p.839]. The Crank-Nicolson scheme is uniformly stable for the linear diffusion equation, but the non-linear version has time step limits [*Hindmarsh and Payne*, 1996]. (See also Section 4).

2.5 Solving the Equations

In order to solve the system for the ice thickness at the next time step, H^{k+1}, all terms associated with the time step $k+1$ are collected on the **left** hand

side and all terms associated with the time step k on the **right** hand side of the equation.

$$H_{i,j}^{k+1} - \frac{\Delta_t}{2}\,\Theta_{i,j}^{k+1} = H_{i,j}^{k} + \frac{\Delta_t}{2}\,\Theta_{i,j}^{k} \tag{2.34}$$

By inserting the above expressions for the diffusivity, the surface gradient and the flux into the **left** hand side of Eq. (2.34) the following expression is obtained:

$$\begin{aligned} & H_{i,j}^{k+1} - \frac{\Delta_t}{2}\,\Theta_{i,j}^{k+1} \qquad (2.35)\\ = \;& H_{i,j}^{k+1} - \frac{\Delta_t}{2}\cdot\Big(\frac{1}{2(\Delta_x)^2}\Big[D_{i+1,j}^{k+1}(S_{i+1,j}^{k+1} - S_{i,j}^{k+1})\\ & + D_{i,j}^{k+1}(S_{i+1,j}^{k+1} - 2S_{i,j}^{k+1} + S_{i-1,j}^{k+1}) - D_{i-1,j}^{k+1}(S_{i,j}^{k+1} - S_{i-1,j}^{k+1})\Big]\\ & + \frac{1}{2(\Delta_y)^2}\Big[D_{i,j+1}^{k+1}(S_{i,j+1}^{k+1} - S_{i,j}^{k+1}) + D_{i,j}^{k+1}(S_{i,j+1}^{k+1} - 2S_{i,j}^{k+1} + S_{i,j-1}^{k+1})\\ & - D_{i,j-1}^{k+1}(S_{i,j}^{k+1} - S_{i,j-1}^{k+1})\Big] + b_{i,j}^{k+1}\Big) \end{aligned}$$

The right hand side is obtained likewise. To find expressions for the ice thickness at the next time step at each grid point the equation is linearized with respect to H. The equation then takes the form:

$$\begin{aligned} & AH_{i,j-1}^{k+1} + BH_{i-1,j}^{k+1} + CH_{i,j}^{k+1} + DH_{i+1,j}^{k+1} + EH_{i,j+1}^{k+1} - \frac{\Delta_t}{2}\,b_{i,j}^{k+1}\\ = \;& KH_{i,j-1}^{k} + LH_{i-1,j}^{k} + MH_{i,j}^{k} + NH_{i+1,j}^{k} + OH_{i,j+1}^{k} + \frac{\Delta_t}{2}\,b_{i,j}^{k} \end{aligned} \tag{2.36}$$

$\{A, B, C, D, E\}$ and $\{K, L, M, N, O\}$ depend on the time dependent variables at time step $k+1$ and k respectively. Writing Eq. (2.36) as a matrix equation we obtain:

$$
\begin{pmatrix}
C & D & & E & & & & & & & \\
B & C & D & & E & & & & & & \\
 & B & C & D & & E & & & & & \\
 & & \ddots & \ddots & \ddots & & \ddots & & & & \\
A & & & B & C & D & & E & & & \\
 & A & & & B & C & D & & E & & \\
 & & A & & & B & C & D & & E & \\
 & & & \ddots & & & \ddots & \ddots & \ddots & & \\
 & & & & A & & & B & C & D & \\
 & & & & & A & & & B & C & D \\
 & & & & & & A & & & B & C
\end{pmatrix}
\cdot
\begin{pmatrix}
H^{k+1}_{i-1,j-1} \\ H^{k+1}_{i,j-1} \\ H^{k+1}_{i+1,j} \\ \vdots \\ H^{k+1}_{i-1,j} \\ H^{k+1}_{i,j} \\ H^{k+1}_{i+1,j} \\ \vdots \\ H^{k+1}_{i-1,j+1} \\ H^{k+1}_{i,j+1} \\ H^{k+1}_{i+1,j+1}
\end{pmatrix}
$$

$$
=
\begin{pmatrix}
M & N & & O & & & & & & & \\
L & M & N & & O & & & & & & \\
 & L & M & N & & O & & & & & \\
 & & \ddots & \ddots & \ddots & & \ddots & & & & \\
K & & & L & M & N & & O & & & \\
 & K & & & L & M & N & & O & & \\
 & & K & & & L & M & N & & O & \\
 & & & \ddots & & & \ddots & \ddots & \ddots & & \\
 & & & & K & & & L & M & N & \\
 & & & & & K & & & L & M & N \\
 & & & & & & K & & & L & M
\end{pmatrix}
\cdot
\begin{pmatrix}
H^{k}_{i-1,j-1} \\ H^{k}_{i,j-1} \\ H^{k}_{i+1,j} \\ \vdots \\ H^{k}_{i-1,j} \\ H^{k}_{i,j} \\ H^{k}_{i+1,j} \\ \vdots \\ H^{k}_{i-1,j+1} \\ H^{k}_{i,j+1} \\ H^{k}_{i+1,j+1}
\end{pmatrix}
$$

$$
+\frac{\Delta_t}{2}
\begin{pmatrix}
b^k_{i-1,j-1} & + & b^{k+1}_{i-1,j-1} \\
b^k_{i,j-1} & + & b^{k+1}_{i,j-1} \\
b^k_{i+1,j-1} & + & b^{k+1}_{i+1,j-1} \\
 & \vdots & \\
b^k_{i-1,j} & + & b^{k+1}_{i-1,j} \\
b^k_{i,j} & + & b^{k+1}_{i,j} \\
b^k_{i+1,j} & + & b^{k+1}_{i+1,j} \\
 & \vdots & \\
b^k_{i-1,j+1} & + & b^{k+1}_{i-1,j+1} \\
b^k_{i,j+1} & + & b^{k+1}_{i,j+1} \\
b^k_{i+1,j+1} & + & b^{k+1}_{i+1,j+1}
\end{pmatrix}
\tag{2.37}
$$

In a more compact form (a double line indicates a matrix):

$$\underline{\underline{\mathbf{P}}}\,\mathbf{H}^{k+1} = \underline{\underline{\mathbf{Q}}}\,\mathbf{H}^{k} + \frac{\Delta_t}{2}(\mathbf{b}^{k+1} + \mathbf{b}^{k}) \tag{2.38}$$

It is now possible to solve for the ice thickness at all the grid points at the next time step, $k+1$, by inverting the matrix, $\underline{\underline{\mathbf{P}}}$, on the left hand side. This is not as straightforward as it may seem because all the elements in this matrix depend on values of the ice thickness at the time $k+1$ which are what we are about calculate. This is solved by the use of the following iteration scheme.

2.5.1 The Iteration Scheme

To solve the system of non-linear equations for the ice thickness at the time step $k+1$ it is necessary to use an iteration scheme due to the dependence of the solution on values not yet calculated. In this model Picard iteration also known as fixed point iteration is applied to find the solution to Eq. (2.39):

$$\mathbf{H}^{k+1} = \phi(\mathbf{H}^{k+1}), \tag{2.39}$$

$$\phi(\mathbf{H}^{k+1}) = \underline{\underline{\mathbf{P}}}^{-1}(\underline{\underline{\mathbf{Q}}}\,\mathbf{H}^{k} + \frac{\Delta_t}{2}(\mathbf{b}^{k+1} + \mathbf{b}^{k})) \tag{2.40}$$

Remembering that $\underline{\underline{\mathbf{P}}}$ depends on $\mathbf{H}^{k+1}$. The model iterates in the following way (n denotes the iteration number): $\mathbf{H}_{n+1}^{k+1} = \phi(\mathbf{H}_{n}^{k+1})$. The iteration stops when: $|\mathbf{H}_{n+1}^{k+1} - \mathbf{H}_{n}^{k+1}| < \epsilon$; if the sequence $\{\mathbf{H}_{n}^{k+1}\}$ converges and this criterion holds the desired accuracy is reached. Other iteration methods exist eg. Newton-Raphson which generally converges faster than Picard iteration, but Picard iteration is very easy to implement and during model runs one or two iterations are sufficient to improve the solution and reach a desired accuracy. The Picard iteration scheme is therefore chosen.

To start the iteration a 'guess' for the ice thickness at the next time step is made by taking an explicit time step. In explicit time discretization the new state of the system is calculated solely using the current state in which all parameters are known:

$$\frac{\partial H}{\partial t} = \frac{H_{i,j}^{k+1} + H_{i,j}^{k}}{\Delta_t} = \Theta_{i,j}^{k}$$

It is a less precise method and much more unstable for larger time steps than the Crank-Nicolson method [*Press et al.*, 2003, p. 838]. Using the explicit guess for the ice thickness vector at the next time step to calculate the values of $\{A, B, C, D, E\}$ we take an implicit time step to calculate the ice thickness vector once again. This ice thickness vector is compared to the ice thickness vector used to calculate $\{A, B, C, D, E\}$. If the difference between the two vectors is 'small enough' the newly calculated ice thickness is accepted; otherwise iteration is continued using the last ice thickness vector as input in $\{A, B, C, D, E\}$ until it is possible to accept [*Eldén and Wittmeyer-Koch*, 2001].

2.5.2 Performing the Calculation

To increase computational speed the number of computations must decrease. As is indicated in Eq. (2.37) the matrices in the calculation are band matrices meaning that only a few diagonals are non-zero. If the indices of the non-zero entries are known it is not necessary to store the complete matrix; only these specific entries must be kept. The first advantage is using less memory; in this way it is possible to work with very large matrices normally using large amounts of memory. The second advantage is when keeping track of the non-zero entries in a matrix multiplication with a vector like in Eq. (2.37) all calculations involving a zero-entry can be skipped and computation time saved. This is implemented in the model using storage and multiplication routines from *Press et al.* [2003](p. 44-46).

When working with large sets of linearized equations round-off errors accumulate when performing calculations as described in *Press et al.* [2003]. As a result the ice thickness, $\mathbf{H}$, is only known with some error, $\delta\mathbf{H}$. In the present case: Outcome $= \mathbf{H} + \delta\mathbf{H}$. It is possible to solve for $\delta\mathbf{H}$ quite easily and improve the solution using a routine from *Press et al.* [2003](see p. 47). This is called iterative improvement because this calculation can be performed a number times depending on how far the outcome is from the real solution. In the model it is done once which should be sufficient for most purposes.

2.6 The Mass Balance Model

The field work resulted in a mass balance parametrization for Hans Tausen Iskappe developed by Reeh et al *Reeh et al.* [2001] using the degree day

approach described in *Reeh* [1989 (1991]. This is the choice of mass balance model in this study.

2.6.1 The Degree Day Model

This degree day model uses the mean annual and mean July temperature as input to calculate the ablation. The surface melt rate, of course, depends on the surface energy balance and the physical approach would be to calculate each of the energy fluxes. In a degree day model, however, only air temperatures are needed making it simpler. Its great advantages is that it uses the best-known meteorological parameter as input and it is computationally cheap [*Van De Wal*, 1996]

The annual temperature cycle is approximated by a cosine function and it is thus assumed that the winter and summer seasons have the same lengths and that the difference between mean annual temperature and summer maximum is the same as winter minimum:

$$TCA = TMA + (TMJ - TMA)\ \cos(\frac{2\pi t}{P})$$

TCA is the annual temperature cycle, TMA and TMJ denotes mean annual and mean July temperatures, t is time and P one year. If the temperature on a given day is 2°C it would be counted as 2 positive degree days (PDD). Counting PDD using only the annual temperature cycle poses a problem: The mean temperature of a given month may be below zero resulting wrongly in zero PDD since the daily cycle and random fluctuations can result in air temperatures above zero. To account for this a stochastic term which is normally distributed around the curve of the TCA is introduced in the calculation. The probability of the temperature T in the small interval dT centered around T is then:

$$p = \frac{1}{s\sqrt{2\pi}} \exp(-\frac{(T - TCA)^2}{2s^2})dT$$

s denotes the standard deviation. The corresponding PDD contribution from this temperature T in the time span dt is then:

$$T\ dt\ p = T\Big\{\frac{dt}{s\sqrt{2\pi}} \exp(-\frac{(T - TCA)^2}{2s^2})\Big\}dT$$

To find the total number of PDD the expression is integrated over all positive temperatures and over the whole annual cycle:

$$PDD = \int_0^\infty T\Big\{\int_0^A \frac{1}{s\sqrt{2\pi}} \exp(-\frac{(T - TCA)^2}{2s^2})\ dt\Big\}dT \qquad (2.41)$$

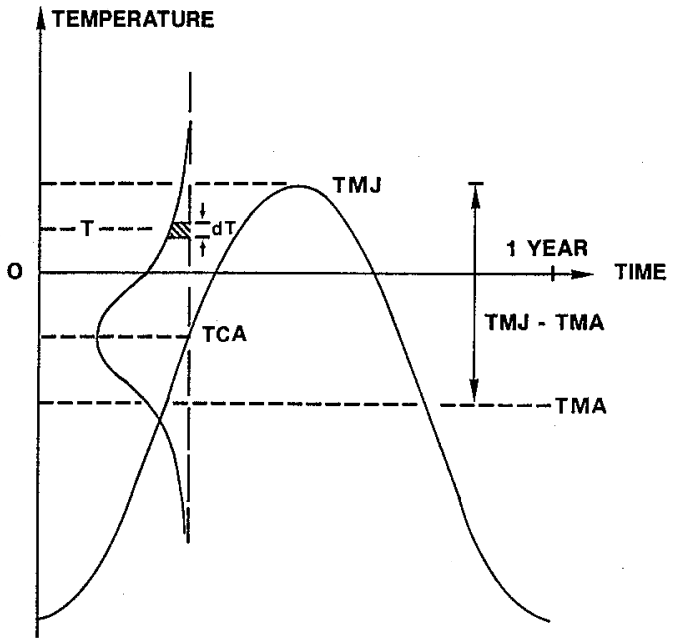

Figure 2.5: *Illustration of the temperature variation used in the degree day model to calculate the number of PDD over a year. Figure from Reeh [1989 (1991] p. 118*

Fig. 2.5 illustrates the PDD calculation.The number of PDD is used to melt snow and ice using different degree day factors for snow, f_{snow}, and ice melt, f_{ice}, in the following way:

1. Snow (if present) is melted using the degree day factor for snow. No run-off occurs before a given fraction P_{max} of the accumulation is melted. This melt water is assumed to percolate into the snow cover and refreeze as superimposed ice.

2. The superimposed ice is melted using the degree day factor for ice.

3. Glacier ice is melted using the degree day factor for ice.

In this model $f_{snow} = 0.0027$ $^{\mathrm{m_{ice}}}/_{\mathrm{PDD}}$, $f_{ice} = 0.0065$ $^{\mathrm{m_{ice}}}/_{\mathrm{PDD}}$, $P_{max} = 0.6$ and $s = 3$ in accordance with *Reeh et al.* [2001]. It is assumed that all precipitation comes in the form of snow, which is not always true.

2.6.2 Programming the Degree Day Model

In order to save computation time the double integral in Eq. (2.41)is not solved for each time step at each grid point. A table was created containing the number of PDD corresponding to a set of the two input parameters: The mean annual and mean July temperature. When the mass balance is updated in the model the temperatures at each grid point are calculated and used to interpolate in the table using bilinear interpolation to find the corresponding number of positive degree days.

To test the method the mass balance corresponding to the present surface of the ice cap was calculated using both the double integral and the look-up table. For a table with a discretization of 0.1 ^{o}C there are only 0.6 % of the grid points that differ by more than 1% when compared to values obtained using the double integral in the same grid points. The mass balance at these points is of the order of millimeters meaning that the method gives results that are precise enough to be used in the model. The maximum difference in mass balance between the to methods is $8.0 \cdot 10^{-5}$ m/yr.

One update of the mass balance takes $7.4 \cdot 10^{-2}$ s which is very fast compared to performing a double integral at each grid point. It is therefore possible to update the mass balance at every time step: At the time step k the mass balance is calculated after the explicit guess for H^{k+1} using H^k and stored in b^{k+1}. The mass balance used for the time step $k+1$ is actually the one corresponding to k, but this is done instead of updating the mass balance at each iteration. Since the time step is $1/4$ yr this error is very small.

In some places a negative mass balance may exceed the amount of ice present and the new calculated ice thickness becomes negative. This is of course not physical and the negative ice surfaces are raised to zero elevation after each time step.

2.7 Model Overview

The overall structure of the model is shown Fig. 2.6. There are some important things which should be noted:

The SIA cannot deal with the dynamics of floating glacier tongues. I have therefore chosen to make the model hydrophobic, meaning that whenever ice starts to flow into the fjords it is removed. This is not physically correct but

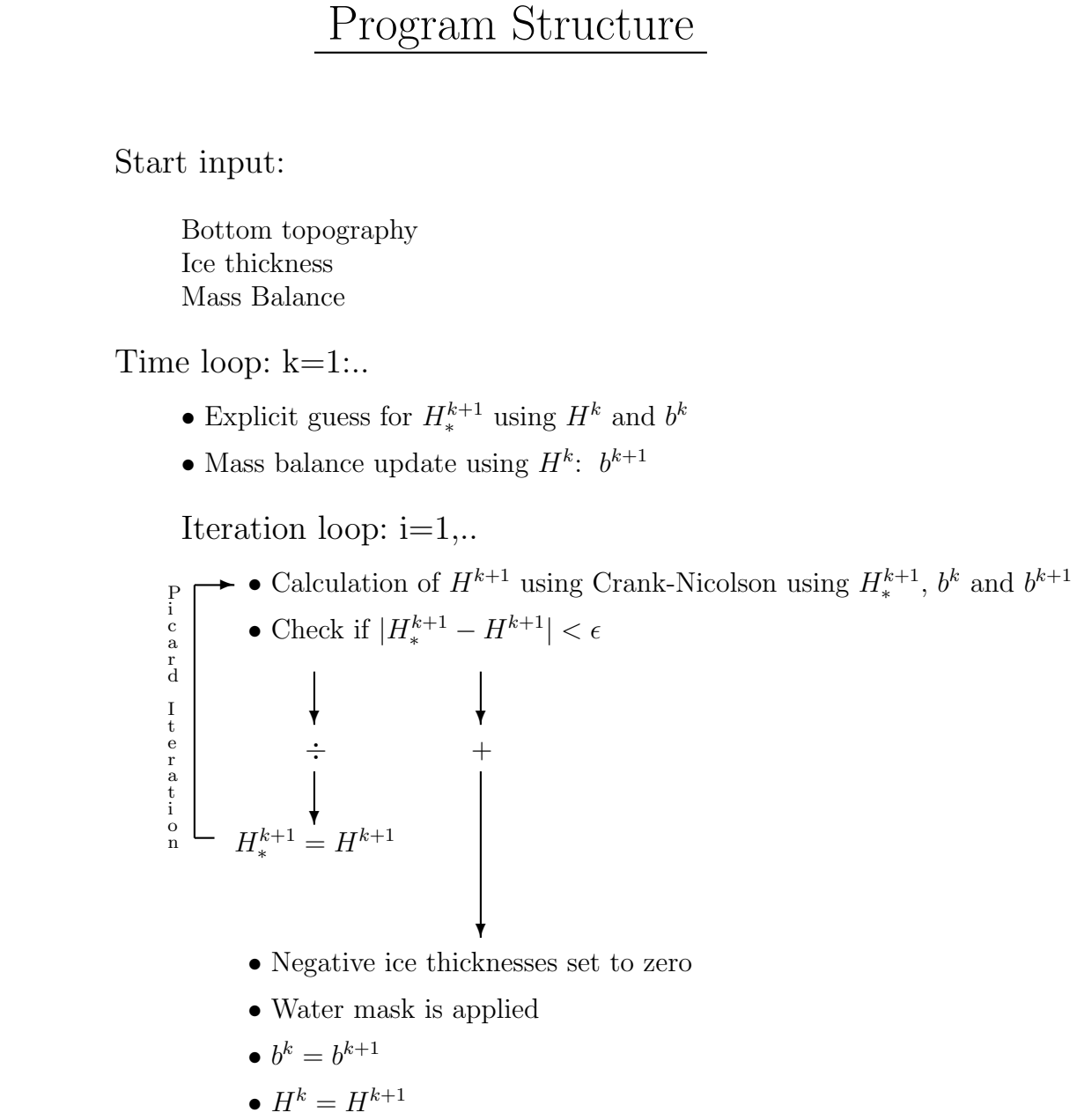

Figure 2.6: *The program structure.*

the necessary physics is not incorporated in the model.

It should also be noted that the model does not account for isostatic uplift and depression. The elevation of the bedrock changes trying to restore isostatic equilibrium as the load of ice on top changes when the ice cap grows or decays. As will be discussed in Section 4.4 this will not greatly influence the result because bedrock changes in the region are small.

Chapter 3

Model validation

3.1 Comparison with the EISMINT Benchmark Tests

An invaluable way to test an ice flow model of the present type is to compare it with the EISMINT benchmark tests *Huybrechts and Payne* [1996]. A part of EISMINT (European Ice Sheet Modelling INiTiative) was the intercomparison between ice flow models at the time organized in order to investigate how well parameters like ice thickness and flux were simulated and to asses the most precise and efficient numerical technique. The level I experiments aimed at defining benchmarks for vertically integrated models based on the SIA using two simple tests and the consensus solutions were reported in *Huybrechts and Payne* [1996]. At this level all boundary conditions and pa-

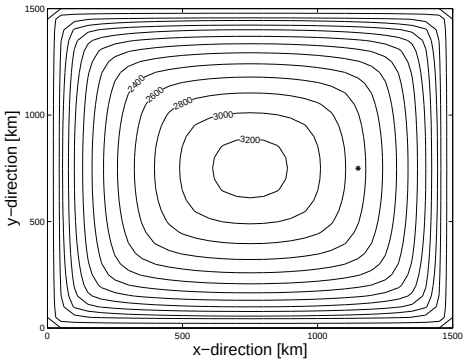

Figure 3.1: *Fixed margin experiment. Contour lines indicate ice thickness. The black star indicates the point where the 'flux at the mid point' is evaluated.*

rameters used in the model are prescribed. Therefore, it can be used as a debugging tool and is a good way to validate models like the present one. I have repeated the tests and compared with the consensus solutions reported in *Huybrechts and Payne* [1996].

3.1.1 The Experiments

Each test consists of a run to steady state and two time dependent runs. All runs are performed using a uniform grid having 31 grid points in each direction with a grid size of 50 km and flat bedrock topography at zero elevation. In 'The Fixed Margin' experiment the ice sheet is artificially bound by the size of the domain and attains a square shape (see Fig. 3.1). The mass balance is constant:

$$M = 0.3 \ \frac{\mathrm{m}}{\mathrm{yr}}$$

and the ice thickness at the boundary is set to zero. In the second experiment, 'The Moving Margin' experiment, the mass balance is a function of distance, d, from the domain center:

$$M = \min\{\frac{1}{2}, g(R_{el} - d)\} \ \frac{\mathrm{m}}{\mathrm{yr}}$$

where:

$$d = \sqrt{(x - x_{\mathrm{summit}})^2 + (y - y_{\mathrm{summit}})^2}$$

$R_{el} = 450$ km and the slope, g, is set to 10^{-2} $^{\mathrm{m_{ice}}}/_{(\mathrm{yr}\cdot\mathrm{km})}$. This experiment investigates how well the model simulates the position of the margin (See Fig. 3.2).

All experiments are run for 200 ka years. The time dependent behavior is investigated using two different periods, $\mathbb{T}$, of 20 ka and 40 ka for the sinusoidal varying climatic boundary conditions. These are for the fixed margin and moving margin experiments respectively:

$$\begin{aligned} M &= 0.3 + 0.2 \cdot \sin\frac{2\pi t}{\mathbb{T}} \quad [\frac{\mathrm{m}}{\mathrm{yr}}] \\ R_{el} &= 450 + 100 \cdot \sin\frac{2\pi t}{\mathbb{T}} \quad [\mathrm{km}] \end{aligned}$$

The present model performs no temperature calculations and therefore it is not necessary to do velocity calculations. I have therefore only compared

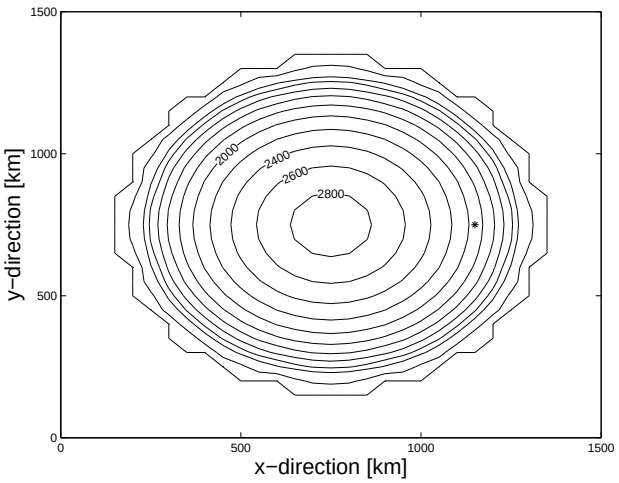

Figure 3.2: *Moving margin experiment. Contour lines indicate ice thickness. The black star indicates the point where the 'flux at the mid point' is evaluated.*

values of the ice thickness and the flux. The results of the runs to steady state for both experiments are shown in Fig. 3.3 and 3.4. The flux is evaluated at the midpoint between the ice divide and the domain margin at the grid point (24,16) indicated by a black star in Figs. 3.1 and 3.2.

3.1.2 Results of the Comparison

Plots of the ice sheet profile and flux for the steady state test of each experiment are displayed in Fig. 3.3 and 3.4. It is sufficient to display only the cross section going from the center of the ice sheet to the right hand margin because of the symmetry. Tables 3.1 and 3.2 show the results of the ice thickness at the divide and flux at the midpoint, defined as the grid point (24,16). The tables show that for the steady state tests the simulated ice thickness at the divide for both experiments and flux at the midpoint for the moving margin experiment lie within the bounds of the consensus results from the EISMINT benchmarks. The mid point flux of the fixed margin experiment is $53^{\mathrm{m}^2}/_{\mathrm{s}}$ from the lower range. The shape of the flux curves, though, does not resemble the type II flux plot in *Huybrechts and Payne* [1996], but more the type I plot. Since this is the case for both types of experiments it not a result of the boundary conditions but must be due to the discretization.

The results of the time dependent experiments are plotted in Fig. 3.5 and 3.6 and Tabels 3.1 and 3.2 show results for the range in ice thickness and flux for

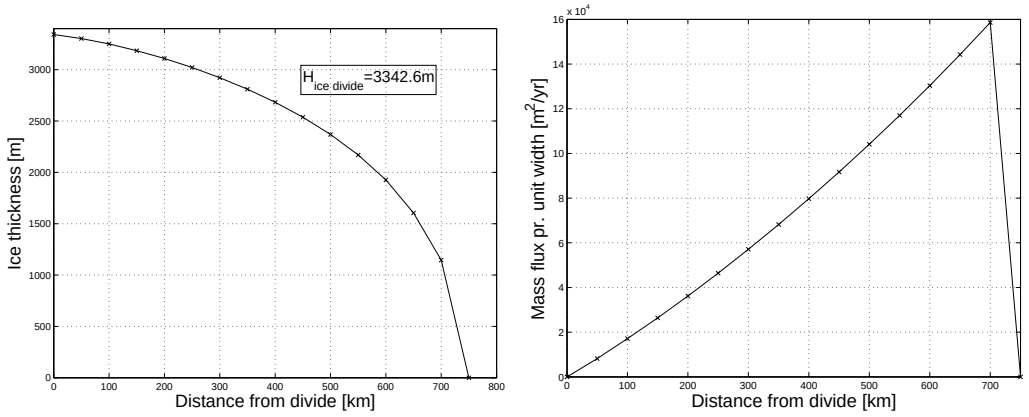

Figure 3.3: *Fixed margin experiment (runs to steady state): The **left** hand figure shows the ice sheet profile and the **right** hand figure shows flux as a function of distance from the ice divide.*

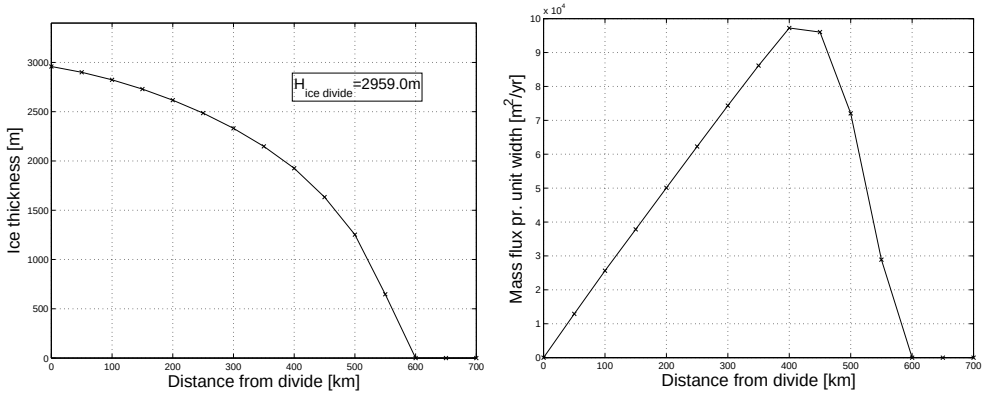

Figure 3.4: *Moving margin experiment (runs to steady state): The **left** hand figure shows the ice sheet profile and the **right** hand figure shows flux as a function of distance from the ice divide.*

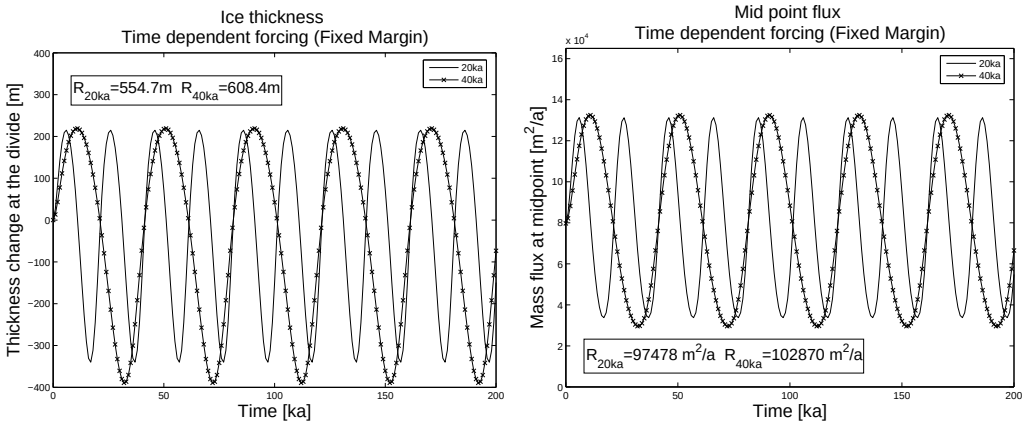

Figure 3.5: *Fixed margin expriment forced by sinussoidal changes in boundary conditions.* ***Left:*** *The deviation from the steady state ice thickness.* ***Right:*** *The change in the flux at the mid point with time. R is defined as the peak-to-peak amplitude of the last oscillation. The values of R for the ice thickness and the* 20 ka *run for the flux lie within the bounds of the uncertainty of the EISMINT experiments, while the value for the* 40 ka *run is* 180 $\frac{\mathrm{m}^2}{\mathrm{s}}$ *too low.*

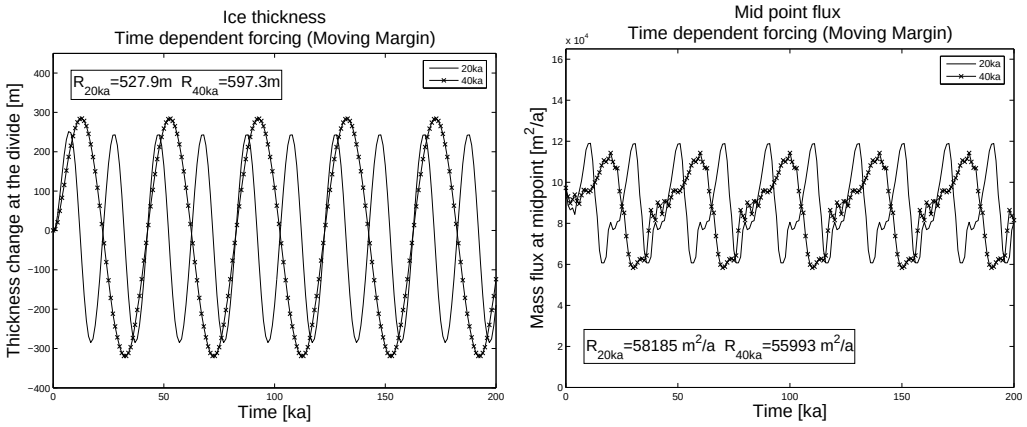

Figure 3.6: *Moving margin experiment forced by sinusoidal changes in boundary conditions.* ***Left:*** *The deviation from the steady state ice thickness. Right: The change in the flux at the mid point with time.* ***Right:*** *The change in the flux at the mid point with time. R is defined as the peak-to-peak amplitude of the last oscillation. For the ice thickness the value of R for the* 20 ka *lies within the standard deviation of the EISMINT experiments while the for the* 40 ka *run the value exceeds the uncertainty by* 0.3 m. *The value of R for the flux for the* 20 ka *run exceeds the uncertainty by* 2344 m^2/s *and for the* 40 ka *run by* 3080 m^2/s *too low.*

Fixed Margin		Hans Tausen Model	EISMINT (Type II)
Steady State	$H_{\text{ice divide}}$	3342.6 m	3342.6 ± 0.4 m
	$\text{Flux}_{\text{mid point}}$	79719 $^{m^2}/_{yr}$	80004 ± 232 $^{m^2}/_{yr}$
T = 20 ka	$H_{\text{at 200 ka}}$	3193.06 m	3195.3 ± 2.6 m
	Range_{H}	554.7 m	556.0 ± 3.5 m
	$\text{Range}_{\text{flux}}$	97478 $^{m^2}/_{yr}$	97980 ± 621 $^{m^2}/_{yr}$
T = 40 ka	$H_{\text{at 200 ka}}$	3269.25 m	3271.4 ± 3.21 m
	Range_{H}	608.4 m	609.0 ± 1.9 m
	$\text{Range}_{\text{flux}}$	102870 $^{m^2}/_{yr}$	103311 ± 261 $^{m^2}/_{yr}$

Table 3.1: *Results from the fixed margin experiment. H is the thickness at the ice divide,* $\text{Flux}_{\text{mid point}}$ *is the flux at the point (24,16) and range is defined as the peak-to-peak amplitude of the last oscillation in the time dependent tests.*

Moving Margin		Hans Tausen Model	EISMINT (Type II)
Steady State	$H_{\text{ice divide}}$	2959.0 m	2958.9 ± 1.3 m
	$\text{Flux}_{\text{mid point}}$	97256 $^{m^2}/_{yr}$	99945 ± 3037 $^{m^2}/_{yr}$
T = 20 ka	$H_{\text{at 200 ka}}$	2769.4 m	2775.7 ± 10.6 m
	Range_{H}	527.9 m	528.5 ± 5.3 m
	$\text{Range}_{\text{flux}}$	58185 $^{m^2}/_{yr}$	54753 ± 1035 $^{m^2}/_{yr}$
T = 40 ka	$H_{\text{at 200 ka}}$	2834.96 m	2846.0 ± 18.6 m
	Range_{H}	597.34 m	599.9 ± 3.1 m
	$\text{Range}_{\text{flux}}$	55993 $^{m^2}/_{yr}$	52221 ± 697 $^{m^2}/_{yr}$

Table 3.2: *Results from the moving margin experiment. H is the thickness at the ice divide,* $\text{Flux}_{\text{mid point}}$ *is the flux at the point (24,16) and range is defined as the peak-to-peak amplitude of the last oscillation in the time dependent tests.*

each experiment. The position of the margin in the time dependent tests of the moving margin experiment is shown in Fig. 3.7. The several maxima and minima displayed by the flux plots correspond to periods where the position of the margin changes [*Huybrechts and Payne*, 1996]. All the plots resemble those of the EISMINT. The tables show that for the fixed margin experiment only the range in flux for the 40 ka test is not within the benchmark range. It lies 180 $^{m^2}/_{s}$ from the lower range. For the moving margin experiments the height ranges are within the EISMINT bounds but both flux ranges are too large. The 20 ka test is 2397 $^{m^2}/_{s}$ above the given range and the 40 ka test is 3075 $^{m^2}/_{s}$ above.

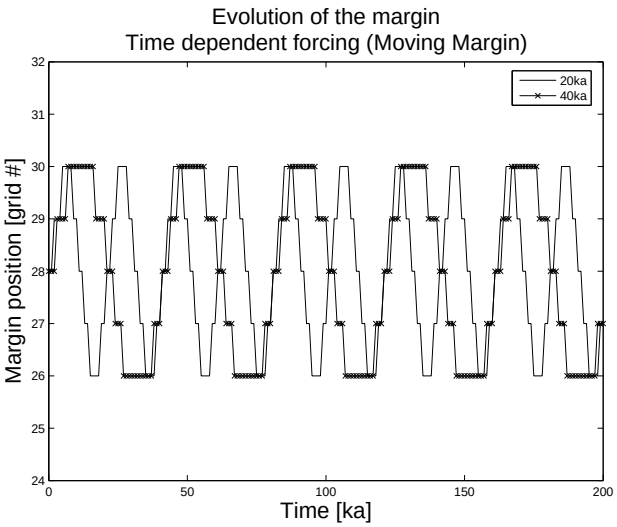

Figure 3.7: *Moving margin experiment forced by sinusoidal changes in boundary conditions. The position of the ice margin.*

Despite some discrepancies the results are very similar to the EISMINT benchmarks. The differences must be due to the discretization method.

3.2 Conservation of mass

In order to verify that the model is mass conserving a check is done using a random model run. At all time steps the change in ice thickness in a certain grid point must be equal the mass balance minus the divergence of the flux. As explained in Section 2.4 the equation is discretized in time using a crank-nicolson method (see Eq. (2.33)) and therefore the equation to be satisfied is:

$$\frac{\partial H}{\partial t} = \frac{\Theta_{i,j}^{k+1} + \Theta_{i,j}^{k}}{2} = \frac{1}{2}\Big(- (\nabla \cdot \mathbf{q})_{i,j}^{k+1} + b_{i,j}^{k+1} - (\nabla \cdot \mathbf{q})_{i,j}^{k} + b_{i,j}^{k}\Big) \qquad (3.1)$$

Table 3.2 shows that $\sum \frac{\partial H_{i,j}}{\partial t} + \sum \frac{1}{2}(\nabla \cdot \mathbf{q}_{i,j}^{k+1} + \nabla \cdot \mathbf{q}_{i,j}^{k}) - \sum \frac{1}{2}(b_{i,j}^{k+1} + b_{i,j}^{k}) = 0$ verifying that no mass is lost or produced during the calculations. The model is thus mass conserving. This check has to be done before raising the ice thickness to zero at grid points where the thickness becomes negative as result of the ablation exceeding the sum of the accumulation and the ice thickness.

Number of grid points	11766
$\sum \frac{\partial H}{\partial t}_{i,j}$	-11163
$\sum \frac{1}{2}(\nabla \cdot \mathbf{q}_{i,j}^{k+1} + \nabla \cdot \mathbf{q}_{i,j}^{k})$	$6.9865 \cdot 10^{-10}$
$\sum \frac{1}{2}(b_{i,j}^{k+1} + b_{i,j}^{k})$	-11163
$\sum(\frac{\partial H}{\partial t}_{i,j} + \mathbf{q}_{i,j} - b_{i,j})$	$-9.0156 \cdot 10^{-9}$

Table 3.3: *Test of mass conservation for the Hans Tausen model. These calculations are done before the ice surface is set to zero where it is negative. As the table shows the model is mass conserving.*

However, the discretization method used has a build-in potential mass conservation error (see *Adalgeirsdottir* [2003] for a thorough analysis). Fig. 3.8 shows an example with a nunatak of how the flux out of a point with no ice can be larger than zero. The flux is calculated at the staggered grid points using the mean of the diffusion and the ice thickness on either side and therefore the flux at $i - \frac{1}{2}$ is non-zero. This leads to $\nabla \cdot \mathbf{q}$ being non-zero at the grid point $i - 1$ and therefore mass flows out from the point even though the ice thickness is zero (see Eq. (2.29) - (2.32)). The value of the ice thickness becomes negative and will need to be raised back to zero at each time step. In *Adalgeirsdottir* [2003] it is described how an upstream method for Type I descretizations can solve the problem. In this study of Hans Tausen Iskappe a smoothed bottom topography is used in order to avoid large gradients and therefore potential nunataks are removed. A check has been done at different time steps during a build up of the ice cap and the problem does not arise at any of them. In runs started with the current ice cap profile there are no nunataks.

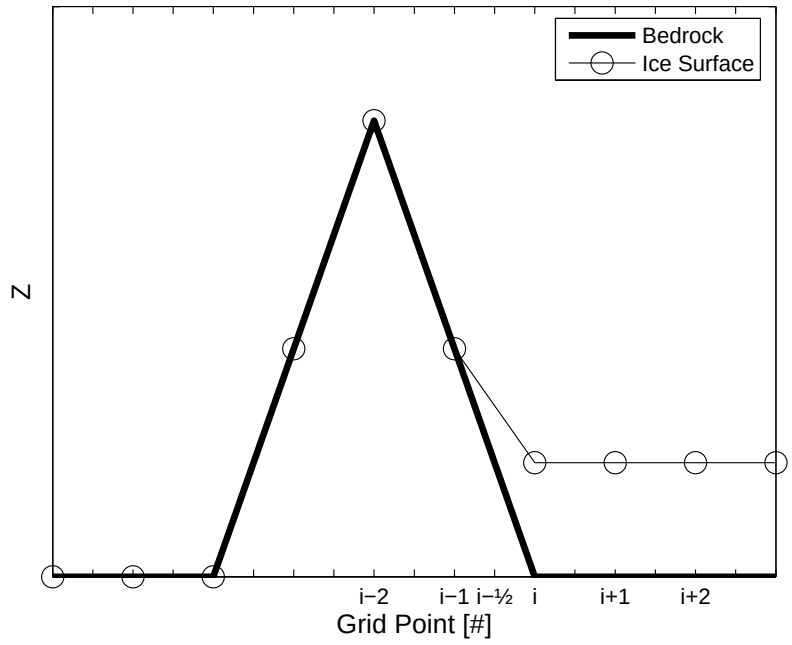

Figure 3.8: *Plot illustrating how ice free points can lead to mass conservation errors The ice thickness is represented by circles.*

Chapter 4

Applying the model to Hans Tausen Iskappe

This chapter describes how the model is set up to investigate the evolution of Hans Tausen Iskappe and presents the digital elevation models and the parameterizations of accumulation and temperature used as input to the model.

4.1 Digital Elevation Models

The input data sets of bedrock topography and ice thickness are the digital elevation models created by and described in *Starzer and Reeh* [2001] as part of the Hans Tausen project. These digital elevation models (DEMs) which also include one for surface topography are based on data from:

- Surface topography data from aerial photographs from 1978
- An airborne radar survey of surface elevation and ice thickness over the central parts in 1993
- Ground radar surveys of surface elevation and ice thickness in 1994 around the central dome and the northeastern part of the ice cap.
- Where no other data existed surface elevation data from a DEM covering the entire Greenland produced by the National Survey and Cadastre of Denmark was applied.

The DEMs are based on a grid of UTM coordinates and stretches from 535000 to 640000 in the West to East direction and from 9120000 to 9230000 in South to North direction in UTM-zone 23. The data are interpolated on to a grid of

500x500 m. Figures 4.1 to 4.3 show contour plots of the surface topography, the ice thickness and the subglacial topography respectively.

4.2 Customizing the DEMs

An important factor when investigating the evolution of an ice cap over large time spans is the computational time used. In order to bring it down I found it necessary to reduce the resolution by interpolating the data by linear interpolation onto a coarser grid with a grid size of 1000x1000 m reducing the number of grid points from 46631 (221x211) to 11766 (111x106).

In the ice flow model the flow is determined by local ice thickness and slope alone ignoring effects exerted by longitudinal stress gradients. Studies of glacier flow by comparison of the observed flow with the local slope show large discrepancies [*Kamb and Echelmeyer*, 1986]. The effective slope needed to explain observations vary much less. This is due to the longitudinal coupling exerted by the longitudinal stress gradients modifying flow at each point from what it would be if determined by local slope and ice thickness. To account for the longitudinal coupling *Kamb and Echelmeyer* [1986] suggest averaging of the ice thickness and slope using a symmetrical triangular averaging window of length $4l$. l is called the longitudinal coupling length and for ice sheets it has a value of 4 to 10 times the ice thickness. The triangular averaging window ensures that the influence of perturbations drop off with distance.

In the present case the smoothing is performed by weighing the value of each data point in the area used to calculate the new value in a certain grid point according to a gaussian distribution. The smoothing is applied over an area of $\sim$ 20 times the ice thickness in each direction. In this way the irregular shape of the ice cap and the steep mountain sides of the plateau are much better conserved. Use of a gaussian bell have the same characteristics as using the triangular averaging window. Contour plots of these smoothed and reduced data sets used as input are displayed in Figs. 4.4 and 4.5.

The effect of these modifications is clearly reflected in the time it takes to do one time step of $\frac{1}{4}$ year: Using the original data set ten time steps takes 72.3 min, while using the original but smoothed data set the time is reduced to 21.7 min. Reducing the number of grid points further reduces the time to 0.12 min making it possible to test many different parameterizations of e.g. temperature and accumulation.

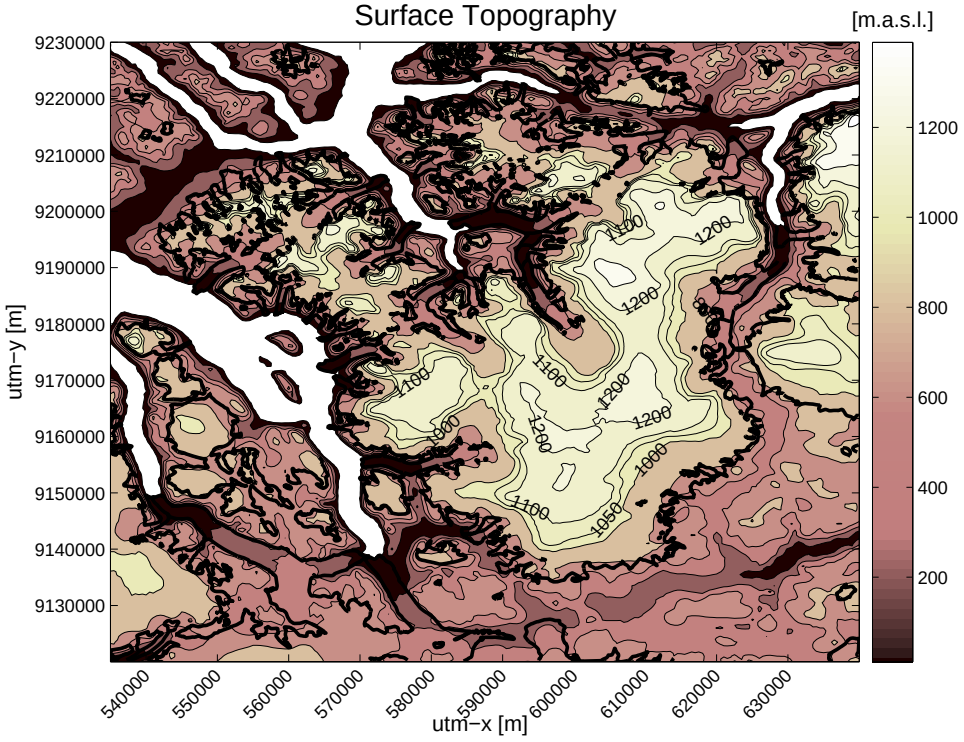

Figure 4.1: *Plot of the surface topography. An equidistance of* 100 m *is used. Data from the DEM described in Starzer and Reeh [2001])*

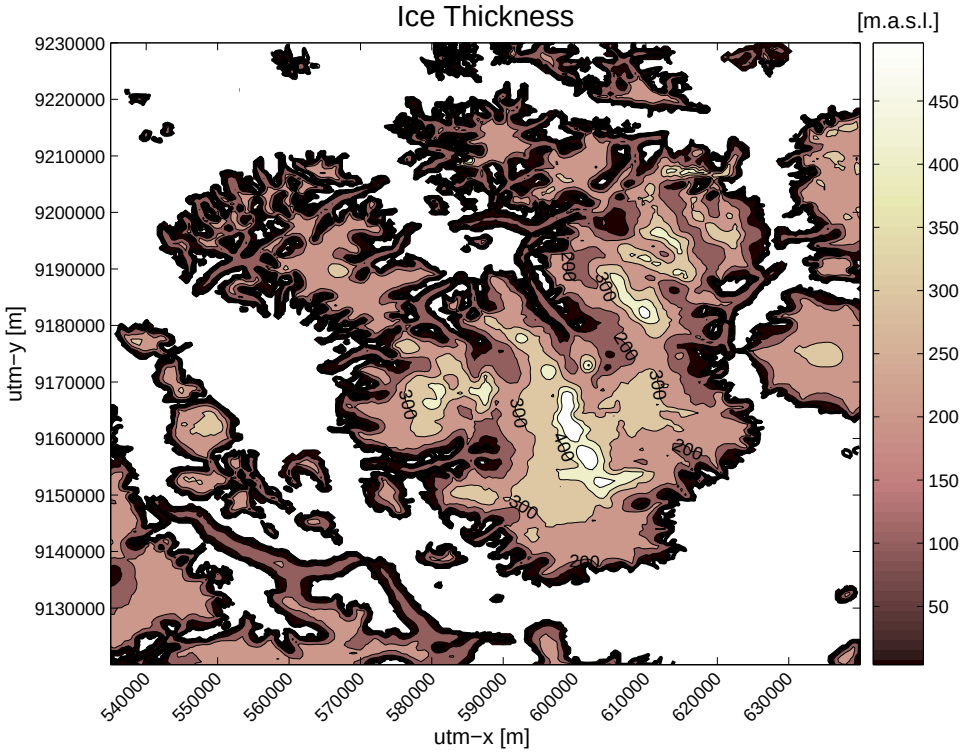

Figure 4.2: *Plot of the ice thickness. An equidistance of* 100 m *is used. Data from the DEM described in Starzer and Reeh [2001])*

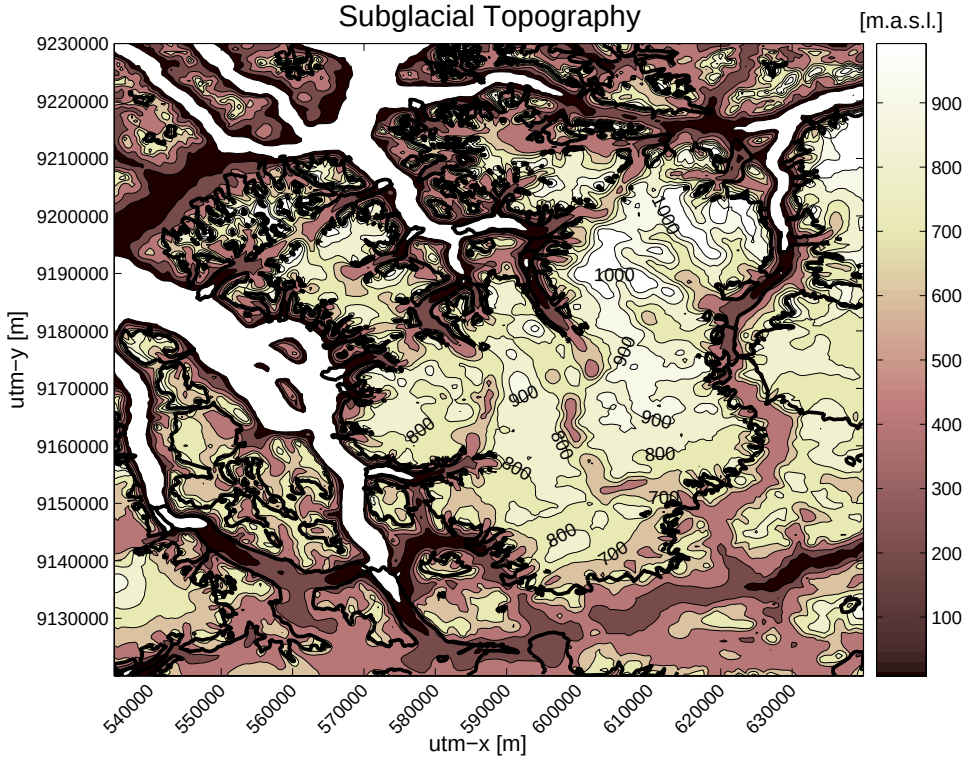

Figure 4.3: *Plot of the subglacial topography. An equidistance of* 100 m *is used. Data from the DEM described in Starzer and Reeh [2001])*

4.3 Parametrization of Accumulation and Temperature

During the summers of 1994 and 1995 mass balance measurements were performed along a flow line extending from the northern dome to the tip of the outflow glacier, Hare Glacier. See Fig. 1.2 for location of Hare Glacier. These measurements included stake readings and snow-pit studies and during the summer of 1995 the air temperature was measured at three of the stakes. These data along with data from the ice core drilled at the central dome and two firn/ice cores drilled in 1975 and 1976 in the southern part, have been used by *Reeh et al.* [2001] to parameterize accumulation and temperature to be used as input to the degree day model described in *Reeh* [1989 (1991] (see also Section 2.6):

The mean annual temperature was never measured on Hans Tausen Iskappe

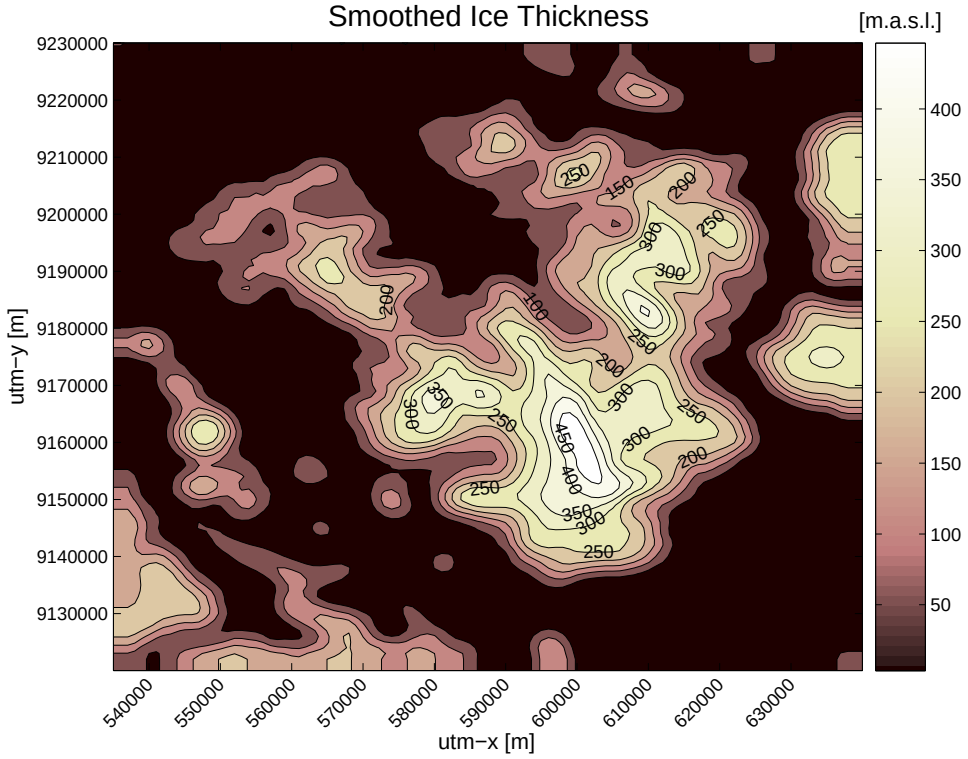

Figure 4.4: *Plot of the smoothed ice thickness. An equidistance of* 50 m *is used.*

so in order to make a parametrization annual temperature data measured at Kap Molkte 100 km South East of the ice cap together with gradients for elevation and latitude derived in *Reeh* [1989 (1991] was used. The parametrization of the mean annual temperature in [°C]:

$$TMA = \begin{cases} 46.8 - 0.751L & \text{for } E < 300m \\ 49.2 - 0.751L - 0.00792E & \text{for } E > 300m \end{cases} \tag{4.1}$$

E denotes the elevation above sea level and L the latitude. The inversion layer near the surface is parameterized by the constant temperature below an elevation of 300 m. The mean July temperature is parameterized using measurements from Hare Glacier and the latitude gradient derived using East Greenland weather stations by *Funder et al.* [1998]. The parametrization of mean July temperature in [°C]:

$$TMJ = 38.74 - 0.4L - 0.0056E \tag{4.2}$$

Data from the snow-pits and stakes together with data from two firn cores and the deep ice core was used to derive the spatial distribution of accumu-

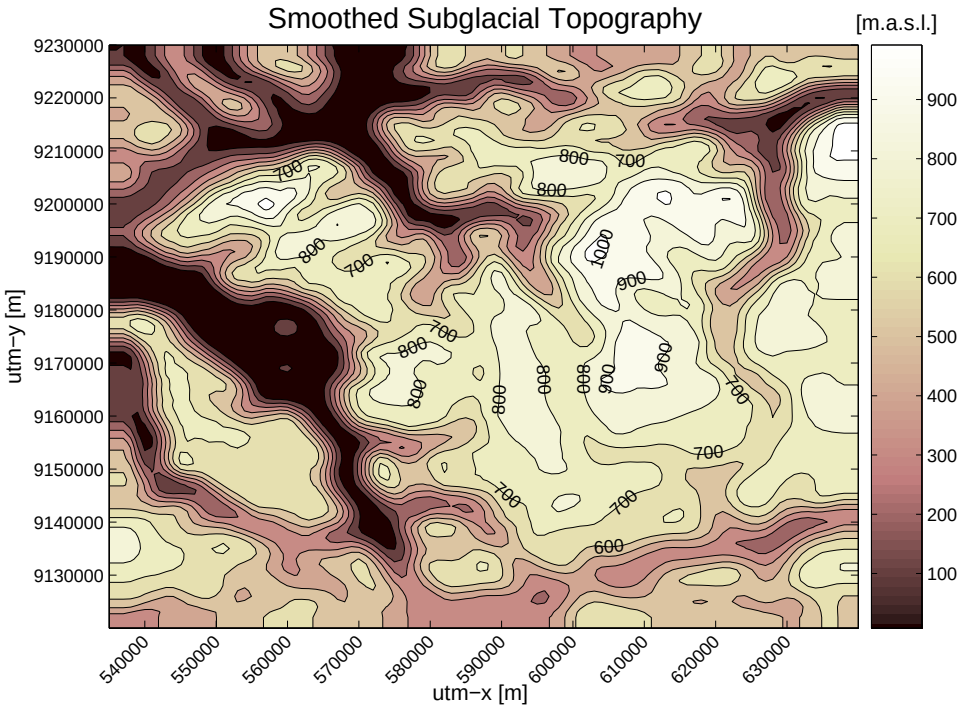

Figure 4.5: *Plot of the smoothed subglacial topography. An equidistance of* 100 m *is used.*

lation. Information from the main ice core and firn cores show that there is a difference in accumulation between the northern and southern part of the ice cap. According to the data from 1994 the mass balance on the northern part is much larger than on the southern part. *Reeh et al.* [2001] ascribes this to be an effect of the weather systems coming in from the north and delivering most of the precipitation here. The southern part lies on the lee side and receives less precipitation. Here the mass balance increases towards the margin maybe as an effect of the catabatic winds. This leads to the following parametrization of the accumulation $[\mathrm{m_{ice}/_{yr}}]$:

$$ACC = \begin{cases} 0.0036E + 0.989L - 81.93 & \text{for } L > 82.51^{o}N \\ -0.307L + 25.46 & \text{for } L > 82.51^{o}N \end{cases} \tag{4.3}$$

The latitudinal gradient between the northern dome and the Central Dome is based on measurements from the 1994 field work while the gradient for the southern part is calculated as the change in accumulation between the central dome and the two firn cores drilled in 1975 and 1976.

The large latitudinal gradient in Eq. (4.3) of 0.989 $^{m_{ice}}/_{L}$ is for the year 1994 where snow fall on Hans Tausen is found to excessive. Strain net observations at the northern dome point to a lower long term balance of ~ 0.25 $^{m_{ice}}/_{yr}$ compared to 0.425 $^{m_{ice}}/_{yr}$ in 1994 *Reeh et al.* [2001]. This suggests a smaller accumulation gradient north of the Central Dome. The effect of a smaller gradient is investigated in Chapter 7. Fig. 4.6 shows the mass balance for the year 1994.

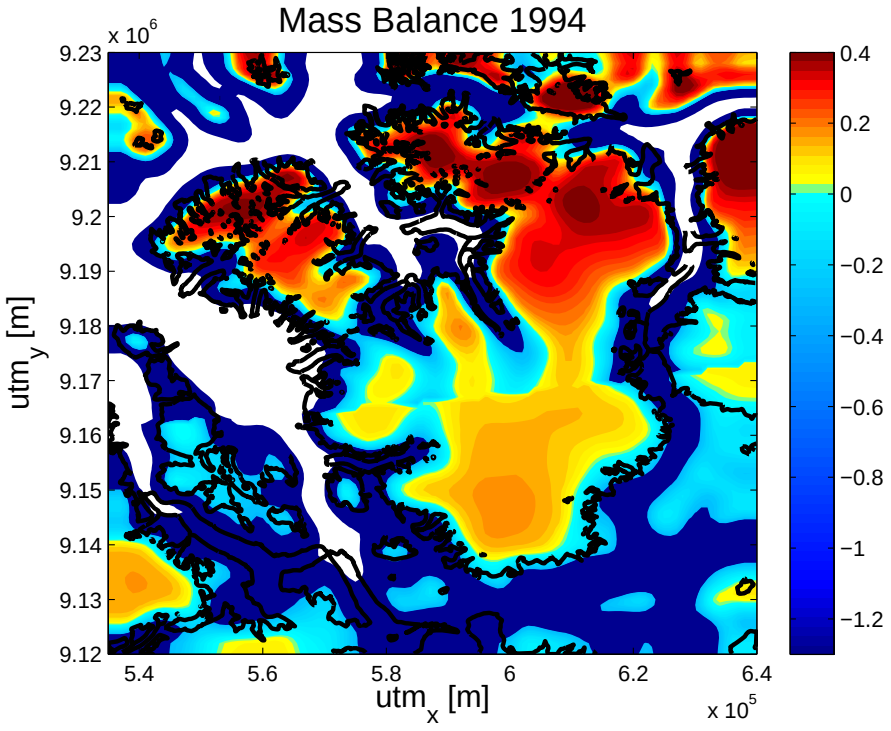

Figure 4.6: *Mass balance for the year 1994. The black outline indicates the ice margin. There is a discontinuity in the parametrization which can be seen in figure.*

4.4 Isostasy

Isostatic effects are not included in the model as they have no effect on the results for the time period and location investigated here. As the Greenland Ice Sheet retreated in response to the warmer climate of the Holocene the elevation of the bedrock started to rise trying to restore isostatic equilibrium. The changes in the marine limit for Jørgen Brønlund Fjord over the

last 8000 years are displayed in Fig. 4.7. This fjord is located to the east of Hans Tausen Iskappe and is displayed on Fig. A.3 in the appendix.

Changes in marine limit includes isostatic effects as well as real changes in sea level e.g. following the immense ice discharge in the beginning of the Holocene. As this happened before the rebuild-up of Hans Tausen it will not affect the emergence curves in Fig. 4.7. Smaller changes in ice volume has happened during Holocene. The small rise in marine limit in the late Holocene is probably caused by neoglacial growth of the ice masses during the Little Ice Age. Looking at the emergence curve a land rise of ~ 10 m has happened over the last 4000 years.

As the ice cap grows it exerts a local isostatic effect which should also be accounted for. *Madsen* [1997] investigated the timing of the build-up using a 1D ice flow model including isostatic effects. In the model an ice cap the size of Hans Tausen Iskappe causes a depression 25% of full isostatic depression amounting to $\frac{1}{12}H$ when equilibrium is obtained. This corresponds to a depression of the order of ~ 30 m. This combined with the overall land rise over the period amounts to a change in bedrock not influencing the results of the model runs. The fraction $\frac{1}{12}H$ is obtained assuming the density of the rock is three times that of ice.

4.5 Parameter values

As discussed above the modified input data is on a grid with a grid size of 1000 m. The grid has 111 points in North/South direction and 106 points in the East/West direction. The size of the time step is a compromise between speed and stability. I have found that for these runs a time step of $\frac{1}{4}$ year is the best choice. The value of the parameter, n, in Glen's Law (2.6) is 3 as mentioned in Section 2.1.3. The ice flow model does not include basal sliding. The ice temperature at the bottom of the ice at the Central Dome and on the outlet glacier Hare Glacier has been measured in both places to be below zero *Reeh* [1995]. The assumption therefore seems reasonable for Hans Tausen Iskappe.

4.5.1 The flow parameter A

The present ice flow model assumes the ice to be isothermal and therefore the value of A in the flow law is assumed constant. Other things influence the value as well, but are not accounted for. Borehole measurements of temper-

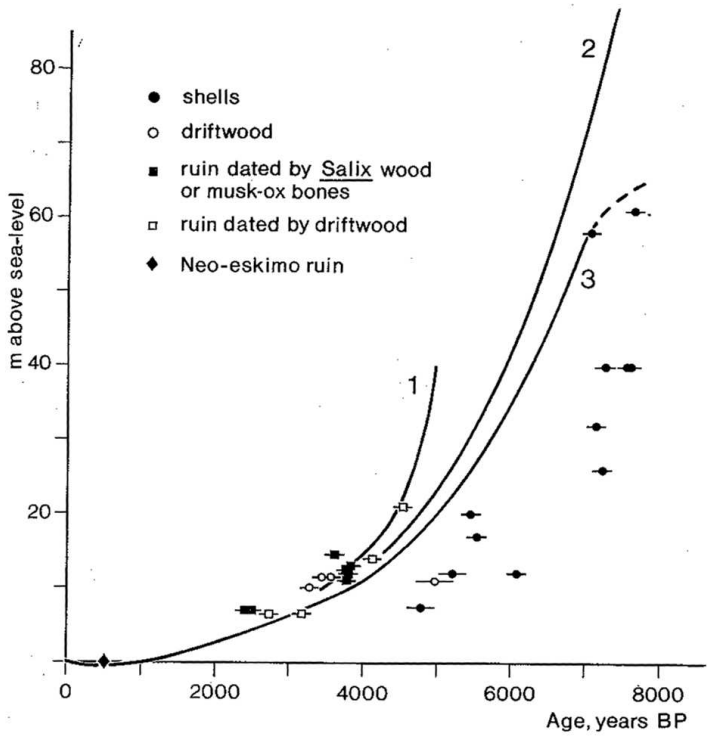

Figure 4.7: *Emergence curves from Jørgen Brønlund Fjord based on finds of e.g. shells and wood. [Bennike, 1987]*

ature at the Central Dome show that the temperature varies almost linearly from -16^oC at the bottom to almost -21^oC at the top [*Reeh*, 1995]. As most of the deformation is assumed to occur near bottom as the ice deforms by simple shear the ice temperature of -16^oC is used as a starting point.

During the field work a strain net was set up around the Central Dome and the surface velocity was measured in three concentric circles. To set a range for the flow parameter using these measurements the ice flow model was run using the 1994 ice thickness applying different values of the A corresponding to ice temperatures in the range $(-17) - (0)^o$C. The surface velocities resulting from the model was then compared to the measured ones at the outer circle at a distance of 10 times the ice thickness away from the dome. The SIA assumptions break down near the dome and therefore only the measured velocities at the outer circle were used. The comparison shows that values of A corresponding to ice temperatures in the range $(-17) - (10)^o$C give

realistic results.

For this study a value of $A = 8.6136 \cdot 10^{-18}$ $^{1}/_{(\mathrm{Pa}^3\mathrm{yr})}$ corresponding to an ice temperature of -16^oC. has been applied. The assumption of isothermal ice is a crude one as the ice temperature varies over the ice cap. On the glacier tongue of Hare Glacier (see Fig 1.4 for location) a bottom temperature of -1^oC was measured [*Reeh*, 1995] meaning that the flow of ice is faster in this place.

In the next chapters different periods of the history of the Hans Tausen Iskappe are investigated using this model setup.

Chapter 5

Past

The ice flow model is now applied to Hans Tausen Iskappe. In this chapter the build-up of the ice cap following the Climatic Optimum is investigated. This is done by studying the size and pattern of the accumulation. The model is run for 4000 years forced by temperature data from the Dye 3 core *Dahl-Jensen et al.* [1998] (See Fig. 1.3).

The Hans Tausen Iskappe is not the only ice cap not to survive the warming of the climate following the last ice age and to regrow in the second half of the Holocene. *Koerner and Fisher* [2002] found from climate proxy data from ice cores that this is the case for many smaller ice caps throughout the Arctic. The end of the last ice age also implied changes for the large ice sheets: The Laurentide Ice Sheet in North America and the Fennoscandian Ice Sheet in Scandinavia disappeared and the Greenland Ice Sheet retreated [*Lowe and Walker*, 1997].

In the following section a short history of Hans Tausen Iskappe is compiled using results of different studies from the vicinity of the ice cap and of the ice cap itself. In Section 5.2 the set-up of the temperature forcing is described. The results are presented in Section 5.3 and discussed in Section 5.4. Conclusions are made in the last section, Section 5.5.

5.1 Hans Tausen Iskappe in the Past

The Hans Tausen Project included glacio-geologic investigations of the area as well as mass balance and ice core studies. This section is split up in glacio-geological studies and studies of the ice core using results of the field work of 1994-1995 but also earlier studies of the area.

5.1.1 The Vicinity of Hans Tausen Iskappe

The present Hans Tausen Iskappe is only 3500-4000 years old as indicated by different studies of the ice core drilled to bedrock at the central dome. With the onset of the Holocene (our present warm period) around 10000 years ago [*Lowe and Walker*, 1997] temperatures started to rise and deglaciation began culminating during the Climatic Optimum 6000-8000 years ago. The Hans Tausen Plateau became ice free prior to 8100 BP while the deglaciation in the outer parts of the Independence Fjord (See Fig A.3 for location) occurred some thousand years before. During the deglaciation even the highest located parts of the ice cap were below the equilibrium line and experienced surface melt. The decay occurred by a lowering of the surface and not by horizontal recession. The warmer climate meant that the fjords were seasonally ice free from the period $6700 - 6300$ years BP documented by finds of driftwood at Kap Bopa and the eastern end of Nordpasset. In Jørgen Brønlund Fjord finds extend this period to $6600 - 2550$ years BP. See Fig. 1.4 for the location of Kap Bopa, Nordpasset and Fig A.3 for location of Jørgen Brønlund Fjord. [*Landvik et al.*, 2001]

During the last ice age Hans Tausen Iskappe is thought to have been confluent with the Greenland Ice Sheet. Studies in Nordpasset show evidence that the northern part of Hans Tausen Iskappe was part of an ice sheet that covered the adjacent area during the same period. [*Landvik et al.*, 2001; *Bennike*, 1987] At present the ice cap lies $\sim$ 20 km north of the Greenland Ice Sheet.

Studies of sedimentation rates from a lake near Jørgen Brønlund Fjord show a richer vegetation than presently in the period 5000-3300 BP probably caused by an increase in precipitation due to the seasonally open fjords [*Landvik et al.*, 2001]. This interval fits well with the age of the ice cap at the drill site, $3500 - 4000$ years assessed by studies of stratigraphy, ice crystals and annual layer thickness by *Madsen and Thorsteinsson* [2001] and *Clausen et al.* [2001]. The build-up of the ice cap probably began as a response to the increased precipitation rate. The sedimentation rate dropped at 3500 years BP and 2100 years BP marking the transition to colder summers.

During the last century up until 1978 the glacier margins seem to be stable or show a slight retreat of 10-100 m from aerial photographs [*Weidick*, 2001]. Recession is generally related to north and western facing glaciers. The oldest moraines in the area are $\sim$ 100 years old, and therefore the culmination of re-advance of local glaciers following the Climatic Optimum is

believed to be at the end of the Little Ice Age (1900 AD) *Weidick* [2001].

5.1.2 The Ice Core

The ice core is an information archive of conditions during build-up of the ice cap. The location of the drill site is marked by a red star in Fig. 1.2. The ice core is drilled to bedrock and is 345 m long [*Hammer et al.*, 2001]. A very characteristic feature is the amount of melt layers present in the core. In the lower 150 m of the core the melt percentage is is above 50% increasing to 100% near the bottom indicating that the build-up was a wet 'summer-affair' during the first few thousand years [*Hammer et al.*, 2001]. Around a depth of

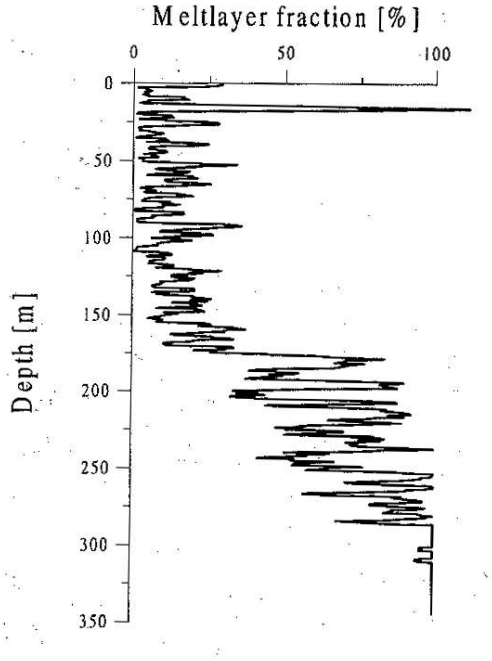

Figure 5.1: *Melt layer fraction in the Hans Tausen ice core. From Madsen and Thorsteinsson [2001].*

175 m there is a distinct drop in the level of melt layer fraction falling below 40%. This drop is thought to be a result of abrupt changes in accumulation or summer temperature. The present level is around 8% indicating that melting occurs at high elevations on the ice cap [*Madsen and Thorsteinsson*, 2001]. Though the age is estimated to 3500-4000 years it has only been possible to create a time scale back to 244 BC due to the melt layers [*Clausen et al.*, 2001]. Melt layer stratigraphy is a product of climate and *Koerner* [1977]

used melt stratigraphy of an ice core from Devon Island to infer information of summer climate and summer sea-ice conditions in the region.

Another interesting feature is the annual layer thickness of $\sim$ 10 cm which is almost constant down to 100 m above the bed [*Clausen et al.*, 2001]. Non-vanishing surface velocities measured in an area around the dome by *Keller et al.* [2001] show that the layers are thinning. This together with studies of the crystal fabric give evidence of an increased accumulation rate back in time [*Madsen and Thorsteinsson*, 2001].

Dust and sea salt concentrations in the ice core are studied by *Steffensen et al.* [2001]. In the upper part of the core the dust particle size and flux are comparable to those at GRIP located on the Greenland Ice Sheet with no local dust sources (see Fig. 1.3). This suggests that the dust in this part of the Hans Tausen core is also of remote origin. In the lower part higher concentrations and increased particle size dominate thought to be of local origin. This is in good agreement with the other results showing that the ice cap was lower at the time (it was rebuilding) and experiencing high melt rates causing an increased dust concentration.

Steffensen et al. [2001] also studied the concentrations of sea salt in the core. There are seasonal variations with higher concentrations during winter compared to summer. Again there is an agreement with results from the GRIP core suggesting a remote source. No changes in concentration are observed with depth indicating that the North Polar Sea never was an important source of sea salt in the area and probably never was ice free during the life time of the ice cap.

$\delta^{18}O$ was measured in the ice core and the profile been interpreted qualitatively back to 2000 years BP. $\delta^{18}O$ is a temperature proxy that can be used to infer past climate when taking different precautions. In the present case the profile can not be interpreted in terms of qualitative changes in past temperature due to lack of knowledge about the rebuilding of the ice cap and the high fraction of summer melt layers. Still some things can be learned about the climatic conditions [*Hammer et al.*, 2001]. The profile has high values in the first millennium and low values in period around 1700-1900 AD indicating higher and lower temperatures respectively. For simulating the build-up of the ice cap a climate curve for the period is needed to be able to give estimates of temperature, accumulation and melt through time. As only a qualitative interpretation of the Hans Tausen ice core has been possible, temperature information of the ice core from Dye 3 will be applied

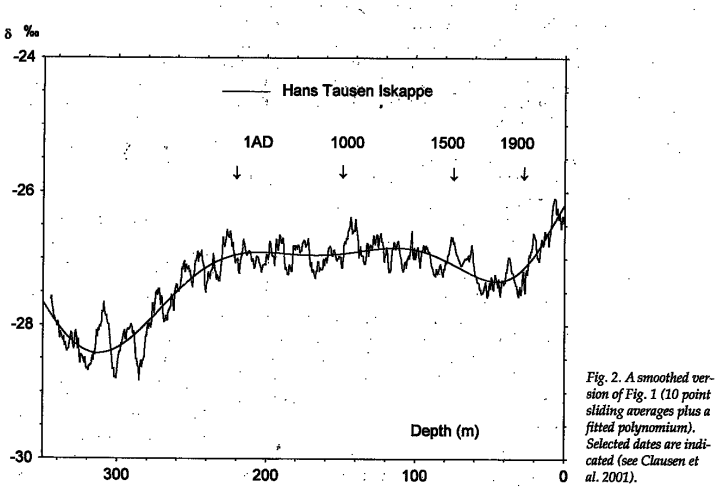

Figure 5.2: *The $\delta^{18}O$ curve of the Hans Tausen ice core. From Hammer et al. [2001].*

as explained in the following section.

5.2 Set-up of the Model

To investigate the build-up of the ice cap the model is run for 4000 years (16000 time steps of $\frac{1}{4}$ year) forced by changes in temperature. The age of the ice cap is as mentioned above set to $3500 - 4000$ years [*Madsen and Thorsteinsson*, 2001; *Clausen et al.*, 2001]. The higher estimate is chosen and will not affect the conclusions made. The data is from the Dye 3 bore hole and the set-up using this data is described below. This forcing is used together with different simple parameterizations of accumulation. The start accumulation needed to initialize the build-up is also investigated.

5.2.1 Temperature Forcing

In subsection 5.1.2 the $\delta^{18}O$-curve is presented. As described it can only be interpreted in a qualitative manner for the past 2000 years and cannot be utilized to force the model for the past 4000 years. Instead past surface temperatures from Dye 3 inferred from borehole temperatures using a Monte Carlo method is used (See fig.5.3) *Dahl-Jensen et al.* [1998]. A surface temperature curve was also extracted using borehole temperatures at GRIP. The two curves are almost identical for the last 7000 years except that the Dye

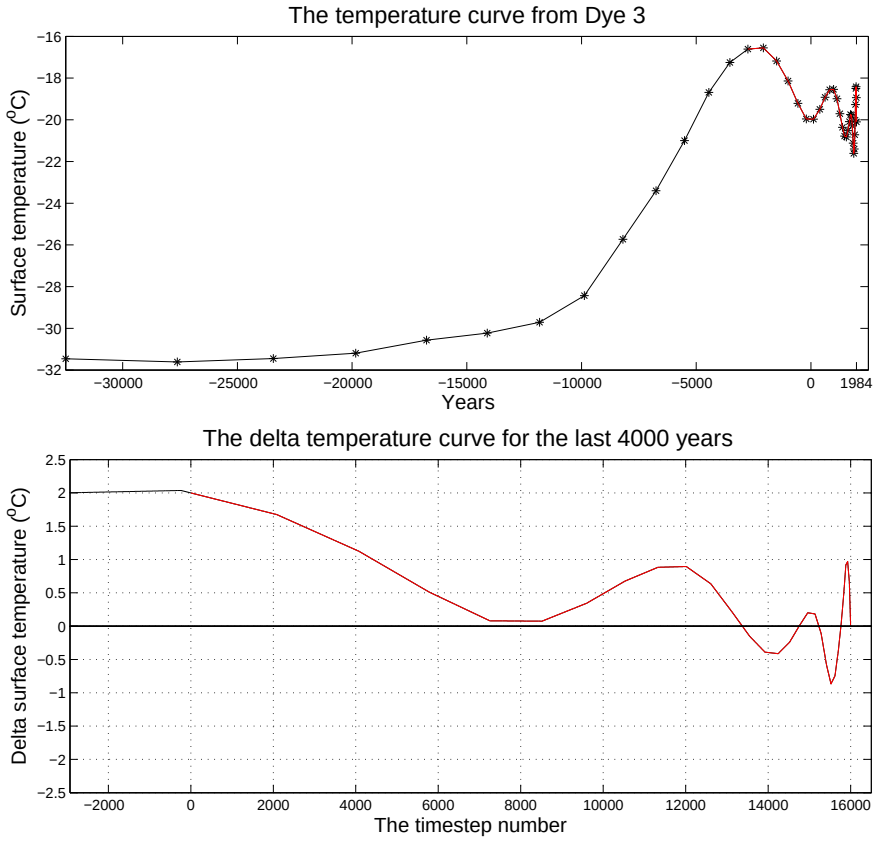

Figure 5.3: ***Upper:*** *The surface temperature at Dye 3 through time from inversion of borehole temperatures by Dahl-Jensen et al. [1998]. The red line indicates the part applied in this study.* ***Lower:*** *The ΔT used as forcing in the model. The deviation is taken from the 1984 value and the amplitude is reduced compared to at Dye 3.*

3 curve has amplitudes 1.5 times those at GRIP. This difference is thought to depend on the different atmospheric variability at the two locations *Dahl-Jensen et al.* [1998]. The two cores show a temperature low ∼2000 years ago, warm temperatures during the Medieval Warming from 500-1200 A.D. and a cooling in the Little Ice Age in the period from 1500 to 1850 A.D. The Hans Tausen $\delta^{18}O$ profile shows some of the same characteristics as the cores from GRIP and Dye 3 as described in the previous section but it is not near a perfect match.

In the build-up experiments only data for the last 4000 years are used as

forcing. These data are then interpolated linearly onto time steps of 1/4 year. The last data point in the series is from 1984 and it is the deviation from the temperature value that year which is used in the model. As a first approximation the temperature deviation from 1984 is added at every grid point at every time step to the value of the mean annual and mean July temperature calculated using the temperature parameterizations of *Reeh et al.* [2001]. This procedure is employed because nothing is known about the response pattern between annual and summer temperatures to a general warming in the area. However, future projections of climate in the Arctic by The Intergovernmental Panel on Climate Change (IPCC) show that the warming is 'very likely' to be more pronounced in this region compared to globally and that the warming will be largest in the winter period [*Christensen et al.*, 2007]. A run over the Greenland region using the regional climate model, HIRHAM4, by *Stendel et al.* [2007] even indicates that summer temperatures might decrease slightly in North Greenland in the future. Results from this run will be discussed in Chapter 7 which deals with the future of Hans Tausen Iskappe. With this in mind a lower bound on the build-up phase is that there is no change in July temperature. The change in mean annual temperature is due to changes in winter and spring temperatures. The effect of a change in July temperature on melt is large and is the topic of a discussion in Chapter 7.

Warmer air can hold more moisture than colder air and this is accounted for by increasing the accumulation by 10 % per degree warming in annual temperature. This increase has also been applied by *Oerlemans et al.* [1998] and *de Woul and Hock* [2005] in their studies of the general response of glaciers to a warming of 1 °C. The value also seems reasonable in the light of the predictions of HIRHAM4 from the run by *Stendel et al.* [2007] of a 2 °C increase in annual temperature. The data set will be presented and discussed in Chapter 7.

The prevailing atmospheric conditions in the Hans Tausen area probably resemble the conditions at GRIP more than those at Dye 3. I have chosen to scale the amplitude of the temperature change so the delta temperature value 4000 years before 1984 is 2 °C. The amplitude is then lower the value of GRIP.

The climate must have been at least slightly warmer than present at the time of the start of the build-up. This is due to the fact that the fjords were seasonally ice free. Today semi-permanent ice covers the fjords. The $\Delta 2$ °C compared to present at 4000 years BP indicated by Fig. 5.3 is probably a high estimate. The temperature increase affects the amount of accumulation needed for build-up of the ice cap, but this will not influence the results as

it is the accumulation pattern that is investigated.

5.3 Results

In this section results regarding the required accumulation for build-up of the ice cap for different changes in July temperature compared to annual temperature are presented. Results from model runs using different parameterizations of accumulation are also presented and will be the basis for the discussion of the conditions during build-up together with results from the field work described previously.

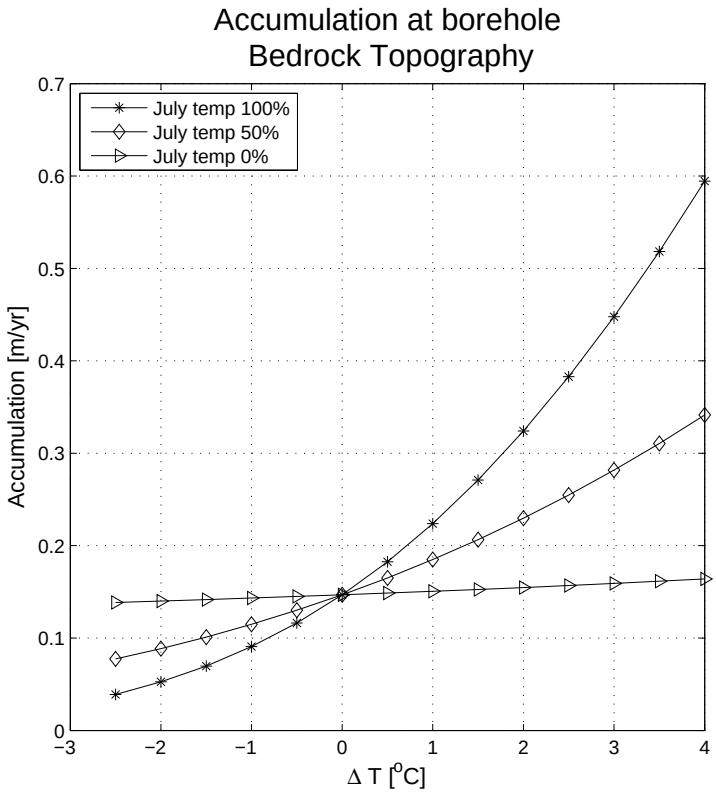

Figure 5.4: *Plot showing the accumulation needed to obtain zero-mass balance for a ΔT change in temperature compared to present at the location of the drill site when starting from zero ice thickness. The height of the surface is then equal to the height of the bedrock. For the ice cap to start rebuilding the accumulation must exceed the given value.*

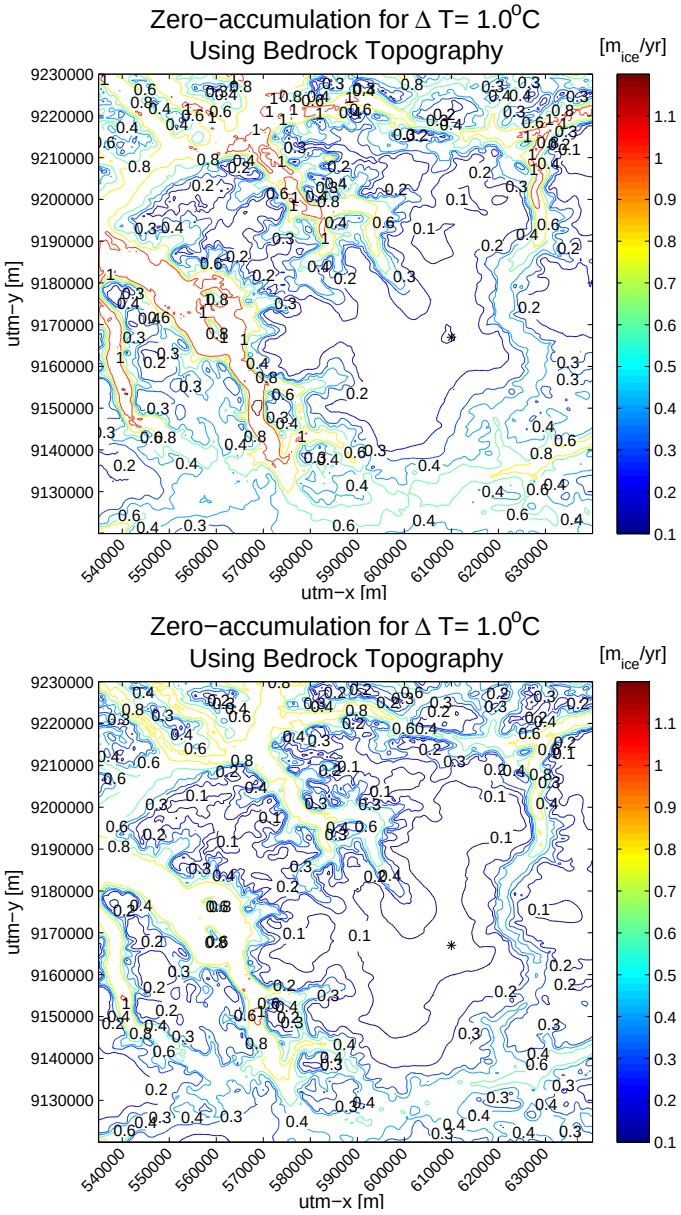

Figure 5.5: ***Upper:*** *Contour plot of the accumulation needed to obtain zero-mass balance for a* 1 °C *rise in temperature compared to present as calculated using the degree day model.* **100**% *of the temperature increase is added to the July temperature.****Lower:*** *Contour plot of the accumulation needed to obtain zero-mass balance for a* 1 °C *rise in temperature compared to present as calculated using the degree day model.* **0**% *of the temperature increase is added to the July temperature.*

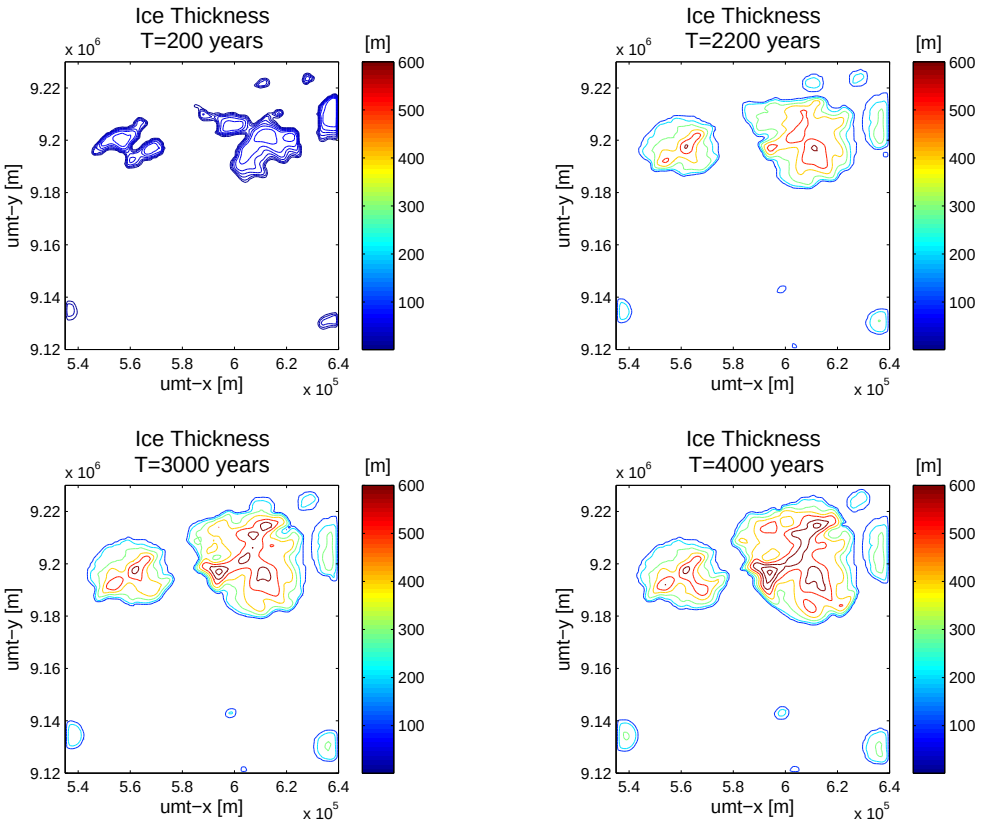

Figure 5.6: *Snap-shots from the simulation of the build-up using the parametrization of accumulation by Reeh et al. [2001]*

5.3.1 Accumulation During the Build-up

Figure 5.4 shows the accumulation necessary at the bore hole location with zero ice thickness to achieve zero mass balance for a given temperature increase/decrease. This means that in order for the build-up of the ice cap to begin the accumulation must exceed the value presented in the graph. Different curves have been calculated depending on the amount of of temperature change added to the July temperature in the degree-day model. The 'July 100%','July 50%' and 'July 0%'-curves refer to calculations where 100%, 50% and 0% of the temperature deviation is added to July temperature in the degree day calculation respectively. As the value of summer temperature greatly affects the melting, the minimum accumulation needed for build-up varies a lot between the curves. The 100% can be taken as the upper bound and 0% as the lower bound.

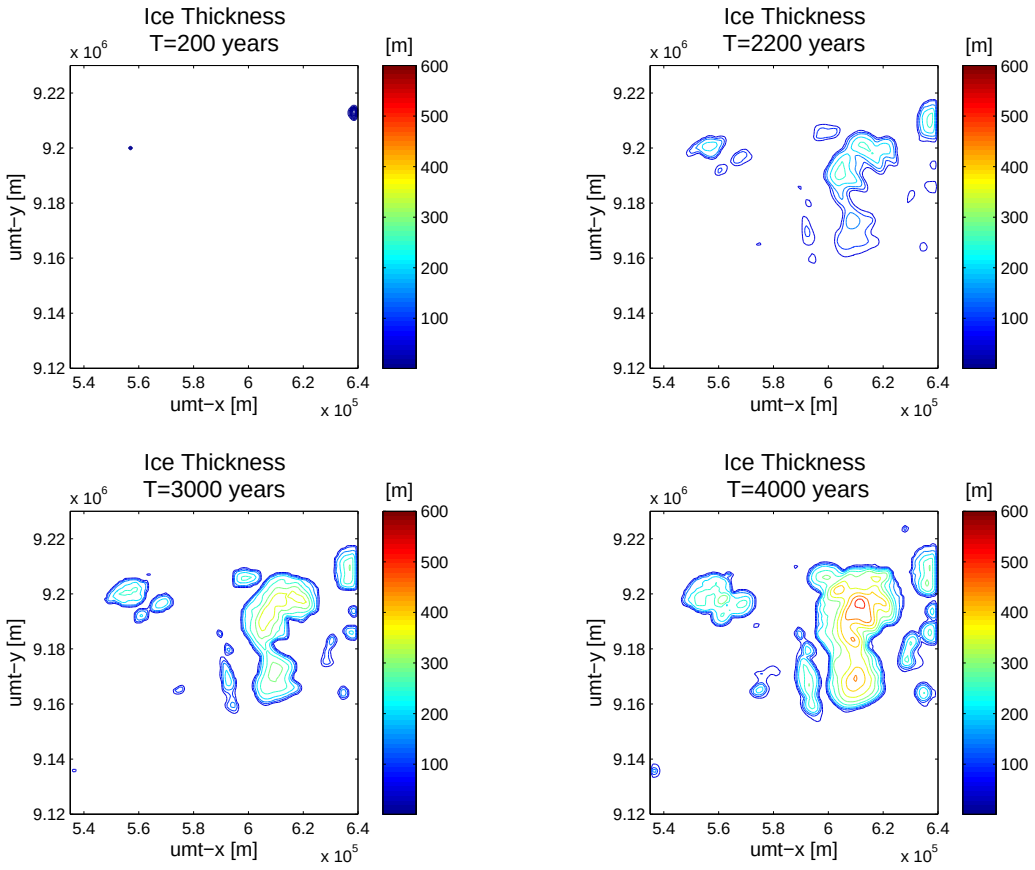

Figure 5.7: *Snap-shots from the simulation of the build-up using constant accumulation over the entire plateau.* **100**% *of the temperature change is added to the July temperature.*

The ´zero-accumulation´ over the entire plateau for a temperature increase of 1 °C for 100% and 0% of the increase added to the July temperature in the degree day model are displayed in Fig 5.5. The two sub-figures resemble the contour plot of bedrock topography in Fig. 4.3. This means that the ablation is largely elevation dependent in this parametrization. Only a slight latitudinal dependence is seen.

5.3.2 Model-runs of the Build-up

In order to investigate conditions during the formation of the ice cap different simple parameterizations of accumulation have been used as input to

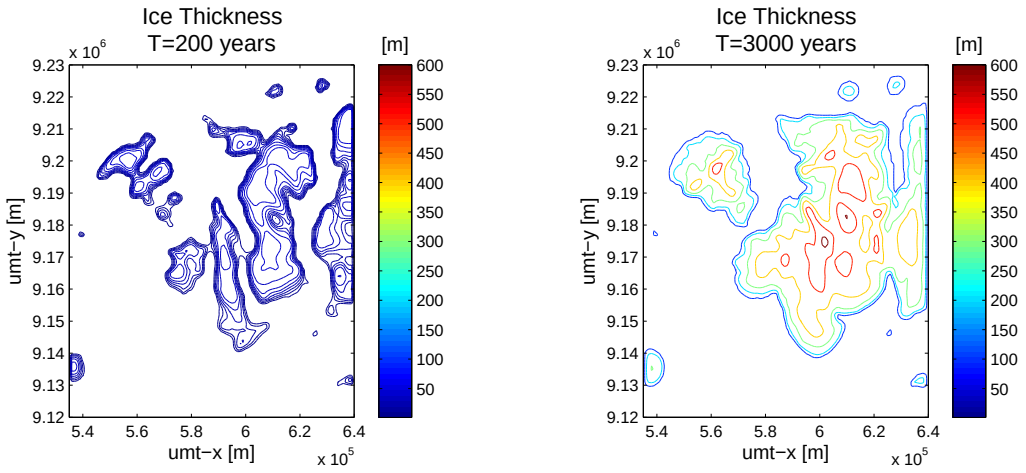

Figure 5.8: *Snap-shots from the simulation of the build-up using constant accumulation over the entire plateau.* **0**% *of the temperature change is added to the July temperature.*

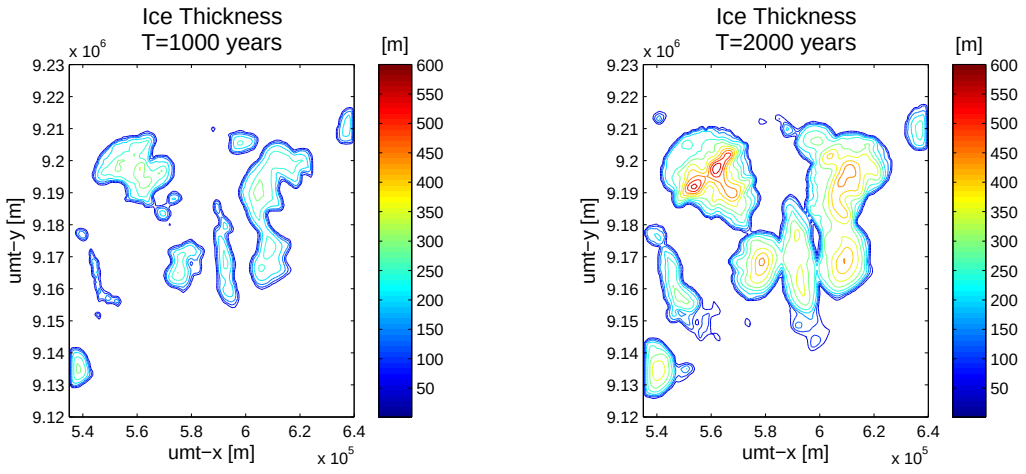

Figure 5.9: *Snap-shots from the simulation of the build-up using constant accumulation plus a longitudinal gradient over the entire plateau.* **100**% *of the temperature change is added to the July temperature.*

the model. The ice cap has an irregular shape and it is very difficult to find the unique time dependent mass balance history leading to the present form of Hans Tausen Iskappe. The different parameterizations presented here are meant to form a basis for a discussion of the build-up conditions together with results from the field work.

Fig. 5.6 shows snap shots of the formation of the ice cap during the 4000 year run using the accumulation parametrization by *Reeh et al.* [2001] which is discussed in Section 4.3. The contour plots in Fig. 5.6 show results of a run with a parametrization where 0 % of the temperature changes is added to the July temperature. The general result does not change whether 100 % is added, a higher value of the flow parameter, A, is applied or a reduced accumulation gradient of $0.5\frac{\mathrm{m_{ice}}}{\mathrm{L}}$ is used rather than $0.989\frac{\mathrm{m_{ice}}}{\mathrm{L}}$. In all cases, formation of ice only occurs on the northern half and it becomes very thick compared to present conditions.

The effect of constant accumulation over the entire plateau is investigated in Figs. 5.7 and 5.8. In both cases acc = $0.21^{\mathrm{m_{ice}}}/_{yr}$ which is increased/decreased according to changes in temperature. In the former case 100 % temperature change is added to July temperature and 0 % in the latter case. Ice forms on the southern half in both cases but not sufficiently on the southwestern part in the former case.

Results from a run including a longitudinal gradient in accumulation. A linear increase in accumulation of $0.1^{\mathrm{m_{ice}}}/_{yr}$ from east to west is superimposed on the constant accumulation shown above for the scenario where the full temperature change is added to the July temperature. Ice now forms on the southwestern part but the ice thickness on the northwestern part is very large.

5.4 Discussion

It is evident from Fig. 5.4 that the change in summer temperature with climate changes has great influence on the accumulation needed for build-up. Under present climatic conditions an accumulation > 0.15 $^{\mathrm{m_{ice}}}/_{\mathrm{yr}}$ is needed for ice to form at the borehole. For comparison the present accumulation at the Central Dome is ~ 0.1 $^{\mathrm{m_{ice}}}/_{\mathrm{yr}}$ with present day ice thickness. For a 1 °C increase in annual temperature the minimum accumulation changes greatly depending on whether this warming is thought be uniform over the whole year (0.22 $^{\mathrm{m_{ice}}}/_{\mathrm{yr}}$), not occurring during summer (0.15 $^{\mathrm{m_{ice}}}/_{\mathrm{yr}}$) or something in

between illustrated by 50 % of the increase added to the July temperature ($0.18\ ^{m_{ice}}/_{yr}$). This effect is also illustrated in Fig. 5.4 showing the 'zero-accumulation' for an increase of 1 °C for the 100 % and 0 % cases. The result is of course dependent on the applied degree day model but it shows that one should take the change in summer temperature into consideration. The influence of July temperature change on melt is as mentioned discussed in Chapter 7.

The shielding of the southern part by the northern part observed at present was not as important during the formation of Hans Tausen Iskappe as seen from Fig. 5.6. Using the present parametrization both with uniform annual warming and warming not occurring during summer no ice is present at any time during build-up on the southern part. This indicates a change in accumulation pattern over time. A possible explanation is that the shielding has increased gradually as the ice thickness on the northern (and southern) part increased. The larger accumulation on the northern part today is ascribed to the path of the weather systems coming in from the North delivering most of the moisture in the North Dome area as described in Section 4.3. It could be interesting to attempt the parametrization of the gradual shift in precipitation pattern.

A more uniform accumulation pattern is investigated in Fig. 5.7 and 5.8. The difference between the two is how much the July temperature contributes to the annual warming. The ice is now able to build-up on the southern part as well, the timing and amount depending on whether warming is thought to occur in summer or not. Ice builds up more readily on the northern part due to its higher elevation and more northerly location both things leading to less ablation in the model. For a uniform accumulation this leads to a thicker ice mass over the northern part compared to at the Central Dome which is not the case in reality (See Fig. 4.2 showing the present ice thickness). In the case of no change in July temperature ice forms over the entire plateau. It fast becomes too thick but resembles the form of the actual ice cap except for the confluence with ice in the eastern part.

Ice has difficulty forming on the southwestern part for the runs where a uniform increase in temperature over the year is assumed. At present the ice thickness in that area is up to 350 m but experiencing melt when looking at Fig. 4.6 showing the 1994 mass balance. No measurements were carried out here, however, and conditions may therefore be different. The fjords were ice free during the time of build-up and probably an important source of moisture [*Landvik et al.*, 2001]. If this is the case the western part closest to the

large open fjords may have experienced increased precipitation during that time compared to later. An attempt has been made to parameterize this by including a longitudinal accumulation gradient in the 100% run above with constant accumulation. This does lead to build up of ice on the southwestern part and even more so on the northwestern part where the present ice thickness is of the order 200 m. For both areas the ice becomes too thick. The linear increase in gradient to acc = 0.1 $^{m_{ice}}/_{yr}$ is obviously to large but indicates that this is a possible scenario. The build up of ice in these areas do not have to coincide with the age of the ice at the Central Dome, the only place where the ice cap has been dated. It could be a little younger.

Using the simple parameterizations of accumulation the ice thickness is easily overestimated. The accumulation needed during the start of the build-up is larger than the accumulation experienced later as seen from the ice core. The near constant annual layer thickness indicates a decrease in accumulation through the life time of the ice cap [*Clausen et al.*, 2001]. In the beginning extensive melting occurred every summer [*Madsen and Thorsteinsson*, 2001] and rain must also have been a part of the accumulation. This is not included in the model but suggests that accumulation must have been even higher than the minimum in order for some ice to survive.

5.5 Conclusions

A change in accumulation pattern over the life time of the ice cap is indicated by the run using the original parametrization of *Reeh et al.* [2001]. No ice forms on the southern part at any time during the simulation. Using a uniform accumulation rate over the entire plateau ice forms also on the southern part. In the experiment where there is no change in July temperature ice forms over the entire plateau while results from the other experiment show smaller coverage. The open fjords at the time have probably played an important role increasing precipitation. This precipitation might have been higher in the areas close to fjords and have helped ice form e.g. on the southwestern part of the plateau. The present observed shielding of the southern part by the northern part has probably been happening gradually as the ice thickness increased. The change perhaps occurring from one of the more uniform patterns suggested above where ice is able to form in most parts.

The minimum accumulation required for build-up to begin has also been investigated. The exact temperature increase during build up is not known but the seasonally open fjords indicate a warmer than present climate. The

minimum accumulation is of course dependent on the summer climate parameterized in the ablation model by July temperature. Future projections of climate in the Arctic [*Christensen et al.*, 2007; *Stendel et al.*, 2007] suggest that the warming will be largest in winter and spring. Therefore the minimum accumulation has been investigated for different increases in July temperature compared to annual temperature. The results vary greatly indicating the influence of summer temperature. Other things also influence the build up accumulation like the effect of rain.

Chapter 6

Present

In this chapter the present state of the ice cap is investigated. The question of steady state is discussed in Section 6.1 by comparing the the 1994 mass balance with the steady state mass balance. New measurements of the Central Dome area are presented in Section 6.2 together with measurements from the field work. These data sets are compared and discussed in Section 6.3 and conclusions for the chapter are in Section 6.4.

6.1 Steady State Mass Balance

In order to investigate the current state of the ice cap the steady state mass balance is calculated, i.e. the mass balance as it would be were the ice cap in a steady state. In a steady state there is no change of the ice thickness in time and Eq. (2.2) reduces to:

$$0 = \nabla \cdot (H\bar{\mathbf{U}}) + b \tag{6.1}$$

Using the present day surface topography and ice thickness this calculation results in the mass balance displayed in the top part of Fig. 6.1. In the lower part shows the mass balance parameterized using the data collected during the field work in 1994-1995. It is clear from Fig. 6.1 that the present mass balance pattern is different from that of a steady state. The steady state mass balance in the figure of course differs from the 'real' steady state mass balance because it is calculated assuming that for a column of ice the gravitational driving stress is balanced by local shear. This means that no down stream effects are considered as discussed in Section 2.2. The accumulation measured in 1994 is thought to be generally higher than the long term accumulation [*Reeh et al.*, 2001]. These things should be kept in mind when looking at Fig. 6.1 but the general structure will not be critically different.

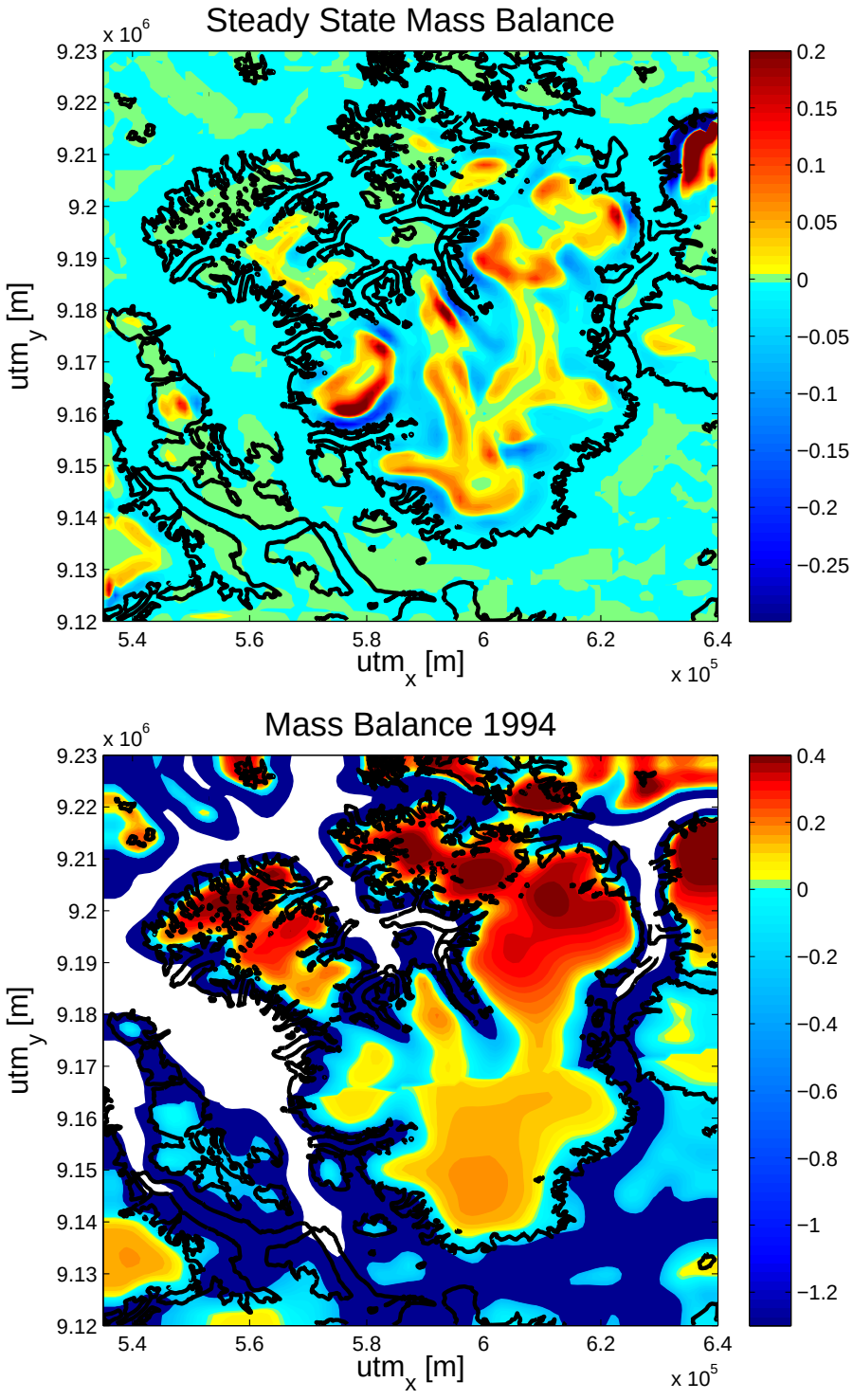

Figure 6.1: ***Upper:*** *The steady state mass balance calculated using Eq. (6.1).The flow parameter A is calculated assuming an ice temperature of* -16^{o}C.***Lower:*** *The mass balance in 1994.*

An important thing to notice is the very negative mass balance of low elevated outlet glaciers of the 1994-mass balance compared to the steady state balance. These glaciers are believed to be relicts formed during the colder Little Ice Age [*Reeh et al.*, 2001] and a slight retreat has been observed by *Weidick* [2001] from vertical photographs taken in 1978. In the steady state case the slightly negative mass balance is per definition compensated by the flow of ice. The very negative mass balance obtained in 1994-case can probably not be compensated by flow of ice and change in glacier volume and extent will occur. Another difference is the gradient between the northern and southern part of the ice cap. Looking at the steady state mass balance this gradient is not necessary to maintain a steady state.

Just by studying Fig. 7.6 it is evident that the ice cap not is in a steady state. Studies at the Central Dome confirm this result and conclude that the Central Dome is presently thickening. As part of the field work in 1994-1995 a strain net was set up around the Central Dome. Results show that the dome area is presently thickening by $1 - 6 {}^{\mathrm{cm}}/_{\mathrm{yr}}$ [*Hvidberg et al.*, 2001; *Keller et al.*, 2001]. The almost constant layer thickness observed for the last 2000 years in the ice core also points in that direction [*Clausen et al.*, 2001].

6.2 Elevation Measurements

The field work in 1994-1995 concluded that the central dome area was thickening at rate of $1 - 6 {}^{\mathrm{cm}}/_{\mathrm{yr}}$ as mentioned in the previous section. New measurements of the area were performed as part of an airborne survey in 2004 by the Danish National Space Center and these results show a decrease in surface height of the order of $\sim 1 - 1.5$ m over the 10-year period. In the following subsections the two data sets of elevation are presented and the decrease in elevation is discussed.

6.2.1 Presenting the data

The elevation data from the summer of 1994 used in this study of the Central Dome area was measured from snow scooter by GPS with a precision of < 1 cm [*Jonsson*, 2001]. The remeasurement in May 2004 was performed using a Riegl scanning laser with a precision of ~ 5 cm and kinematic GPS with a precision of the position of $25 - 50$ cm [*Dalå et al.*, 2005]. The tracks of both surveys are displayed in Fig. 6.2.

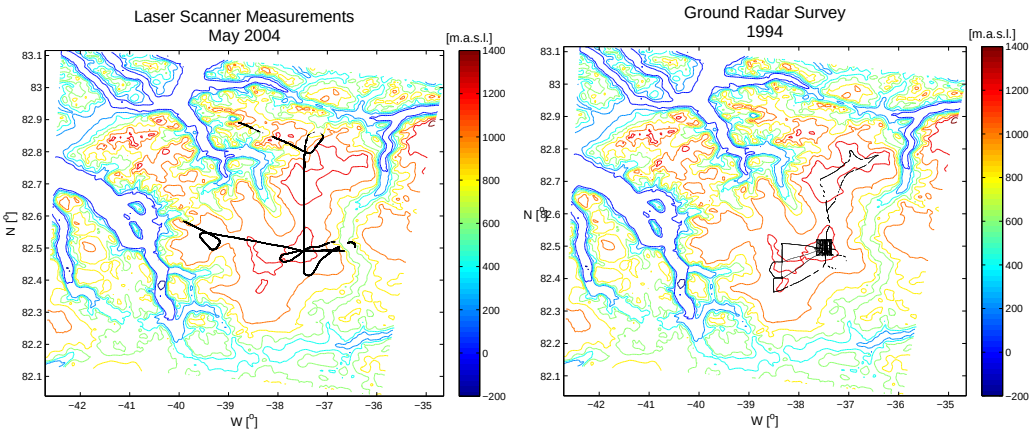

Figure 6.2: ***Left:****Plot showing the flight tracks of the airborne survey in 2004.* ***Right:*** *Plot showing the snow scooter tracks in 1994.*

Comparison of the two sub-figures show that the measurements of the 1994 survey are much more evenly spaced in the Central Dome area than those of the airborne survey. Both data sets are gridded using the griddata function in MATLAB®. This function grids unevenly spaced data by triangle based linear interpolation. Contour plots of the elevation of the dome area in 1994 and 2004 are displayed in Fig. 6.3 together with the measurement points displayed by the small, black dots. The changes in elevation of the dome area between the two measurements are contoured in Fig. 6.3.

The simple gridding method combined with the distribution of measurement points affects the elevation change plot in Fig. 6.4. The flight tracks of the 2004 survey are clearly visible in the plot. When studying the elevation change plot one should take care and only use the result where there is measurement coverage from both data sets. The measurement points are indicated in the figure. A better gridding method will improve the result. Using only these areas the elevation change is generally $1 - 1.5$ m $\pm$ 0.5 m and a little larger in the northeast corner of the figure. This decline in elevation is larger than the error estimate meaning that there is an actual decrease in surface height.

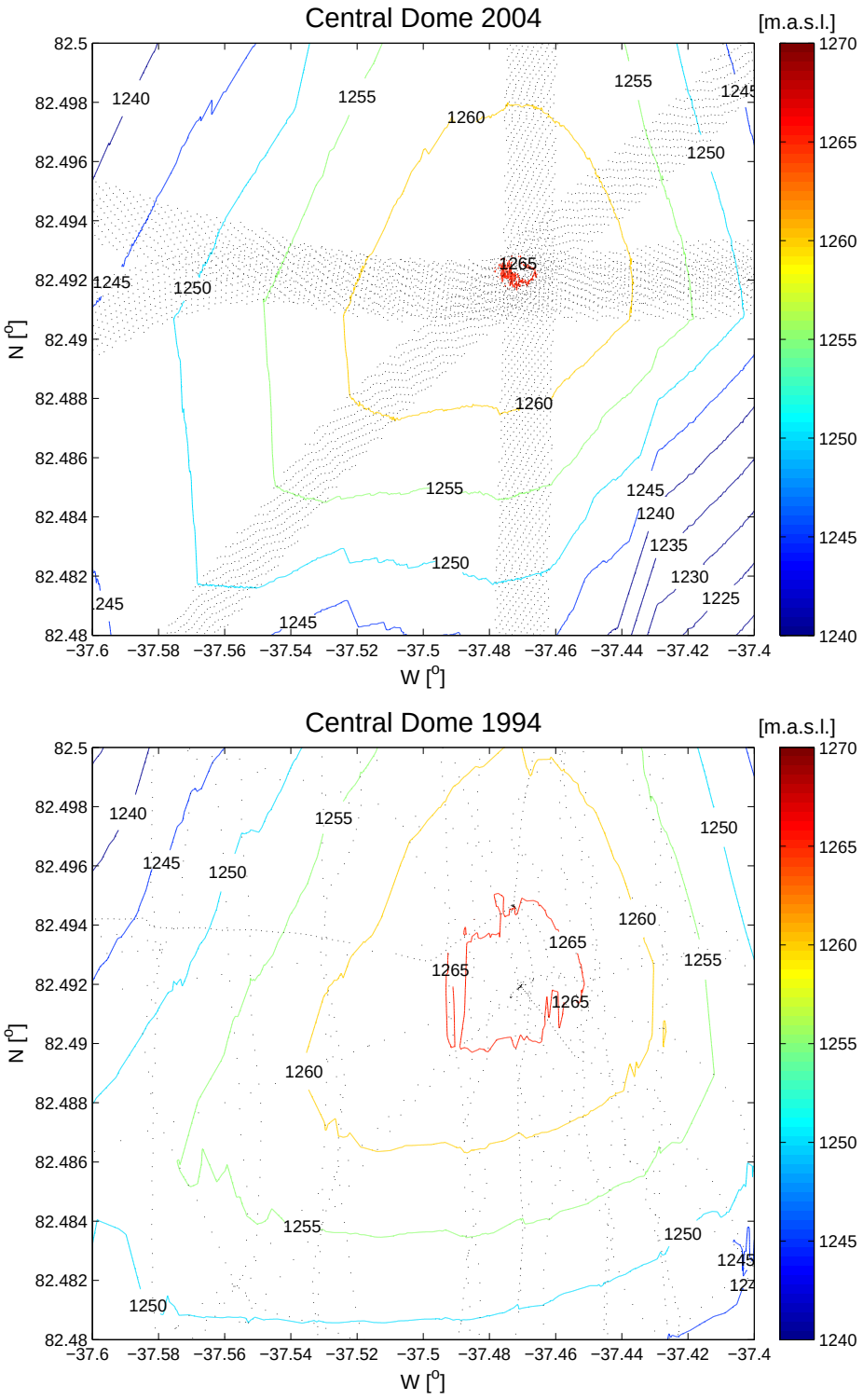

Figure 6.3: ***Upper:*** *Contour plot of the gridded data of surface elevation from the 2004 survey.* ***Lower:*** *Contour plot of the gridded data of surface elevation from the 1994 survey. The measurement points are represented by small black dots.*

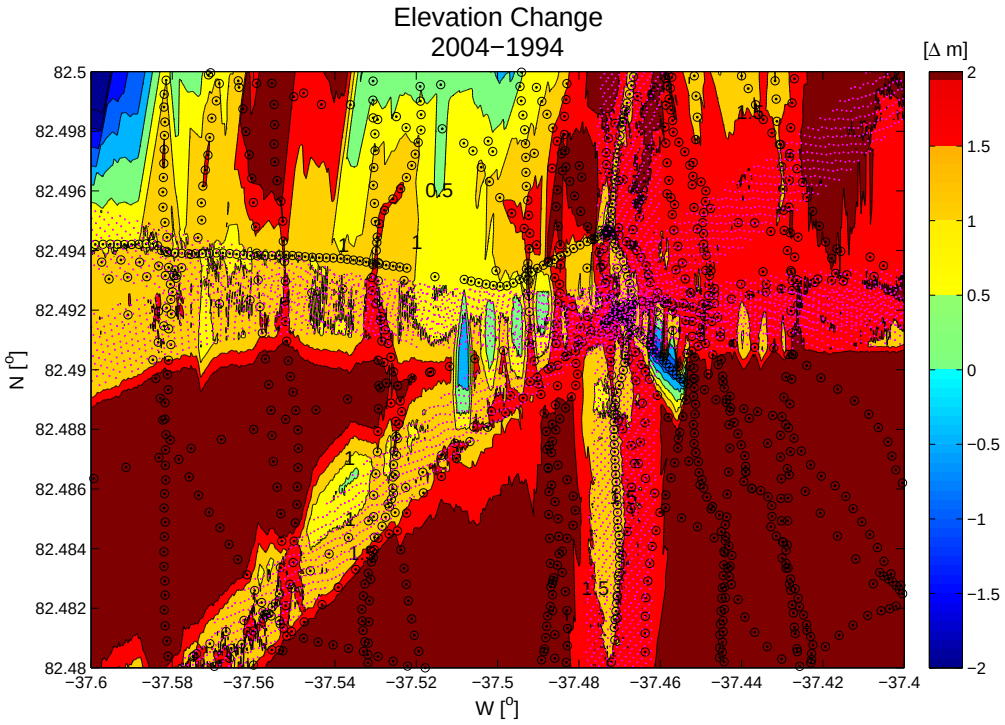

Figure 6.4: *Contour plot showing the changes in elevation height of the dome area from* 1994 *to* 2004 *obtained by subtracting the two gridded data sets displayed in Fig. 6.3.* ***Positive*** *values imply a* ***decrease*** *in elevation over the period. The error estimate is* ~ 0.5 m. *The* ***black*** *dots show the 1994 measurements and the* ***purple*** *dots indicate the 2004 measurements.*

6.3 Discussion of Elevation Changes

In this section the decrease in elevation measured in the Central Dome area is discussed and different causes are explored. The elevation change has been measured over a short period of time and the causes are therefore thought to be local. As mentioned in the discussion of the present and steady state mass balance retreat of outlet glaciers is observed. Thinning of the ice margin areas will of course affect the general flow and thereby the central parts of the ice cap but not over the time span discussed here. Therefore possible local mechanisms of elevation decrease are discussed in the following. These are: surface melting, run-off, mass balance, ice flow, measurement timing and densification of the snow and firn.

On the local dome there are no melt water streams [*H. Clausen pers. com.*] meaning that the decrease cannot be explained by simple melting combined with run-off. The decrease is not due to the timing of the measurements with respect to the melt season as this drags the result in the other direction: The lowest surface (2004-surface) is measured in May before the onset of summer, that is at its highest elevation. The highest surface (1994-surface) is measured during summer when the snow starts to compact and elevation decreases.

6.3.1 Mass Balance and Ice Flow

It is possible to observe a decrease in elevation without having a negative mass balance. If the accumulation is smaller than the amount of ice transported away by flow the surface height will decrease as illustrated in Fig. 2.2. I have investigated the possible elevation change by this effect in the Central Dome area.

This is done by applying an accumulation in the dome area that results in a mass balance of approximately zero. The Hans Tausen model is then run for a period of 87 years using different values of the flow parameter, A. These values correspond to ice temperatures in the range $(-17) - (0)^o$C. The results are displayed in Fig. 6.5. Looking at the results of runs using realistic values of A corresponding to ice temperatures in range $(-17) - (-10)^o$C (see Section 4.5) the change in ice thickness amounts to $1 - 2$ m over the 87 years. This is a fall of approximately 10 to 20 cm over a 10 year period. Assuming the ice cap to be at the melting point results in a significantly larger elevation decrease of 3.3 m in 10 years.

A period with low mass balance at the dome area can contribute to surface lowering observed but cannot be the only cause.

6.3.2 Densification

When measuring elevation changes of ice caps and ice sheets attention should be drawn to short-term changes in accumulation rate and firn densification. In the dry-snow zone of the Greenland Ice Sheet *Zwally and Li* [2002] observed and modelled interannual changes in elevation on the decimeter scale due to variations in temperature and accumulation which affected the densification of the firn layer.

The above mentioned results are from the dry snow zone and a possibil-

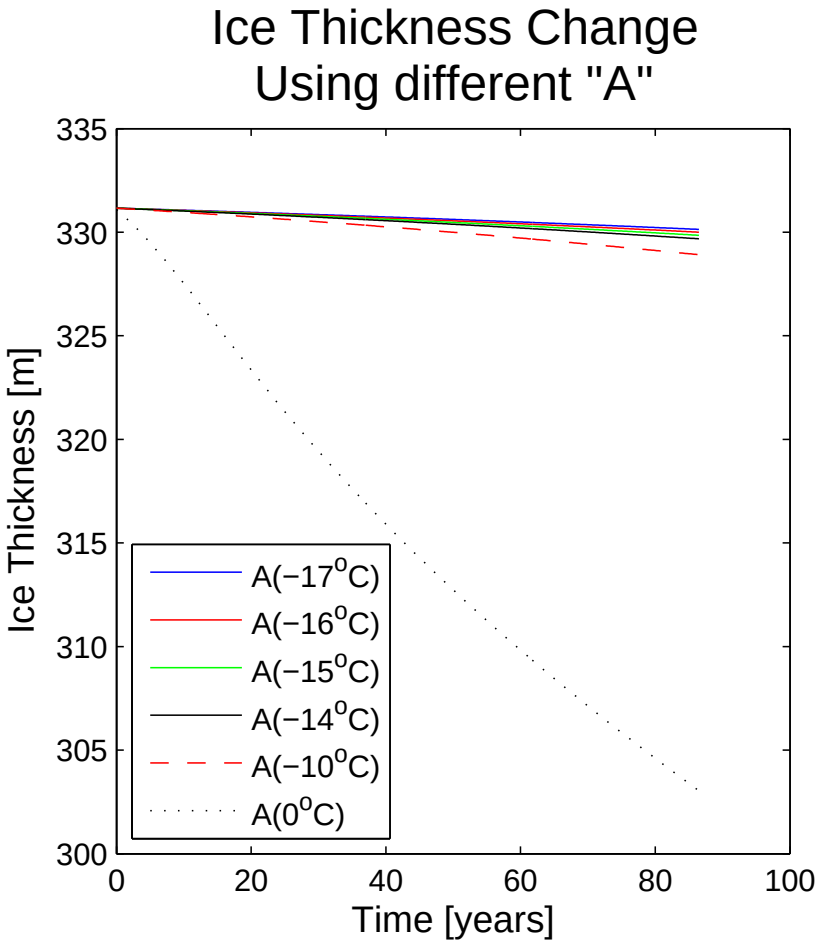

Figure 6.5: *Elevation change of the dome area in response to a near zero mass balance combined with different values of the flow parameter, A using the ice flow model.*

ity is that the dome area has experienced an increase in surface melt and perhaps rain during the period. Results from the ice core show 100 % fraction of melt layers in the bottom part of the core decreasing to 8 % in the top part [*Madsen and Thorsteinsson*, 2001] meaning that melt can occur with only slight increases in temperature. In order to obtain an estimate of the elevation change due to increased melt the following considerations are made: At present the accumulation in the dome area is 0.1 $^{m_{ice}}/_{yr}$. The precipitation falls as snow and the density of packed snow/firn is approximately half that of ice [*Paterson*, 1994] resulting in an accumulation of 0.2 $^{m_{firn/snow}}/_{yr}$. As-

suming that over the the ten year period the dome area has experienced an increase in temperature leading to melt, then a high estimate would be that half of the snow melts and refreezes as ice. This would lead to a reduction in height of ~ 5 $^{\text{cm}}/_{\text{yr}}$ and ~ 50 cm over the 10 year period.

6.4 Conclusions

Hans Tausen Iskappe is presently not in a steady state as indicated by several studies: Comparison of the 1994 measured and parameterized mass balance with the steady state mass balance show large differences, observations of retreat of lowing lying outlet glaciers that probably are remnants of the colder times during the Little Ice Age, the constant layer thickness in the ice core, strain net observations showing thickening of the ice in the Central Dome area of $1 - 6$ $^{\text{cm}}/_{\text{yr}}$ and the remeasurement of the dome area showing an elevation decrease of the order $1 - 1.5$ m $\pm$ 0.5. The elevation decrease is shown in Fig. 6.4. Care should be taken when interpreting the plot due to the simple gridding method applied combined with the data coverage.

Several local mechanisms that can decrease elevation has been investigated. The two main effects are thought to be increased densification of the firn and flow away from the dome combined with low accumulation. The two mechanisms can explain the lower bound of the decrease. However, estimates of elevation decrease from the two mechanisms cannot explain decreases in the high range of $1 - 1.5$ m $\pm$ 0.5. If densification is the dominant process the elevation decrease does not have to be in contradiction with the measured thickening in the same area. It would be very interesting if the dome area were remeasured over a larger area in order to asses the magnitude of the lowering.

Chapter 7

Future

Predictions of future climate are essential when trying to asses changes in e.g. surface temperature and sea level important for our future life on Earth. A very important contributor to sea level rise is the decrease in land ice volume. Projections of future warming predict preferential warming of Arctic regions [*Christensen et al.*, 2007]. This makes studies of mass balance of Arctic glaciers important when assessing sea level rise. *Meier et al.* [2007] estimates that $\sim$ 60 % of the rise in sea level not attributable to thermal expansion stems from ice loss from glaciers and ice caps not connected to the two great ice sheets. Generally, Arctic glaciers and ice caps are losing mass, though there are great inter annual and spatial variations [*Dowdeswell and Hagen*, 2004].

In this chapter the future of the Hans Tausen Iskappe is investigated by testing the sensitivity to changes in temperature and precipitation. This is done using predictions of temperature and precipitation of the Greenland area up until 2080 by *Stendel et al.* [2007] using the regional climate model (RCM) HIRHAM4. These results used as input to the Hans Tausen model is described in Section 7.1. This is followed by a description of the different experiments applied to the ice cap in Section 7.2. In Sections 7.3 to 7.5 the results are presented and discussed and conclusions of this chapter are drawn.

7.1 Model Forcing

The regional climate model HIRHAM4 has been used by *Stendel et al.* [2007] to simulate the climate of the Greenland region in the period 1950-2080. Earlier tests show that HIRHAM4 is able to simulate the present climate realistically [*Christensen et al.*, 1998]. Results from the transient run are used

to force the Hans Tausen model in order to investigate the future state of the ice cap. The advantage of a regional climate model (RCM) is the high horizontal resolution compared to a general circulation model (GCM), but this also restricts the size of the model area. HIRHAM4 is forced by results from a transient run with a GCM. The grid resolution of the RCM is 25 km and the results of the transient run from a grid point located near the drill site at 82.5° N, 37.5° W at 278 m.a.s.l. are presented in Fig. 7.1 [*Stendel et al.*, 2007]. It should be noted, when looking at Fig. 7.1, that the result of the HIRHAM4 model run shows the trend of temperature and precipitation in the future and is not a prediction of how the values of the parameters are going to be in a specific year.

The Intergovernmental Panel on Climate Change (IPCC) provides predictions for climate changes through a wide range of studies. Climate changes are modelled using different storylines representing different futures also known as SRES scenarios. These 'futures' are different scenarios of how fast new technology becomes available across borders, how demographic structure changes, how economics of different regions evolve and how environmental issues are faced. The output of these scenarios of the prediction concerning the atmospheric concentration of greenhouse gasses has great interest. This is one of the important inputs to general circulation models (GCM) trying to predict future climate.

The HIRHAM4 simulation uses observed concentrations of the well-mixed greenhouse gases for the period up to 2000 and future concentrations as prescribed by the A1B scenario (one of the IPCC 'futures') described in *Nakicenovic et al.* [2000]. The A1 storylines implicate a fast economic but low population growth and a rapid introduction of new and efficient technologies resulting in low greenhouse gas emissions over time. Different letters following A1 describes the alternative directions that changes in the energy system can follow depending on what the dominant source is: oil, coal, natural gas or alternative sources. The A1B is a scenario with a balance between the sources - no single source is dominant. By the start of the next century this scenario predicts a CO_2 concentration of 700 ppm -more than twice the pre-industrial level- and a rise in global mean temperature of 3.5 °C.

The HIRHAM4 model run predicts overall increases in temperature in the Greenland region. In general temperature increases in winter (3 °C) and spring (4 °C) will be higher than increases in summer and fall (2 °C) for the period 2021-2051 compared to the period 1961-1990. For the period 2051-2080 the increase in winter temperature will accelerate even more. This is

the general trend in the run, but the situation differs from place to place. In North Greenland the summer temperatures are predicted to decrease a little related to changes in lower tropospheric winds [*Stendel et al.*, 2007]. Increases in precipitation are also predicted with great differences over the region. These results agree with the changes in Arctic regions projected by the IPCC. It is found that it is very likely that increases in mean annual temperature in polar regions will exceed global rise in temperature and that the warming will be greatest in the winter [*Christensen et al.*, 2007]. Also precipitation is expected to increase with the largest changes during winter.

Looking at Fig. 7.1 most of these trends can be seen. There is a clear increase in both mean annual temperature and precipitation during the period. The aforementioned decrease in summer temperature is not clearly seen in the plot of July temperature in Fig. 7.1 due to the large interannual variations, but the mean temperatures of the periods 2021 - 2050 and 2051 - 2080 decreases by $\sim$ 0.2 °C and $\sim$ 0.21 °C compared to 1961-1990. The increase in mean annual temperature for the two periods compared to 1961-1990 are $\sim$ 2 °C and $\sim$ 4 °C, respectively. The mean of the precipitation also increases compared to 1961-1990: For the period 2021-2050 the increase is $\sim$ 20 mm and for the period 2051-2080 it is $\sim$ 67 mm. The increase in mean annual temperature does not stem from a rise in July temperature but mostly from increases in winter and spring temperatures. The largest increase is found in May (*Martin Stendel pers. comm.*). The fact that the increase in temperature is greatest in winter and spring in the future fits well with observations of temperatures in the Arctic from 1980 to 2007 where this trend is also evident [*Anisimov et al.*, 2007].

The output grid point is located very close to the location of the drill site as mentioned above. For location of the drill site see Fig. 1.2. The predicted values of precipitation for the end of the last century fits well with observations at the drill site and the values are therefore used as values for the drill site. There is, however, a large difference in elevation between the HIRHAM4 output point at 278 m.a.s.l. and the real elevation of the ice cap, which is 1271 m.a.s.l. and this influences the HIRHAM4 output values of temperature. The values are much too high compared to values at the drill site. Therefore they are corrected for this elevation difference using the lapse rates for mean annual and mean July temperature in Eqs. (4.1) and (4.2), before being used as temperatures at the drill site.

After these corrections the HIRHAM4 output values can be used as input to the Hans Tausen model. The values at the drill site are parameterized to

the entire ice cap using the gradients in temperature and accumulation with elevation and latitude described in Section 4.3.

7.2 Model Experiments

In order to investigate the sensitivity of Hans Tausen Iskappe to changes in temperature, precipitation and accumulation pattern different experiments are carried out using the result from the model run of HIRHAM4 by *Stendel et al.* [2007] described above. The experiments are simulated over a period of 87 years using either constant values of temperature and precipitation or the HIRHAM4 output data in the period 1994-2080. The smoothed DEMs of ice thickness and bedrock topography for 1994 obtained as part of the Hans Tausen Project described in Section 4.1 are used as input surfaces. When I discuss e.g. the ice thickness in 2078 it is rather the ice thickness after running the Hans Tausen model over 85 years.

There are three groups of experiments with some sub-scenarios: The **Original** group uses the output values from HIRHAM4 plotted in Fig 7.1 from 1994 to 2080. The **Present** and **Future** groups represent mean values of temperature and precipitation predicted by HIRHAM4 for the end of the last and the end of this century, respectively. For these two groups the input values are constant during the 87 year long model run. I have chosen to use the 30 year averaging periods 1961-1990 and 2051-2080 also discussed in [*Stendel et al.*, 2007] to represent the present and future values of temperature and precipitation together with two shorter averaging periods.

In the case of the **Present** and **Future** groups the temperature is parameterized to the whole ice cap as described above while the accumulation is kept constant in both time and space. For the **Original** group experiments the input values vary from year to year. In these experiments both temperature and accumulation are parameterized to the entire ice cap. In the following subsections the three different groups of experiments are described.

7.2.1 Present Scenarios

There are two sub-scenarios in this group: $\mathbf{Start}_{(1992-1995)}$ and $\mathbf{Start}_{(1961-1990)}$. The subscripts indicate the period over which output values of temperature and precipitation are averaged -both years included. The input values can be seen in Tab. 7.1.

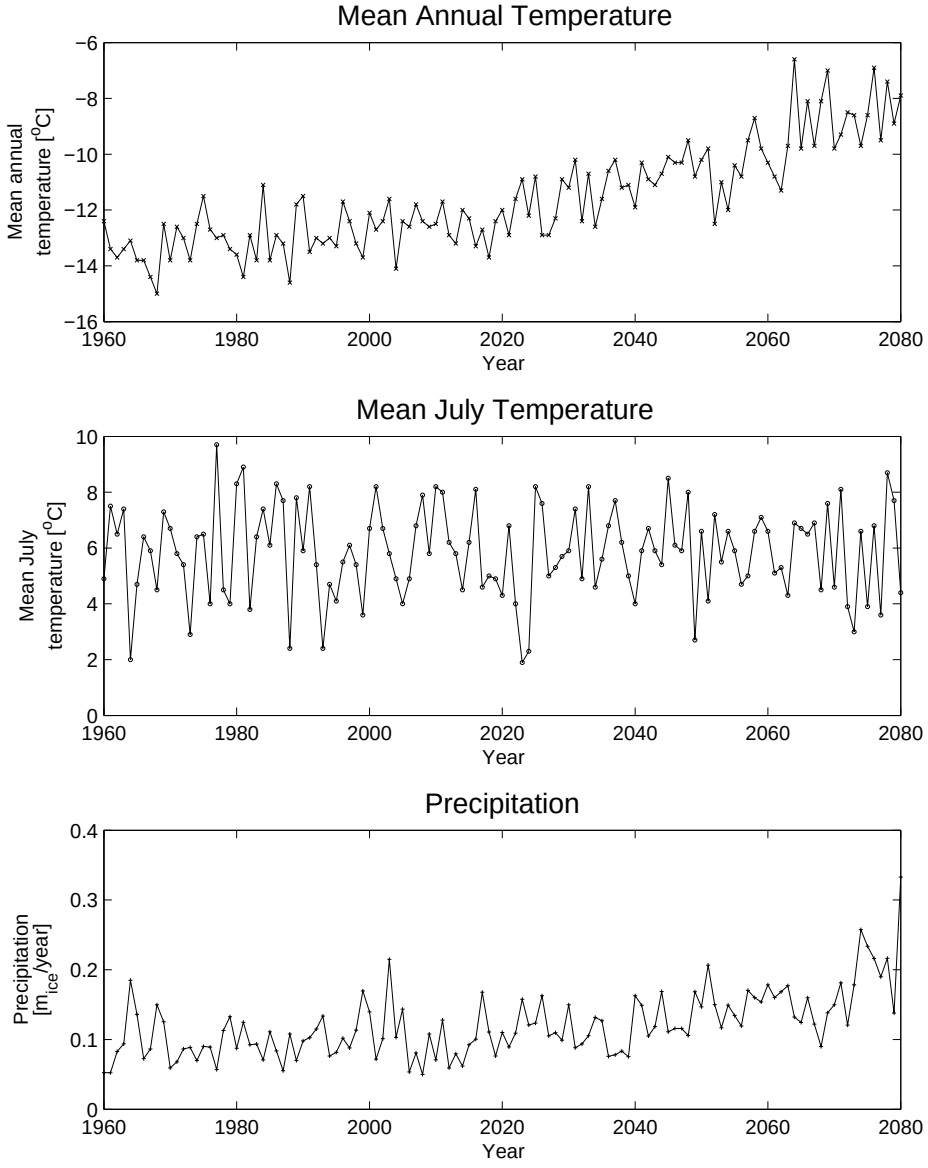

Figure 7.1: *Future values used as input to the ice flow model of annual mean temperature, mean July temperature and precipitation as predicted by a run with the regional climate model HIRHAM4 by Stendel et al. [2007]. The data is from a grid point located at* $(82.5^oN, 37.5^oW)$ 278 *m.a.s.l. Note: The results of the model is not a forecast in the way that a specific year will be colder or warmer than another year. The result shows trends.*

Experiment	Mean Annual Temperature [°C]	July Temperature [°C]	Precipitation [m_{ice}/yr]
Present Scenarios			
$\mathbf{Start}_{(1992-1995)}$	-13.1	4.2	0.102
$\mathbf{Start}_{(1961-1990)}$	-13.3	6.0	0.093
Future Scenarios			
$\mathbf{End}_{(2071-2080)}$	-8.5	5.7	0.206
$\mathbf{End}_{(2051-2080)}$	-9.4	5.8	0.168

Table 7.1: *Table showing the values of temperature and precipitation for the Present and End scenarios. The values are averages of the HIRHAM4 output data over the period given in the subscripts. Both years are included.*

The averaging period 1992-1995 is chosen because of the low values of annual and July temperature. These values are also very similar to the values discussed in [*Reeh et al.*, 2001] and are inputs of $\mathbf{Start}_{(1992-1995)}$. The sub-scenario with average values over 30 years, $\mathbf{Start}_{(1961-1990)}$, is more representative for the values of the end of the last century predicted by HIRHAM4.

7.2.2 Future Scenarios

This group also consists of two sub-scenarios: $\mathbf{End}_{(2051-2080)}$ and $\mathbf{End}_{(2071-2080)}$. The values of temperature and precipitation are displayed in Tab. 7.1.
$\mathbf{End}_{(2051-2080)}$ is the average over the last 30 years of the HIRHAM4 simulation and is taken as the most representative of the **Future** scenario. The input values of $\mathbf{End}_{(2071-2080)}$ is the average over the last 10 years of the simulation period and has higher values of mean annual temperature and precipitation and colder July temperature.

7.2.3 Original Scenarios

This group consists of three sub-scenarios. In this group all sub-scenarios are forced by the full output series in the period from 1994-2080. The difference lies in how the accumulation is parameterized to the whole ice cap. $\mathbf{Org}_{(\mathrm{Const})}$ uses a constant accumulation over the entire area only varying in time. $\mathbf{Org}_{(0.989)}$ and $\mathbf{Org}_{(0.5)}$ both uses the parametrization by *Reeh et al.* [2001] (see Eq. (4.3)), but have different gradients in accumulation between the Central Dome and the northern part of the ice cap. $\mathbf{Org}_{(0.989)}$ uses the

gradient of 0.989 $^{m_{ice}}/_{L}$ measured in 1994, while $\mathbf{Org}_{(0.5)}$ uses a smaller gradient of 0.5 $^{m_{ice}}/_{L}$, where L is latitude.

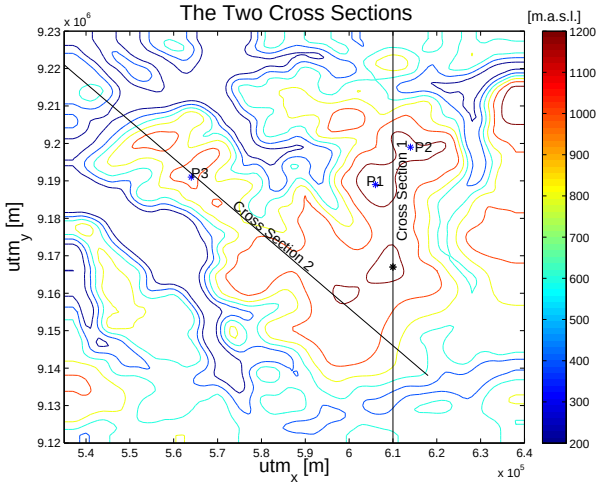

Figure 7.2: *The two cross sections discussed in Sections 7.3 and 7.4. Plots of the ice thickness along these cross sections are shown in Figs. 7.3 and 7.4.* P1, P2 *and* P3 *indicate points on the northern half of the ice cap discussed in Section 7.4.1.*

7.3 Results

The results of the model runs for the 7 experiments are plotted in Figs. 7.3 to 7.9. Two cross sections defined in Fig. 7.2 are used to display changes in ice thickness over 85 years (Figs. 7.3 and 7.4) while changes in total ice volume, specific mass balance and grid points covered by ice are shown in Figs. 7.5 to 7.7. All these figures describe model runs over 85 years using results from HIRHAM4 run for the period 1994-2078.

The 'jumps' in ice covered area in Fig. 7.7 happens as a response to the short periods of positive mean specific mass balance. Slight increases in volume can also be detected in Fig. 7.5.

In Figs. 7.8 and 7.9 the ice thicknesses resulting from three experiment simulations over 1000 years are displayed. These runs illustrate the effect of a certain climate parametrization over a longer time span than the 87 year runs.

To test the sensitivity of the results to the value of the flow parameter A,

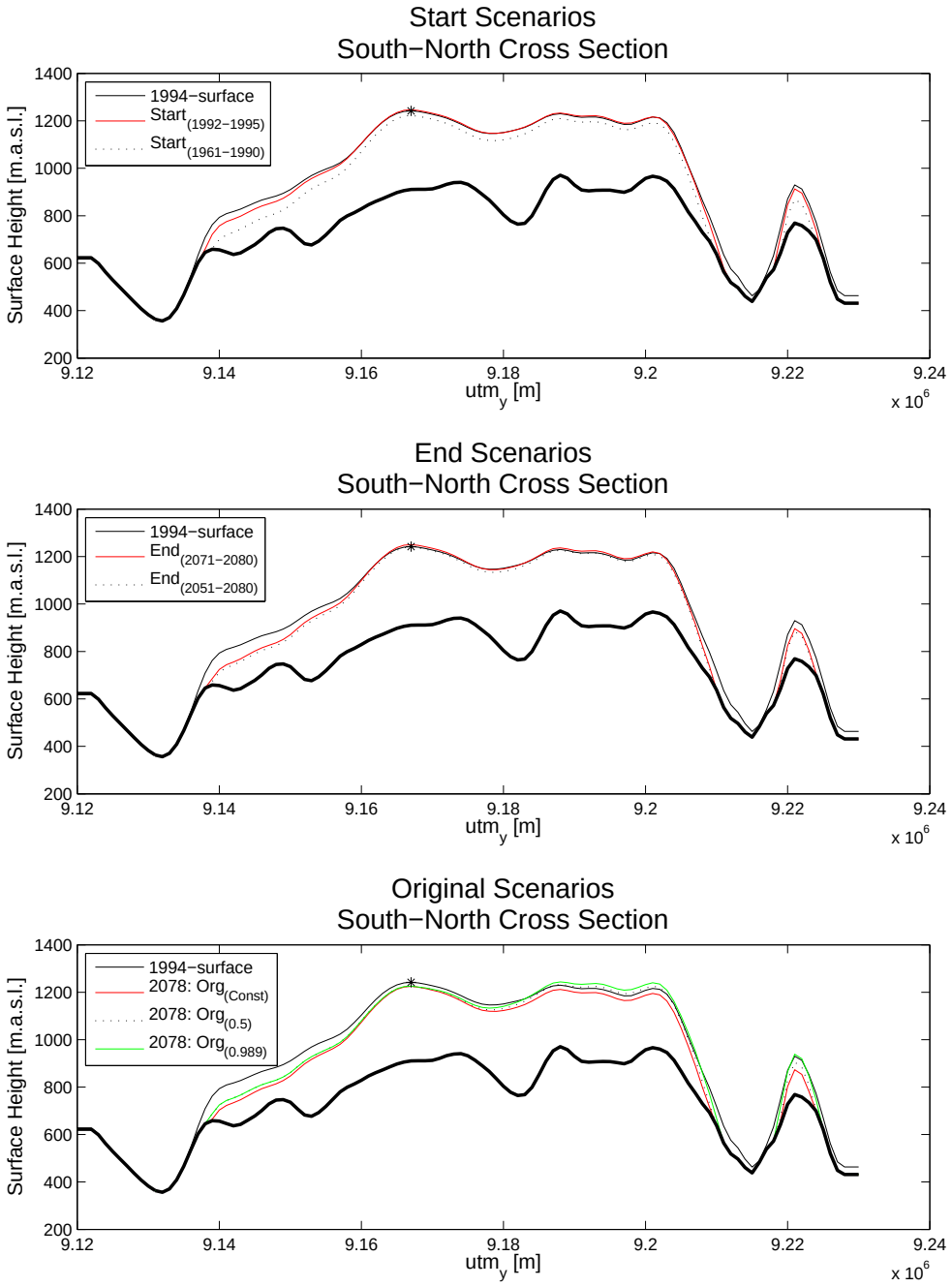

Figure 7.3: *Cross section 1 (South to North): Ice thickness after 85 years compared to the initial surface. For the Original experiments 85 years correspond to 2078. The thick black line indicates bedrock. The black star indicates the drill site.*

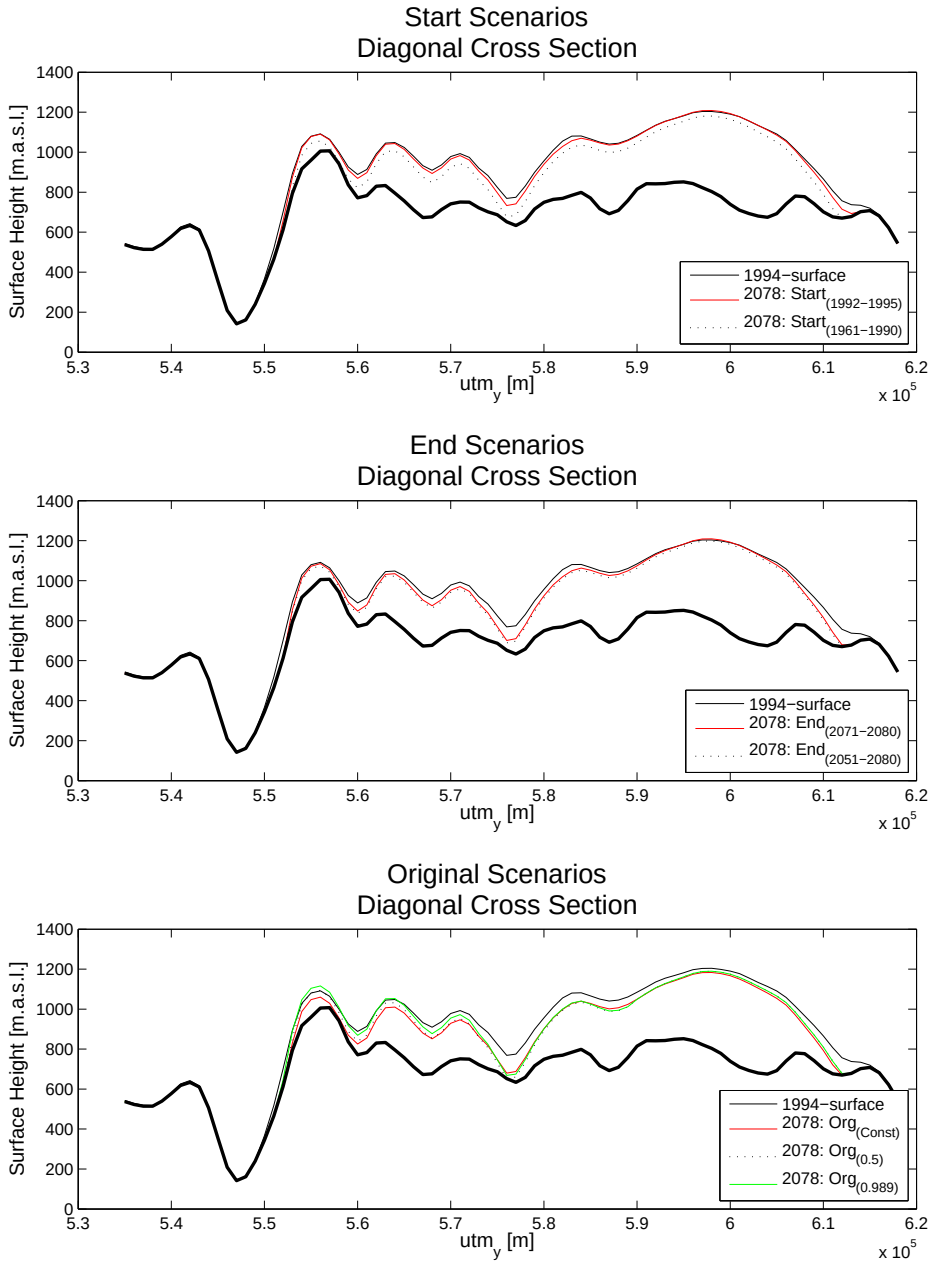

Figure 7.4: *Cross section 2 (Diagonal): Ice thickness after 85 years compared to the initial surface. For the Original experiments 85 years correspond to 2078. The thick black line indicates bedrock.*

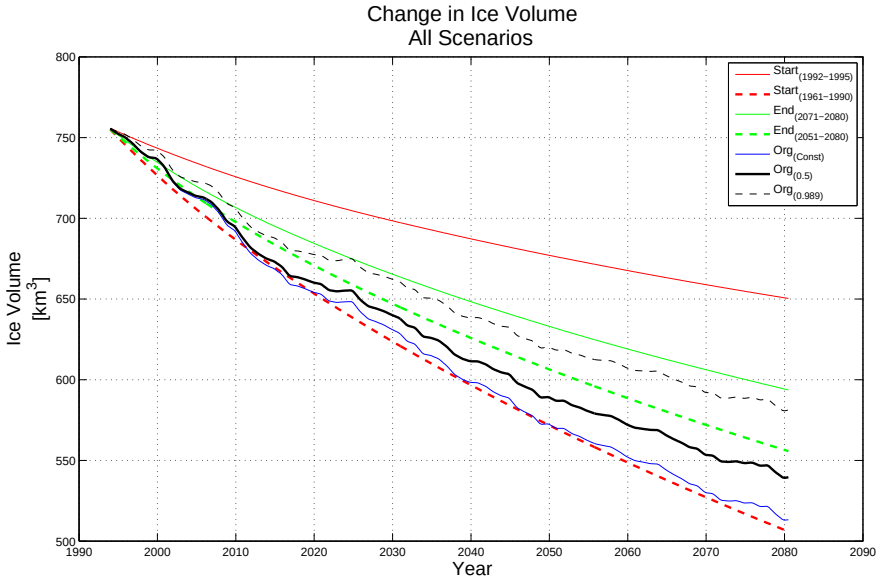

Figure 7.5: *Evolution of the ice volume with time.*

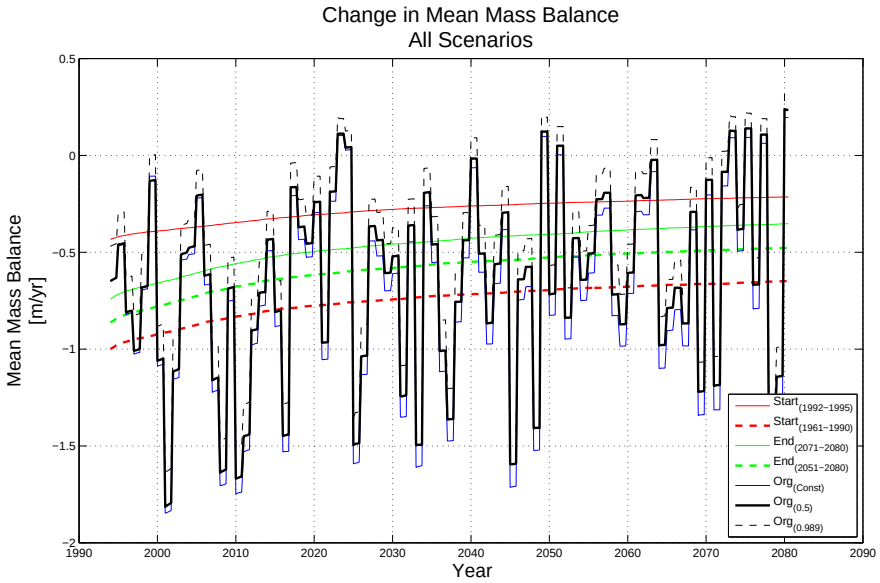

Figure 7.6: *Changes in mean mass balance with time.*

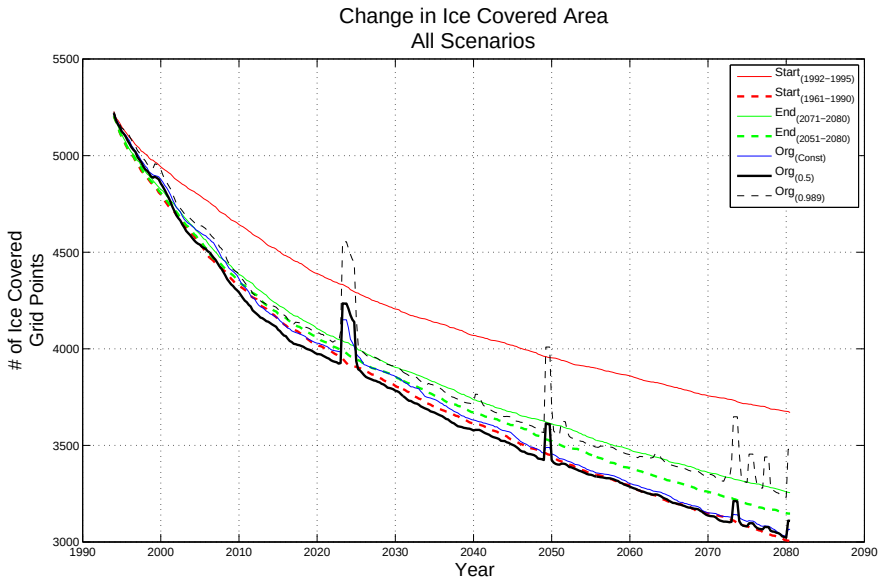

Figure 7.7: *Changes in the number of ice covered grid points (ice covered area) with time.*

the $\mathbf{Start}_{(1992-1995)}$ runs were repeated using the range of values discussed in Section 4.5. No significant differences were observed and it was concluded that within the given range the value of A will not influence the results. For all runs a value of A corresponding to -16 °C was applied.

7.4 Discussion

Looking at the plots of the cross sections (Figs. 7.3 and 7.4) it is easily seen that all experiments agree on a thinning in low elevation areas and a retreat of the margin. The magnitude and extent of recession, though, vary greatly between the scenarios: Up to 40-50 m in the margin areas and up to 10-30 m in the central parts of the ice cap. There is not the same consensus regarding the interior and high elevation areas. Four of the sub-scenarios predict an increase in ice thickness in at least one area: $\mathbf{Start}_{(1992-1995)}$, $\mathbf{End}_{(2071-2080)}$, $\mathbf{Org}_{(0.989)}$ and $\mathbf{Org}_{(0.5)}$. The three remaining sub-scenarios predict lowering of the entire surface. Figs. A.1 and A.2 in the Appendix show the shape and size of the ice cap the resulting from the different sub-scenarios after 87 years.

The thinning and retreat of the ice is also clear from Figs. 7.5 and 7.7. All experiments show decrease in volume and extent. The smallest changes are

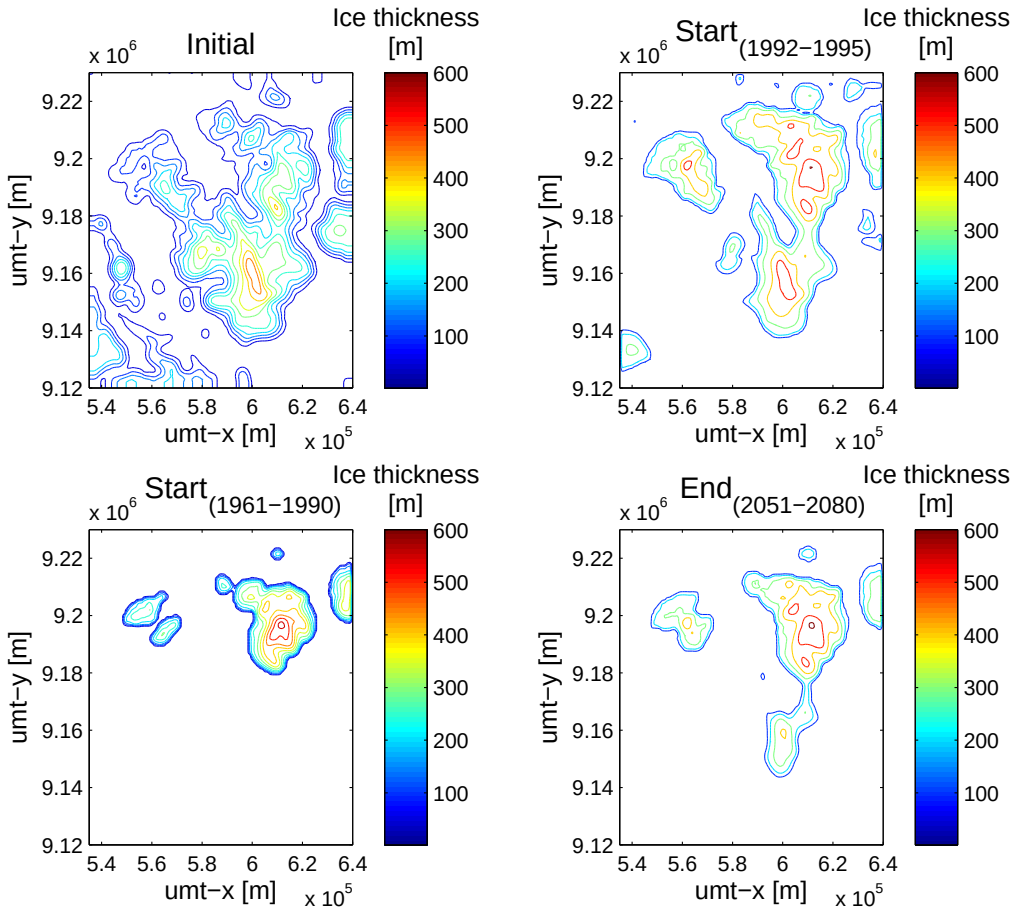

Figure 7.8: *Contour plots of the ice thickness after running the model using different climate scenarios for 1000 years using a reduced gradient between the northern and southern parts.* Initial *is the smoothed ice thickness from 1994 used as input.*

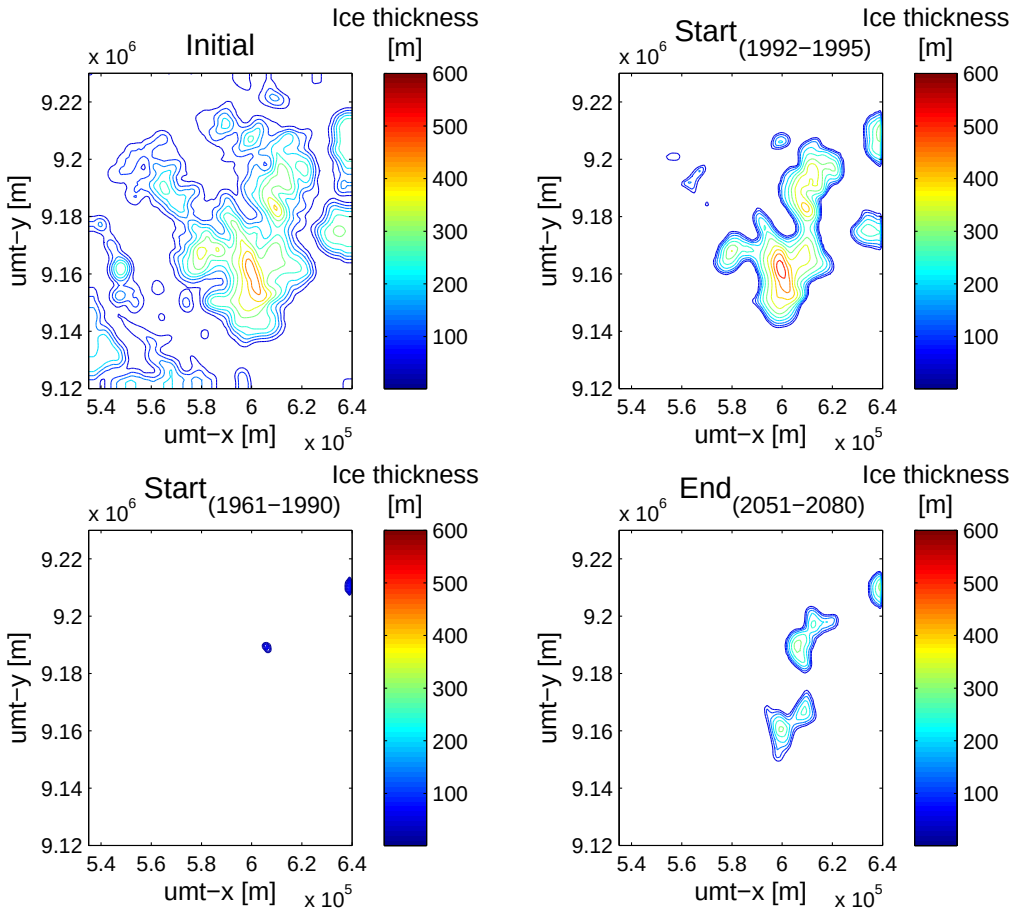

Figure 7.9: *As in Fig. 7.8 but with constant accumulation over the entire ice cap.* Initial *is the smoothed ice thickness from 1994 used as input.*

predicted by **Start**$_{(1992-1995)}$ and the greatest predicted by **End**$_{(2051-2080)}$. Although the mean specific mass balance (Fig. 7.6) increases for the four **Present** and **End** experiments as the low lying areas melt away it is still negative at the end of the run and the ice cap will continue to decrease for some time after. The trend in mean specific mass balance for the **Original** experiments also increases. The range of mean specific mass balance of the different sub-scenarios is the same as observed for other Arctic glaciers and ice caps [*Braithwaite*, 2005]. In the following subsections different aspects of the results will be discussed.

Influence of gradient	Start [m]	$\mathbf{Org}_{(\mathrm{Const})}$ [m]	$\mathbf{Org}_{(0.5)}$ [m]	$\mathbf{Org}_{(0.989)}$ [m]
P1	1303.2	1326.9	1293.3	1317.7
P2	1235.9	1265.1	1220.6	1251.5
P3	1051.4	1052.2	1012.1	1032.0

Table 7.2: *Table illustrating the influence of the accumulation gradient between the northern and southern part of Hans Tausen Iskappe. Simulations using the HIRHAM4 data. The positions of* P1, P2 *and* P3 *is displayed in Fig. 7.2. The first column is the elevation at the start of the run. The three other columns contain the elevation after the simulation depending on the experiment.*

7.4.1 The Accumulation Gradient

As mentioned in Section 4.3 the snowfall on Hans Tausen Iskappe for the year of mass balance measurements was found to be excessive [*Reeh et al.*, 2001]. This was also the case at the northern dome where the accumulation rate was measured to be 0.425 $^{\mathrm{m_{ice}}}/_{\mathrm{yr}}$. Strain net observations point to a much lower long term value of $0.2-0.3$ $^{\mathrm{m_{ice}}}/_{\mathrm{yr}}$. For this reason the three experiments in the **Original** scenario had different values of the accumulation gradient between the north and central domes in Eq. (4.3) in order to test the sensitivity of the result to the magnitude. A larger gradient implies an increase in accumulation on the northern half.

Figs. 7.3 and 7.4 show that for the two scenarios $\mathbf{Org}_{(0.989)}$ and $\mathbf{Org}_{(0.5)}$ the ice thickness grows on the northern dome while on the northwestern part only $\mathbf{Org}_{(0.989)}$ is significantly higher than the 1994-surface. $\mathbf{Org}_{(0.5)}$ shows only slight growth. For the $\mathbf{Org}_{(0.989)}$ scenario the ice thickness increases by 24 m and 29 m in the points P1 and P2 on Fig. 7.2, respectively. In P3 the increase is less than 1 m. The $\mathbf{Org}_{(0.5)}$ sub-scenario also yields an ice thickness increase in P1 (14 m) and P2 (15 m) but results in a decrease of 20 m in P3. For the last sub-scenario, $\mathbf{Org}_{(0.989)}$, the ice thickness decreases over the entire ice cap. In P1 the decrease is 10 m, in P2 15 m and for P3 on the northwestern part the decrease is largest amounting to 40 m. The results are summarized in Table 7.2 which shows the elevation of the three points before and after the simulations.

The northern part of the ice cap is very sensitive to the gradient in accumulation between the northern and southern part of the ice cap. The northern dome is less sensitive than the northwestern part of the ice cap due to its

high elevation.

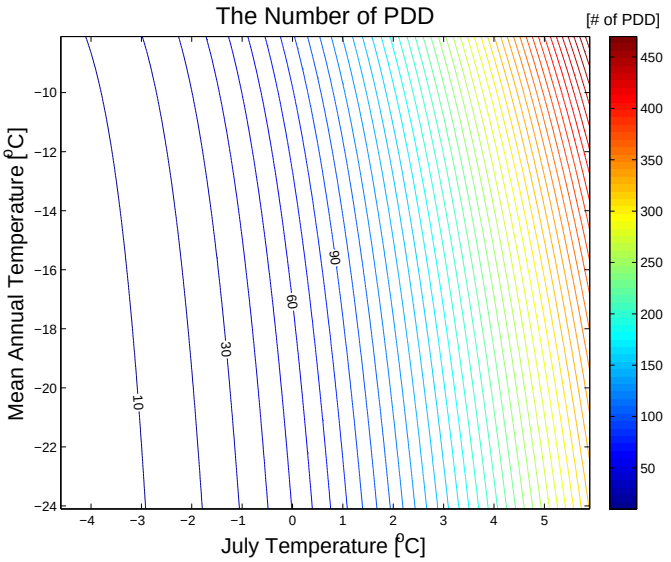

Figure 7.10: *The number of positive degree days (PDD) as a function of July and mean annual temperature. It is clearly seen that a change in July temperature results in a much larger change in PDD as compared to the same change in mean annual temperature. The equidistance between contour lines is 10 PDD.*

7.4.2 Sensitivity to July Temperature

The amount of ablation predicted by the degree day model is greatly dependent on the July temperature as seen in Fig. 7.10. The change in PDD with a small change in July temperature is much greater than the change resulting from a small change in mean annual temperature. The amount of melt is therefore strongly determined by the mean July temperature. For the runs using the variations in temperature and precipitation predicted by HIRHAM4 (**Original** scenarios) there is strong correlation between the mean July temperature and the mean specific mass balance with a correlation coefficient of $\mathrm{Conf}_{95\%}\{-0.938 < \mathrm{r} < -0.908\}$. The correlation coefficient between accumulation and mean specific mass balance is lower, $\mathrm{Conf}_{95\%}\{0.322 < \mathrm{r} < 0.496\}$, while there is no correlation for the mean annual temperature, $\mathrm{Conf}_{95\%}\{-0.086 < \mathrm{r} < 0.123\}$.

For ice caps in the Canadian High Arctic *Koerner* [2005] found that the

net mass balance almost entirely depends on summer climate because variations in winter balance are very small. The Hans Tausen Iskappe is also located in the High Arctic and has low accumulation combined with a high annual temperature variability. It is therefore reasonable that the conditions of the Canadian ice cap should also be prevailing for Hans Tausen Iskappe and the result of the degree day model seems sensible.

Increasing the mean annual temperature but keeping the mean July temperature constant prolongs the melt season slightly in the degree day model. The amplitude of the cosinus curve imitating the annual temperature cycle is reduced and is shifted towards warmer temperatures increasing the number of PDD calculated using Eq. (2.41). The maximum of the temperature curve is the same as before the increase. This increase does not have the same effect as increasing both the mean July temperature which prolongs the melt season more by increasing the amplitude and the maximum of the annual temperature cycle. This simplified annual temperature cycle could underestimate the effects of increase in temperature during other part of the year. In the simulation by *Stendel et al.* [2007] the largest temperature increases are observed in May possibly influencing the melt season.

The influence of mean July temperature on mass balance is also illustrated by the differences in volume at the end of the model period between $\mathbf{Start}_{(1992-1995)}$ and $\mathbf{Start}_{(1961-1990)}$. The volume decrease for $\mathbf{Start}_{(1961-1990)}$ is more than twice that of $\mathbf{Start}_{(1992-1995)}$ after 87 years. The two sub-scenarios have similar values of mean annual temperature and precipitation but the July temperature of $\mathbf{Start}_{(1961-1990)}$ is almost 2 °C warmer than $\mathbf{Start}_{(1992-1995)}$.

Reeh et al. [2001] studied changes in mean specific mass balance to changes in temperature and precipitation. The temperature increase was uniformly distributed over the year and they used the parameterizations of temperature and accumulation described in their article which are also applied in the Hans Tausen model [*Reeh et al.*, 2001]. They find that the already negative mean specific mass balance doubles for a temperature increase of 1 °C and an 20 % increase in precipitation. Performing the same calculation with no change in mean July temperature the mass balance only decreases ~ 10 %. This again confirms the influence of mean July temperature on ablation.

7.4.3 Present and Future

An interesting feature of the plots of volume and ice covered area in Fig. 7.5 and 7.7 is that $\mathbf{End}_{(2051-2080)}$ predicts smaller changes than $\mathbf{Start}_{(1961-1990)}$.

This is due to the slightly colder July temperature and the increase in precipitation of $\mathbf{End}_{(2051-2080)}$ compared to $\mathbf{Start}_{(1961-1990)}$. Many ice margins in Peary Land have previoulsy been observed to be very stable. The slow movement of the ice is thought to be an important factor but *Weidick* [2001] also points to a partial control by precipitation. He discusses the question of the relationship of precipitation to fjord conditions: Whether ice free fjords imply increased precipitation that rule out the effect of the temperature rise. The ice free fjords might have been an important factor for the increased precipitation during the build-up of the ice cap. As temperature increases in the future this could be a stabilizing factor for Hans Tausen Iskappe. At present the fjords are covered by semi-permanent ice [*Weidick*, 2001].

Braithwaite [2005] discusses the implications for Arctic glaciers of an even higher increase in temperature. If the climate warms sufficiently and sea ice melts away in the vicinity of the glaciers the relationship discussed above could change leading to a marine setting with reduced annual temperature range. For lower annual temperature amplitudes the fraction of precipitation that falls as rain will increase to a greater extent for maritime than for continental glaciers if temperature increases and they are thus more sensitive to a warming of the climate [*de Woul and Hock*, 2005; *Braithwaite*, 2005].

Comparing the results of $\mathbf{End}_{(2051-2080)}$ and $\mathbf{Start}_{(1961-1990)}$ with the results of the **Original** scenarios it is clear that the effect of individual years is important for changes in volume and ice covered area. Looking at Fig. 7.5 displaying the changes in volume $\mathbf{Org}_{(\mathrm{Const})}$ starts out following the curve of $\mathbf{End}_{(2051-2080)}$. A few years of very negative mean specific mass balance around the year 2010 causes the volume to decrease and the $\mathbf{Org}_{(\mathrm{Const})}$ curve almost follows the $\mathbf{Start}_{(1961-1990)}$ for the rest of the period. Both $\mathbf{Org}_{(0.5)}$ and $\mathbf{Org}_{(0.989)}$ have greater volumes due to the gradient in accumulation between the northern and southern parts of the ice cap increasing the precipitation on the northern part. Though the volume of $\mathbf{Org}_{(0.5)}$ is greater than for $\mathbf{Org}_{(\mathrm{Const})}$ the ice covered area is practically the same and very similar to that of $\mathbf{Start}_{(1961-1990)}$ except for the year 2080 where a positive mean mass balance of the **Original** causes the areas to increase. The down wasting in the $\mathbf{Org}_{(\mathrm{Const})}$ experiment is larger than in $\mathbf{Org}_{(0.5)}$ on the northern half.

Both $\mathbf{End}_{(2051-2080)}$ and $\mathbf{Start}_{(1961-1990)}$ predicts melt and negative mass balance at the Central Dome. Studies of the ice core by *Madsen and Thorsteinsson* [2001] show that presently some melting occurs but not every year. The remeasurement of the Central Dome shows a decrease in elevation indicating a change in the state of the ice cap.

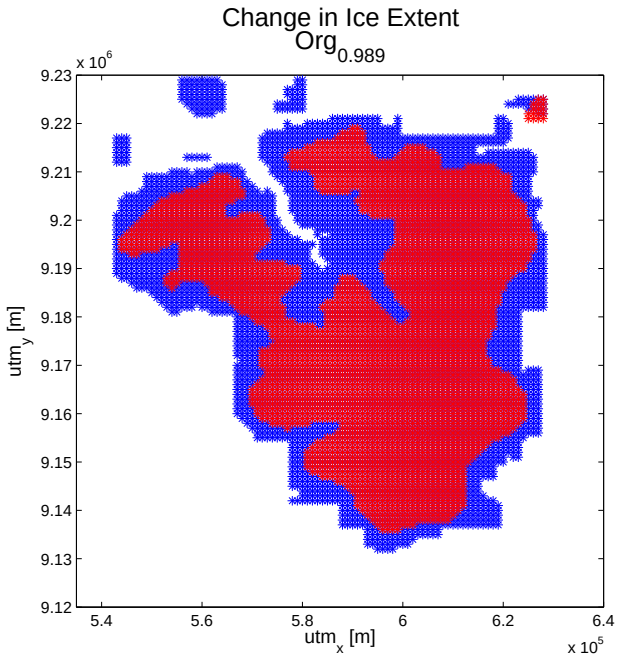

Figure 7.11: *The change in ice covered area for the* $\mathbf{Org}_{(0.989)}$ *experiment. The blue area indicates the areal extent of the ice cap at the start of the simulation and the red area the extent after running the model for* 87 *years.*

7.4.4 Shape and Area

As mentioned earlier all experiments agree on thinning of low elevation areas and retreat of the margin leading to a steeper ice cap. The extent of this is, however, very different from sub-scenario to sub-scenario. Since there is consensus between all experiments, the thinning and retreat is not happening as a response to future changes but is most likely already happening. Outlet glaciers at low elevations are probably relicts formed during the colder climate of the Little Ice Age and are beginning to retreat in response to the warming since then [*Reeh et al.*, 2001]. *Weidick* [2001] conclude a modest net recession of glaciers in the area from aerial photographs taken in 1978. Fig. 7.11 shows the change in ice covered area from the initial ice coverage to the ice coverage at the end of the 87 year model run for $\mathbf{Org}_{(0.989)}$. Some of the other sub-scenarios have larger decreases than $\mathbf{Org}_{(0.989)}$.

7.4.5 Hans Tausen Ice Cap in 1000 Years

Model predictions of the size and shape of the ice cap after running the model over 1000 years are shown in Figs. 7.8 and 7.9. Fig. 7.8 shows results using the parametrization of temperature as well accumulation described in Section 4.3 from *Reeh et al.* [2001] using a reduced gradient while Fig. 7.9 shows runs with constant accumulation over the ice cap. The results support those obtained in the previous subsections. The $\mathbf{Start}_{(1992-1995)}$ sub-scenario has the smallest changes in shape and size. $\mathbf{Start}_{(1992-1995)}$ has a low value of July temperature but also of precipitation. The low summer temperature diminishes melt to an extent that only a small part of the precipitation is melted away. These results emphasize the effect of July temperature in the model. It is also clear from the two figures that the accumulation gradient between the northern and central dome is important for maintaining the northern part of ice cap. In the parametrization there is also a gradient on the southern part increasing the accumulation towards the southern margin. This gradient is important for the ice on the southern part of the ice cap. For these scenarios the ice thickness at the northern and southern domes increases. Comparison between the two 30-year averaging periods, $\mathbf{Start}_{(1961-1990)}$ and $\mathbf{End}_{(2051-2080)}$, shows that for the latter climate the disappearance of the southern part is delayed a bit. For both scenarios the northern dome will survive and grow. Without the gradients the ice cap almost disappears in the 1000 years.

7.5 Conclusions

The experiments using the Hans Tausen model projects downwasting of low elevation areas and retreat of the margin for Hans Tausen Iskappe irrespective of scenario type. This leads to a steepening of the ice cap. All experiments show a decrease in volume and ice covered area. The mean specific mass balance increases through the period in response to the disappearance of low lying areas. There is no consensus regarding the central areas and the increase/decrease in elevation of the northern part of the ice cap is very dependent on the difference accumulation gradient between the Northern and Central Dome and the summer temperature.

The degree day model is very sensitive to small changes in mean July temperature and shows high correlation between mean mass balance and summer temperature for the **Original** scenario runs. This prediction seems reasonable as a similar result is seen from observations in the Canadian High Arctic. Here *Koerner* [2005] finds high correlations between mean specific mass bal-

ance and summer climate. The high influence of mean July temperature on melt was also observed and discussed in Chapter 5.

$\mathbf{Start}_{(1961-1990)}$ and $\mathbf{End}_{(2051-2080)}$ representing the present and future climate show differences in mass balance. The increase of mean annual temperature does not affect the amount of melting enough to outweigh the increase in precipitation. This leads to a slowdown in retreat of $\mathbf{End}_{(2051-2080)}$ compared to $\mathbf{Start}_{(1961-1990)}$. If the projections of precipitation and temperature for North Greenland are correct the near-future of Hans Tausen Iskappe is not more threatening than the present. However, the effect of individual years with extreme values is important.

Chapter 8

Conclusion and Outlook

A 2D vertically integrated ice flow model was developed in order to investigate Hans Tausen Iskappe, a local ice cap in North Greenland. The ice flow model is based on the shallow ice approximation and is well suited for studying the evolution of an ice cap over long periods of time. The model was validated using the EISMINT benchmarks and proved to perform well,

Using changes in surface temperature inferred from the Dye 3 borehole [*Dahl-Jensen et al.*, 1998] studies of the build-up show, that there has been a change in accumulation pattern during the life time of the ice cap. Using the present parametrization no ice forms at any time on the southern part of the plateau during the 4000 year simulation. The shielding of the southern part by the northern part observed at present probably happened gradually as the ice thickness increased. The open fjords at the time of build up infer a climate that was at least slightly warmer than present and were probably an important source of moisture at the time [*Landvik et al.*, 2001].

Laser scanner measurements of the Central Dome area in 2004 show an elevation decrease of $1 - 1.5$ m ± 0.5 m in the period from 1994. The short time span over which the decrease has been observed suggests local effects rather than larger changes in ice flow. The main causes are thought to be increased melting in the Central Dome area over the period and flow away from the dome combined with lower mass balance. This explains the lower bound of the decrease but is not sufficient to account for a larger elevation decline. Hans Tausen Iskappe is presently not in a steady state as indicated by several sources: The elevation measurements from 2004, the comparison of the 1994 mass balance with the steady state mass balance, the constant layer thickness in the ice core and the strain net observations from the field work showing thickening of the dome area.

The future state of Hans Tausen Iskappe was investigated by forcing the ice flow model using future predictions of precipitation and temperature by *Stendel et al.* [2007]. All the applied scenarios agree on thinning and recession of the ice margin resulting in a steeper ice cap over the next century. The present and future climate were represented by 30 year averages of the model predicted temperature and precipitation. The mean July temperature is projected to decrease slightly and the large increase in mean annual temperature is not sufficient to enlarge melting enough to outweigh the large increase in precipitation. This means that the average future climate will not accelerate the decrease of the ice cap. However, the effect of individual years with extreme temperatures and/or precipitation should be taken into account.

The nature of the projected warming is important for the future of ice masses. Model simulations investigating both the build-up and the future state of Hans Tausen Iskappe are very dependent on whether the temperature increase is uniformly distributed over the year or whether it increases mostly during winter and spring.

All studies in this thesis suggests an ice cap very sensitive to changes in climate. The mass balance is very important for its size and shape and a key to improving the results would be longer time series of temperature and mass balance observations over larger areas of the ice cap. This would enable much better parameterizations of accumulation and melt. A remeasurement of larger parts of the ice cap would help determine the size and extent of the elevation decrease.

The ice flow model assumes isothermal ice conditions but the ice temperatures measured in the boreholes both at the Central Dome and on the outlet glacier, Hare Glacier, display large differences. The temperature near bedrock in the former case is ~ -16 °C while it is ~ -1 °C in the latter case. To be able to better account for the flow, including ice temperature calculations in the model would improve the value of the flow parameter A.

Appendix A

All Future Scenarios

Figs. A.1 and A.2 show the shape and size of the ice thickness resulting from the 87 year runs in Chapter 7. The top left subplot in Fig. A.1 shows the starting point ice thickness in 1994. The thinning and retreat of the ice margin is evident in all plots. The influence of the accumulation gradient between the Central Dome and northern part of the ice cap is seen in Fig. A.1.

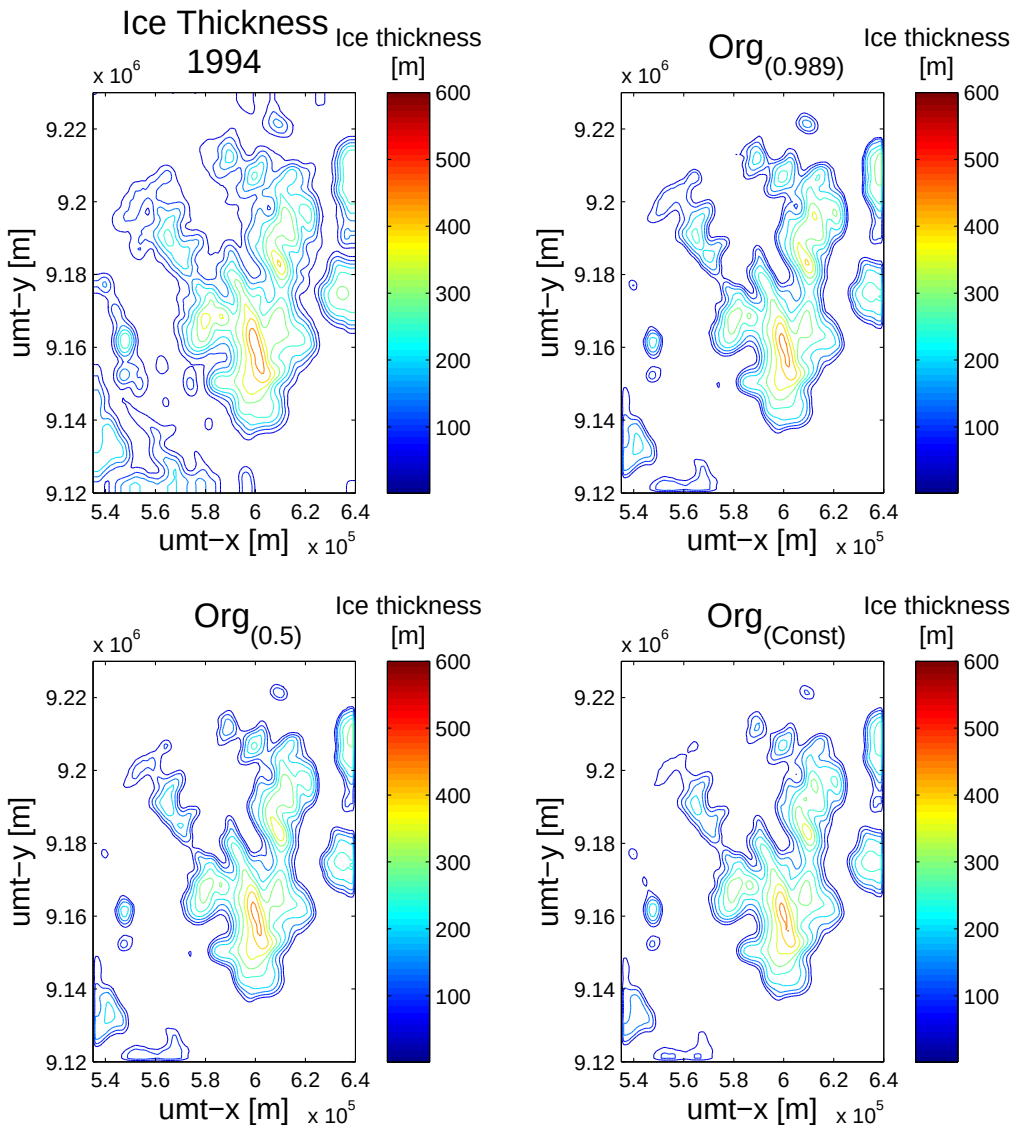

Figure A.1: *The shape and size of the ice thickness after 85 years. In this plot the 1994 ice thickness is shown together with the results of the* ***Original*** *scenarios.*

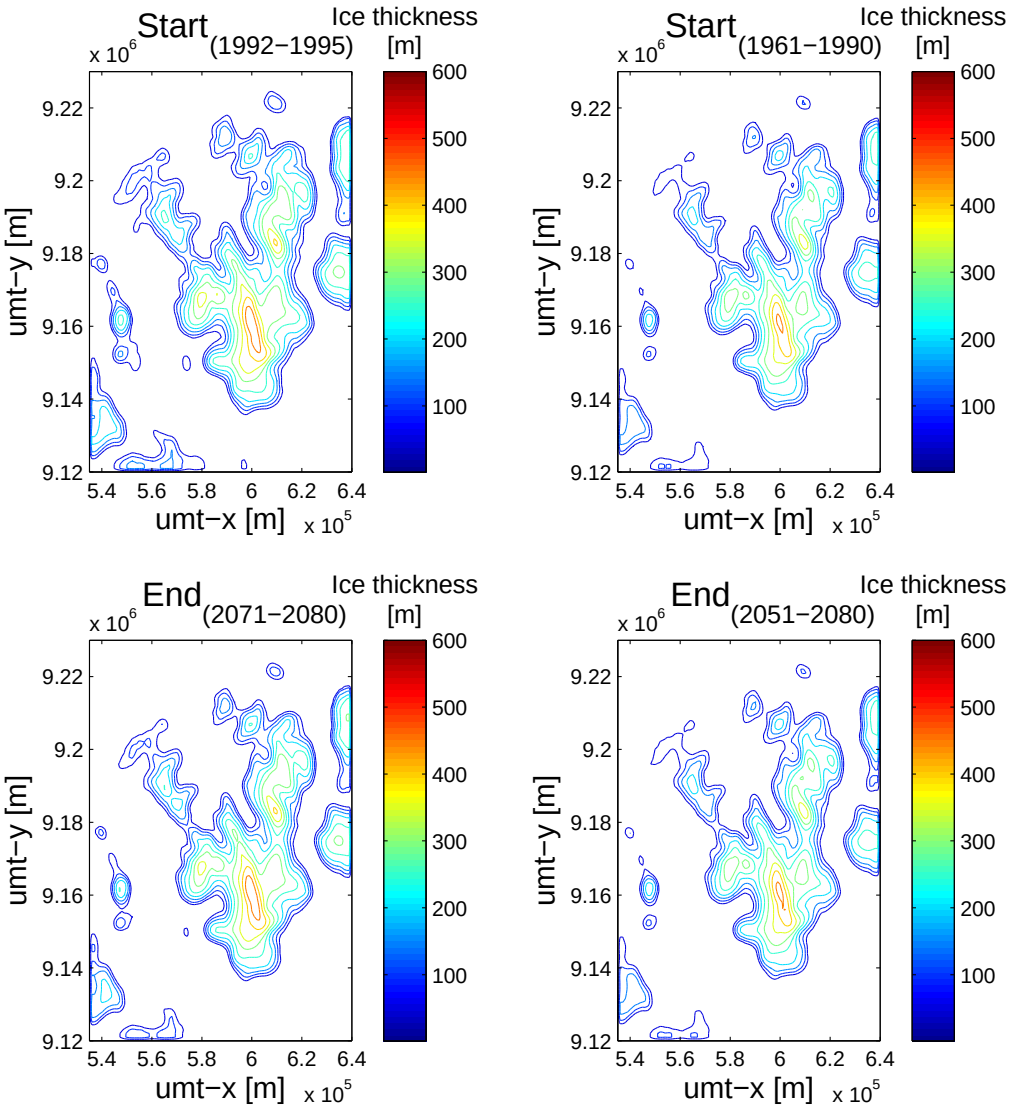

Figure A.2: *The shape and size of the ice thickness after 85 years. In this plot the* ***Present*** *and* ***Future*** *scenarios are shown.*

Map of Peary Land

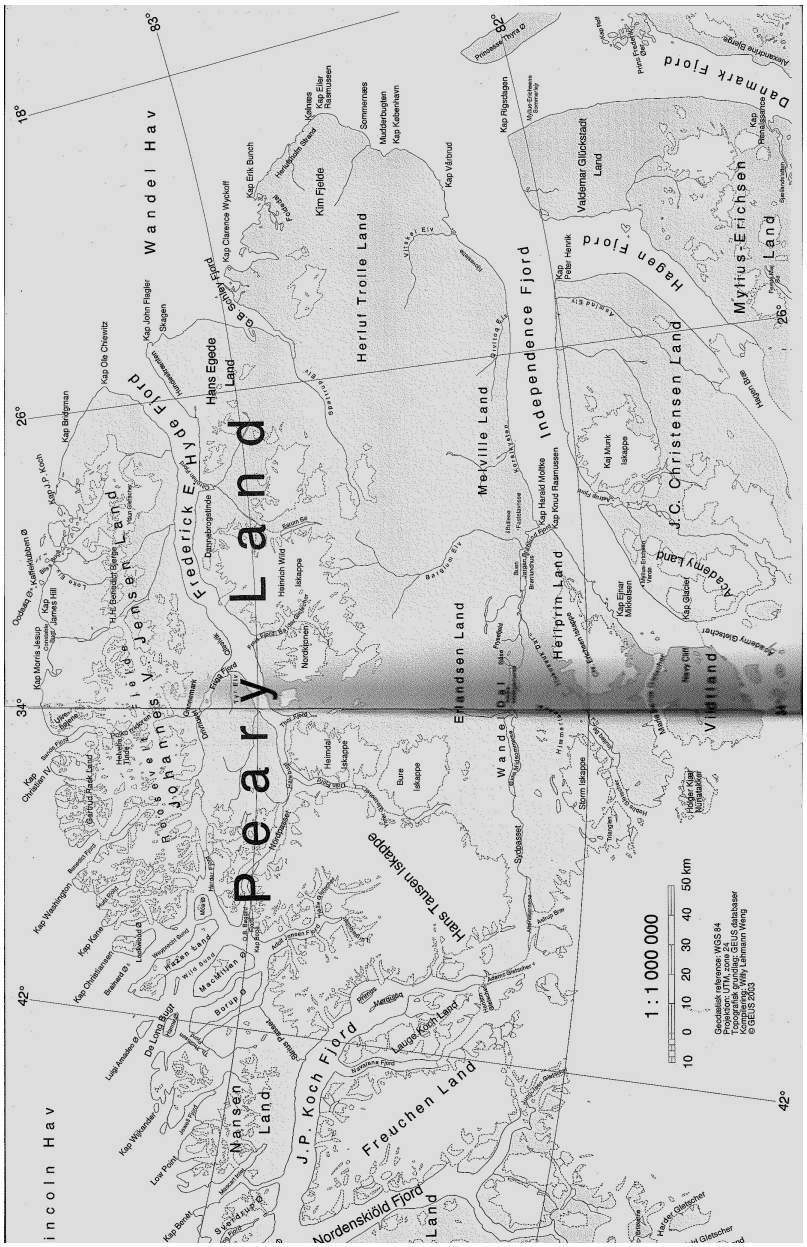

Figure A.3: *Figure showing the vicinity of Hans Tausen Iskappe in Peary Land, North Greenland.Map: GEUS 2003 from the anthology: Peary Land At tænke sig til Peary Land - Og kommer der. Redaktion: Gunnar Martens, Jens Fog Jensen, Morten Meldgaard og Hans Meltofte.*

Bibliography

Adalgeirsdottir, G., Flow dynamics of Vatnajökull ice cap, Iceland, Ph.D. thesis, Versuchanstalt für Wasserbau Hydrologie und Glaziologie der Eidgenössischen Technishen Hochschule Zürich, 2003.

Anisimov, O., D. Vaughan, T. Callaghan, C. Furgal, H. Marchant, T. Prowse, H. Vilhjalmsson, and J. Walsh, Polar regions (Arctic and Antartic), *Climate change 2007: Impacts, adaptation and vulnerability. contribution of working group ii to the fourth assessment report of the intergovernmental panel on climate change*, IPCC, 2007.

Bennike, O., Quarternary geology and biology of the Jørgen Brønlund Fjord area, North Greenland, *Meddelelser om Grønland, Geoscience*, *18*, p.3–20, 1987.

Braithwaite, R., Mass-balance characteristics of artic glaciers, *Annals of Glaciology*, *42*, p.225–229, 2005.

Cappelen, J., B. Jørgensen, E. Laursen, L. Stannius, and R. Thomsen, The Observed Climate of Greenland, 1958-99 -with Climatological Standard Normals, 1961-90, *Technical report, ministery of transport*, Danish Meteorological Institute, 2001.

Christensen, J., et al., Regional Climate Projections, *Climate change 2007: The physical science basis. contribution of working group i to the fourth assessment report of the intergovernmental panel on climate change*, IPCC, 2007.

Christensen, O., J. Christensen, B. Machenhauer, and M. Botzet, Very high-resolution regional climate simulations over Scandinavia - present climate, *Journal of Climate*, *11*, 3204–3229, 1998.

Clausen, H., M. Stampe, C. Hammer, C. Hvidberg, D. Dahl-Jensen, and J. Steffensen, Glaciological and Chemical Studies on ice Cores from Hans

Tausen Iskappe, Greenland, *Meddelelser om Grønland, Geoscience*, *39*, p.123–149, 2001.

Dahl-Jensen, D., K. Mosegaard, N. Gundestrup, G. Clow, S. Johnsen, A. Hansen, and N. Balling, Past Temperatures Directly from the Greenland Ice Sheet , *Science*, *282*, p.268–271, 1998.

Dalå, N., R. Forsberg, K. Keller, H. Skourup, L. Stenseng, and S. Hvidegaard, Airborne Lidar Measurements of Sea Ice North of Greenland and Ellesmere Island 2004. GreenICE/SITHOS/CryoGreen/a76 Projects - Final Report, *Reports No.2*, Danish National Space Center, 2005.

Dawes, P., Udforskning af Peary Land gennem 4000 år, *Peary Land: At tænke sig Peary Land - og komme der*, pp. 59–138, 2003.

de Woul, M., and R. Hock, Static mass-balance sensitivity of Arctic glaciers and ice caps using a degree-day approach, *Annals of Glaciology*, *42*, 217–224, 2005.

Dowdeswell, J., and J. Hagen, *Mass Balance of the Cryosphere*, chap. 14, pp. 527–557, Cambridge University Press, 2004.

Eldén, L., and L. Wittmeyer-Koch, *Numeriska beräkningar -analys och illustrationer med MATLAB®*, Studentlitteratur, 2001.

Fowler, A., and D. Larson, On the flow of polythermal glaciers; II. Surface wave analysis, *Preceedings of the Royal Society, London*, *A370*, 155–171, 1978.

Funder, S., C. Hjort, J. Landvik, S. Nam, N. Reeh, and R. Stein, History of a Stable Ice Margin - East Greenland during the middle and upper Pleistocene, *Quarternary Science Reviews*, *17*, p.77–123, 1998.

Glen, J., The Creep of Polycrystalline Ice, *Proceedings of the Royal Society of London*, *228*, p.519–538, 1955.

Hammer, C., S. Johnsen, H. Clausen, D. Dahl-Jensen, N. Gundestrup, and J. Steffensen, The Paleoclimatic Record from a 345 m long Ice Core from the Hans Tausen Iskappe, *Meddelelser om Grønland, Geosience*, *39*, p.87–95, 2001.

Hindmarsh, R., and A. Payne, Time-step limits for stable solutions of the ice-sheet equation, *Annals of Glaciology*, *23*, p.74–85, 1996.

Hooke, R., *Principles of Glacier Mechanics*, 2nd ed., Cambridge University Press, 2005.

Huybrechts, P., and T. Payne, The EISMINT benchmarks for testing ice-sheet models, *Annals of Glaciology*, *23*, p.1–12, 1996.

Hvidberg, C., K. Keller, N. Gundestrup, and P. Jonsson, Ice-divide flow at Hans Tausen Iskappe, North Greenland, from surface movement data, *Journal of Glaciology*, *47*, p.78–84, 2001.

Jonsson, P., An impulse radar measurement in NE Greenland, *Meddelelser om Grønland, Geoscience*, *39*, 81–86, 2001.

Kamb, B., and K. Echelmeyer, Stress-gradient coupling in glacier flow: I. Longitudinal averaging of the influence of ice thickness and surface slope, *Journal of Glaciology*, *32*, p.267–284, 1986.

Keller, K., C. Hvidberg, N. Gundestrup, and P. Jonsson, Surface Movement and Mass Balance at the Hans Tausen Drill Site determined by use of GPS, *Meddelelser om Grønland, Geosience*, *39*, p.115–122, 2001.

Koerner, R., Devon Island Ice Cap: Core Stratigraphy and Paleoclimate, *Science*, *196*, p.15–18, 1977.

Koerner, R., Mass balance of glaciers in the Queen Elizabeth Islands, Nunavut, Canada, *Annals of Glaciology*, *42*, p.417–423, 2005.

Koerner, R., and D. Fisher, Ice-core evidence for widespread Arctic glacier retreat in the Last Interglacial and the early Holocene, *Annals of Glaciology*, *35*, p.19–24, 2002.

Landvik, J., A. Weidick, and A. Hansen, The glacial history of the Hans Tausen Iskappe and the last glaciation of Peary Land, North Greenland, *Meddelelser om Grønland, Geoscience*, *39*, p.27–44, 2001.

Le Meur, E., O. Gagliardini, T. Zwinger, and J. Ruokolainen, Glacier flow modelling: a comparison of the Shallow Ice Approximation and the full-Stokes solution, *Comptes Rendus Physique*, *5*, 709–722, 2004.

Leysinger Vieli, G. J.-M. C., and G. Gudmundson, On estimating length fluctuations of glaciers caused by changes in climatic forcing, *Journal of Geophysical Research*, *109*, 1–14, 2004.

Lowe, J., and M. Walker, *Reconstructing Quaternary Environments*, Pearson Education Limited, 1997.

Madsen, K., Hans Tausen Iskernen -studier af krystalstruktur, datering og smeltelagsstratigrafi, Master's thesis, University of Copenhagen, 1997.

Madsen, K., and T. Thorsteinsson, Textures, fabrics and meltlayer stratigraphy in the Hans Tausen ice core, North Greenland - indications of late Holocene ice cap generation, *Meddelelser om Grønland, Geoscience*, *39*, p.97–114, 2001.

Marshall, S., Recent advances in understanding ice sheet dynamics, *Earth and Planetary Science Letters*, *240*, p.191–204, 2005.

Meier, M., M. Dyurgerov, U. Rick, S. O'Neel, W. Pfeffer, R. Anderson, S. Anderson, and A. Glazovsky, Glaciers Dominate Eustatic Sea-Level Rise in the 21st Century, *Science*, *317*, 1064–1067, 2007.

Nakicenovic, N., et al., *Special Report on Emissions Scenarios*, Cambridge University Press, 2000.

Oerlemans, J., *Glaciers and Climate Change*, A.A Balkema Publishers, 2001.

Oerlemans, J., et al., Modelling the response of glaciers to climate warming, *Climate Dynamics*, *14*, p.267–274, 1998.

Paterson, W., *The physics of Glaciers*, 3rd ed., Pergamon, 1994.

Press, W., S. Teukolsky, W. Vetterling, and B. Flannery, *Numerical Recipes in FORTRAN 77*, Cambridge University Press, 2003.

Reeh, N., Parameterization of Melt Rate and Surface Temperature on the Greenland Ice Sheet, *Polarforshung*, *59/3*, p.113–128, 1989 (1991).

Reeh, N., *Report on acivities and results 1993-1995 for Hans Tavsen Ice Cap Project -Glacier and Climate Change Research, North Greenland*, NMRs miljøforskningsprogram -klimaforskning, 1995.

Reeh, N., O. Olesen, H. Thomsen, W. Starzer, and C. Bøggild, Mass balance parameterisation for Hans Tausen Iskappe, Peary Land, North Greenland, *Meddelelser om Grønland, Geosience*, *39*, p.57–69, 2001.

Saito, F., A. Abe-Ouchi, and H. Blatter, An improved numerical scheme to compute horizontal gradients at the ice sheet margin: its effect on the simulated ice thickness and temperature, *Annals of Glaciology*, *46*, 2007.

Starzer, W., and N. Reeh, Digital elevation models of the Hans Tausen ice cap, *Meddelelser om Grønland, Geoscience*, *39*, p.44–56, 2001.

Steffensen, J., M. Siggard-Andersen, M. Stampe, and H. Clausen, Microparticles, soil derived chemical components and sea salt in the Hans Tausen Ice Cap Ice Core from Peary Land, North Greenland, *Meddelelser om Grønland, Geoscience*, *39*, p.151–160, 2001.

Stendel, M., J. Christensen, G. Adalgeirsdottir, N. Kliem, and M. Drews, Regional climate change for Greenland and Surrounding Seas. Part I: Atmosphere and Land Surface, *Danish Climate Centre Report 07-02*, Danish Meteorological Institute, 2007.

Van De Wal, R., Mass-balance modelling of Greenland ice sheet: a comparison of an energy-balance and a degree-day model, *Annals of Glaciology*, *23*, p.36–46, 1996.

Van den Berg, J., R. Van de Wal, and J. Oerlemans, Effects of spatial discretization in ice-sheet modelling using the shallow-ice approximation, *Journal of Glaciology*, *52*, p.89–98, 2006.

Weidick, A., Neoglacial Glaciations around Hans Tausen Iskappe, Peary Land, North Greenland, *Meddelelser om Grønland, Geoscience*, *39*, p.5–26, 2001.

Zwally, H., and J. Li, Seasonal and interannual variations of firn densification and ice-sheet surface elevation at the Greenland summit, *Journal of Glaciology*, *48*, p.199–207, 2002.